

**Obesity-linked dysfunction of
hypothalamic and pituitary circuits
in regulation of energy homeostasis**

Inaugural-Dissertation

zur

Erlangung des Doktorgrades

der Mathematisch-Naturwissenschaftlichen Fakultät

der Universität zu Köln

vorgelegt von

Bengt-Frederik Belgardt

aus Köln

Köln 2009

Berichterstatter: Prof. Dr. Jens C. Brüning
Prof. Dr. Peter Kloppenburg
Prof. Dr. Tamas Horvath

Tag der mündlichen Prüfung: 14.01.2010

“By three methods we may learn wisdom:
First, by reflection, which is noblest;
second, by imitation, which is easiest;
and third, by experience, which is the bitterest.”

-Confucius

Table of contents

<i>Table of contents</i>	4
<i>Figure index</i>	8
<i>Table index</i>	10
<i>Abbreviations</i>	11
<i>1 Introduction</i>	15
1.1 The obesity pandemic and associated diseases	15
1.2 Energy homeostasis	15
1.3 The adipokine leptin	16
1.4 Leptin signalling	16
1.5 The pancreatic hormone insulin	18
1.6 Insulin signalling	18
1.7 The brain as a regulator of energy homeostasis	20
1.8 The hypothalamus as a regulator of energy homeostasis	21
1.9 Leptin, insulin and the melanocortin circuit	23
1.10 Lipid-induced insulin and leptin resistance	26
1.11 The role of NFκB and JNK signalling in energy homeostasis	27
1.12 Central and peripheral inflammation and energy homeostasis	30
1.13 ER stress and energy homeostasis	31
1.14 Objectives	32
<i>2 Materials and Methods</i>	33
2.1 Chemicals and Biologicals	33
2.2 Molecular Biology	35
2.2.1 Isolation of genomic DNA	35
2.2.2 Quantification of nucleic acids	35
2.2.3 Polymerase chain reaction	35
2.2.4 RNA extraction, RT-PCR and Quantitative Real-Time PCR	36
2.3 Cell Biology	38
2.3.1 Histological analysis and immunohistochemistry	38

2.4 Biochemistry	39
2.4.1 Enzyme-linked Immunosorbent Assay (ELISA)	39
2.4.2 Protein extraction	39
2.4.3 Western Blotting	40
2.4.4 C-jun N-terminal kinase assay	40
2.4.5 Hepatic lipid content analysis	41
2.5 Mouse experiments	41
2.5.1 Animal care	42
2.5.2 Mice	42
2.5.3 Blood collection and determination of glucose levels	43
2.5.4 Food intake and indirect calorimetry	43
2.5.5 Glucose, insulin and pyruvate tolerance test	43
2.5.6 Analysis of body composition	44
2.5.7 Restraint stress	44
2.5.8 Intracerebroventricular indwelling catheter implantation	44
2.5.9 Intraperitoneal leptin sensitivity tests	45
2.5.10 Implantation of osmotic minipumps	45
2.5.11 Behavioural analysis	46
2.6 Cell culture	46
2.7 Computer analysis	47
2.7.1 Densitometrical analysis	47
2.7.2 Statistical methods	47
3 Results	48
3.1 Generation of POMC cell-specific PDK1 knockout mice	48
3.2 Increased body weight and hyperphagia in young PDK1^{ΔPOMC} mice	51
3.3 Secondary hypocortisolism in PDK1^{ΔPOMC} mice	53
3.4 Corticosterone replacement prolongs hyperphagia and increased body weight in PDK1^{ΔPOMC} mice	57
3.5 Restoration of energy homeostasis in PDK1^{ΔPOMC} mice by FOXO1 inhibition <i>in vivo</i>	58
3.6 Corticotroph cell loss in PDK1^{ΔPOMC} mice is FOXO1-independent	62
3.7 Hypothalamic JNK activity is increased by HFD	64
3.8 HFD induces an inflammatory response in the hypothalamus	65
3.9 TNFα has both anorexigenic and orexigenic properties in the CNS	66
3.10 HFD-induced hypothalamic expression of cytokines is not readily reversible	67
3.11 Generation of JNK1^{ΔNES} mice	68

3.12 JNK activity is increased in pituitaries of diet-induced obese mice	70
3.13 Unchanged behaviour in JNK1^{ANES} mice	71
3.14 Decreased weight but unchanged body composition in JNK1^{ANES} mice	73
3.15 Improved glucose homeostasis in JNK1^{ANES} mice under ND conditions	74
3.16 JNK1^{ANES} mice show decreased body weight but are not protected from diet-induced obesity	75
3.17 Improved glucose homeostasis in obese JNK1^{ANES} mice	76
3.18 JNK1^{ANES} mice show increased hypothalamic insulin but not leptin sensitivity	77
3.19 Unchanged hypothalamic expression of neuropeptides, cytokines and ER stress mediators in JNK1^{ANES} mice	80
3.20 HFD induces ER stress in the pituitary in a JNK1-independent manner	81
3.21 JNK1^{ANES} mice show decreased activation of the somatotrophic axis	82
3.22 JNK1^{ANES} mice show increased activation of the thyroid axis	85
3.23 JNK1^{ANes} mice are protected from hepatic dysfunction upon HFD	88
3.24 JNK1^{ANes} mice are protected from HFD-induced adipose tissue inflammation and dysfunction	91
<i>4 Discussion</i>	96
4.1 Inactivation of PDK1 in POMC cells	97
4.2 PDK1 in POMC cell function	97
4.3 The PDK1-FOXO1 axis in hypothalamic POMC expression	98
4.4 The PDK1-FOXO1 axis in corticotroph cell survival	99
4.5 Hypothalamic cytokine expression in diet-induced obesity	100
4.6 Hypothalamic/pituitary JNK activation in obesity	102
4.7 JNK1 as a regulator of somatic growth	102

4.8 JNK1 as a negative regulator of the thyrotrophic axis	104
4.9 JNK1 action and hypothalamic insulin sensitivity	105
4.10 Systemic effects of CNS/pituitary JNK1 signalling	105
4.11 Caloric restriction, aging and JNK1	108
4.12 Perspective	109
5 Summary	110
6 Zusammenfassung	111
7 References	112
8 Acknowledgements	121
9 Erklärung	122
10 Curriculum vitae	123

Figure index

Figure 1: Canonical leptin signalling.	17
Figure 2: Canonical insulin signalling.	19
Figure 3: The melanocortin system regulates energy homeostasis.	26
Figure 4: Multiple pathomechanisms of insulin resistance.	29
Figure 5: Targeted genomic loci in PDK1 ^{f1Δneo/f1Δneo} and POMC-Cre mice.	48
Figure 6: Ablation of the PDK1 protein in POMC neurons.	49
Figure 7: Unchanged PDK1 protein content in peripheral tissues and total brain.	50
Figure 8: PDK1 deletion follows endogenous POMC expression.	50
Figure 9: PDK1 deletion does not affect generation and survival of POMC neurons.	51
Figure 10: Increased body weight and hyperphagia in young PDK1 ^{ΔPOMC} mice.	52
Figure 11: POMC mRNA expression is impaired in PDK1 ^{ΔPOMC} mice.	53
Figure 12: Elevated insulin sensitivity in PDK1 ^{ΔPOMC} mice.	54
Figure 13: Reduced plasma corticosterone and adrenal ACTH insensitivity in PDK1 ^{ΔPOMC} mice.	55
Figure 14: Loss of POMC cells in pituitaries of PDK1 ^{ΔPOMC} mice.	56
Figure 15: Corticosterone restoration maintains hyperphagia and increased body weight in PDK1 ^{ΔPOMC} mice.	58
Figure 16: Generation of mice with inducible FOXO1 ^{Δ256} expression.	59
Figure 17: Expression of FOXO1 ^{Δ256} rescues the hypothalamic phenotype of PDK1 ^{ΔPOMC} mice.	60
Figure 18: Unchanged orexigenic and PVN neuropeptide expression in PDK1 ^{ΔPOMC} mice. ...	62
Figure 19: Corticotroph loss is not FOXO1-dependent in PDK1 ^{ΔPOMC} mice.	63
Figure 20: Pituitary pro-apoptotic gene expression in young PDK1 ^{ΔPOMC} mice.	64
Figure 21: High-fat diet induces hypothalamic JNK activation.	65
Figure 22: High-fat diet induces hypothalamic transcription of cytokines.	66
Figure 23: TNFα elicits orexigenic and anorexigenic effects in a dose-dependent manner ...	67
Figure 24: Diet-induced up-regulation of cytokine expression is not readily reversible by diet modulation.	68
Figure 25: Nestin cell-specific deletion of JNK1.	69
Figure 26: Generation of JNK1 ^{ΔNes} mice.	70
Figure 27: Pituitary JNK activation upon high-fat feeding.	71

Figure 28: Unchanged locomotor control and anxiety in JNK1 ^{ΔNes} mice.....	72
Figure 29: Unchanged water maze performance by JNK1 ^{ΔNes} mice.....	73
Figure 30: Decreased weight but unchanged body composition in JNK1 ^{ΔNES} mice on Normal Diet.....	74
Figure 31: Improved insulin sensitivity and glycemic control in JNK1 ^{ΔNES} mice on Normal Diet.....	75
Figure 32: Decreased weight but unchanged body composition in JNK1 ^{ΔNES} mice on HFD..	76
Figure 33: Improved glucose tolerance and insulin sensitivity in obese JNK1 ^{ΔNES} mice.....	77
Figure 34: Unaltered leptin sensitivity in JNK1 ^{ΔNES} mice	78
Figure 35: Elevated hypothalamic insulin sensitivity in JNK1 ^{ΔNES} mice.....	79
Figure 36: Hypothalamic neuropeptide, cytokine and ER stress marker expression is unchanged in JNK1 ^{ΔNES} mice	81
Figure 37: HFD induces ER stress marker expression in the pituitary	82
Figure 38: Serum IGF-1 is reduced in JNK1 ^{ΔNES} mice	83
Figure 39: Somatic growth is reduced at the control level of the pituitary in JNK1 ^{ΔNES} mice	84
Figure 40: Pituitary expression of PIT-1 and its target GHRHR is regulated in JNK1 ^{ΔNES} mice	85
Figure 41: Corticosterone levels are normal in JNK1 ^{ΔNES} mice.....	86
Figure 42: JNK1 ^{ΔNES} mice show increased activation of the thyrotropic axis.....	86
Figure 43: Elevated pituitary activation of the thyrotropic axis in JNK1 ^{ΔNES} mice.....	87
Figure 44: JNK inhibition increases TRHR expression <i>in vitro</i>	88
Figure 45: JNK1 ^{ΔNES} mice are protected from diet-induced hepatosteatosis	89
Figure 46: Reduced hepatic triglyceride content in HFD-fed JNK1 ^{ΔNES} mice.....	89
Figure 47: Ameliorated hepatic glucose production in diet-induced obese JNK1 ^{ΔNES} mice....	90
Figure 48: Elevated hepatic insulin sensitivity in diet-induced obese JNK1 ^{ΔNES} mice.....	90
Figure 49: Increased eWAT mass in diet-induced obese JNK1 ^{ΔNES} mice	91
Figure 50: Obese JNK1 ^{ΔNES} mice are protected from adipocyte hypertrophy	92
Figure 51: JNK1 ^{ΔNES} mice show ameliorated lipid metabolism enzyme expression in eWAT93	
Figure 52: JNK1 ^{ΔNES} mice are protected from obesity-induced WAT inflammation	94
Figure 53: GLUT4 expression in eWAT is increased in obese JNK1 ^{ΔNES} mice	95
Figure 54: Model of post-developmental POMC neuron activity and POMC mRNA expression.....	99

Table index

Table 1: Chemicals.....	33
Table 2: Enzymes	35
Table 3: Primer sequences.....	36
Table 4: Real-Time analysis probes	37
Table 5: Custom Real-Time analysis probes.....	38

Abbreviations

°C	degrees Celsius
3'	three prime end of DNA sequences
5'	five prime end of DNA sequences
A	adenosine
ACTH	adrenocorticotrophin
AgRP	agouti-related peptide
AKT	protein kinase B
Arc	arcuate nucleus
Avertin	tribromoethyl alcohol and <i>tert</i> -amyl alcohol
BAT	brown adipose tissue
BMI	body mass index
C	cytosine
CART	cocaine-and-amphetamine-related transcript
cAMP	cyclic adenosine monophosphate
cDNA	complementary DNA
CNS	central nervous system
Cort	corticosterone
Cre	site specific recombinase from phage P1 (causes recombination)
Da	Dalton
DAPI	4',6-diamidino-2-phenylindole
ddH ₂ O	double distilled water
DG	diglyceride
DMH	dorsomedial hypothalamic nucleus
DMSO	dimethylsulfoxide
DNA	desoxyribonucleic acid
DNase	desoxyribonuclease
dNTP	desoxyribonucleotide-triphosphate
DTT	Dithiothreitol
e.g.	<i>exempli gratia</i>
ECL	enhanced chemiluminescence
EDTA	ethylenediamine tetraacetate
eGFP	enhanced green fluorescent protein
ELISA	enzyme-linked immunosorbent assay
EtBr	ethidium bromide
EtOH	ethanol
FFA	free fatty acid
floxed	loxP flanked
fMol	femto-Mol
FOXO1	forkhead-O transcription factor 1
g	gram
G	guanine
G6P	glucose-6-phosphatase
GABA	gamma-aminobutyric acid
GFP	green fluorescent protein
GH	growth hormone
GHRH	GH-releasing hormone
GHRHR	GHRH receptor

GLUT4	glucose transporter 4
GTT	glucose tolerance test
Gusb	glucuronidase beta
h	hour
H&E	hematoxylin/eosin
HCl	hydrochloric acid
HEPES	N-2-hydroxyethylpiperazine-N'-2-ethansulfonic acid
HFD	high-fat diet
HGP	hepatic glucose production
Hprt	hypoxanthine guanine phosphoribosyl transferase-1
HSL	hormone sensitive lipase
icv	intracerebroventricular
IGF-1	insulin-like growth factor-1
IL1 β	interleukin 1 beta
IL6	interleukin 6
ip	intraperitoneal
IR- β	insulin receptor, beta subunit
IRES	internal ribosome entry site
IRS	insulin receptor substrate
ITT	insulin tolerance test
JAK	Janus kinase
JNK	c-Jun N-terminal kinase
k	kilo
kb	kilobase pairs
KCl	potassium chloride
kDa	kilodalton
KOH	potassium hydroxide
l	liter
<i>lacZ</i>	gene encoding the enzyme beta-galactosidase
LH	lateral hypothalamic area
loxP	recognition sequence for Cre (<u>l</u> ocus of <u>x</u> -ing over phage <u>P</u> 1)
LPL	lipoprotein lipase
m	milli
M	molar
MAPK	mitogen-activated protein kinase
MCR	melanocortin receptor
ME	median eminence
MgCl ₂	magnesium chloride
min	minute
mRNA	messenger RNA
MSH	melanocyte-stimulating hormone
n	nano
Na ₂ HPO ₄	disodium hydrogen phosphate
Na ₃ O ₄ V	sodium orthovanadate
NaCl	sodium chloride
NaF	sodium fluoride
NaH ₂ PO ₄	monosodium phosphate
NaHCO ₃	sodium bicarbonate
NaOH	sodium hydroxide
ND	normal diet
NF κ B	nuclear factor kappa-light-chain-enhancer of activated B cells

NMR	nuclear magnetic resonance
NPY	neuropeptide Y
ObRb	leptin receptor, long isoform
OD	optical density
p/P	phospho-
PAGE	polyacrylamid gel electrophoresis
PB	phosphate buffer
PBS	phosphate buffered saline
PCR	polymerase chain reaction
PDK1	3-phosphoinositide-dependent protein kinase 1
PFA	paraformaldehyde
PH	pleckstrin homology
PI3K	phosphatidylinositol 3-kinase
PIP ₂	phosphatidylinositol-4,5-bisphosphate
PIP ₃	phosphatidylinositol-3,4,5-trisphosphate
PIT-1	Pituitary-specific positive transcription factor 1
PKC	protein kinase C
pMol	pico-Mol
POMC	proopiomelanocortin
PTB	phosphotyrosine binding
PTEN	phosphatase and tensin homolog
PTT	pyruvate tolerance test
PVN	paraventricular nucleus
Raf	proto-oncogene serine/threonine protein kinase
Ras	small GTPase (<u>R</u> at <u>s</u> arcoma)
RNA	ribonucleic acid
RNAi	RNA interference
RNase	ribonuclease
RT	room temperature
SDS	sodiumdodecylsulfate
sec	second
SEM	standard error of the mean
SGK1	serum- and glucocorticoid regulated kinase 1
SH	src homology
Shp-2	tyrosine phosphatase-2
SOCS	suppressor of cytokine signalling
STAT	signal transducer and activator of transcription
T3	triiodothyronine
T4	thyroxine
TAE	Tris-acetic acid-EDTA buffer
TBS	Tris buffered saline
TG	triglyceride
TNF α	tumor necrosis factor alpha
TRH	thyrotrophin releasing hormone
TRHR	TRH receptor
Tris	2-amino-2-(hydroxymethyl)-1,3-propanediol
TSH β	thyroid stimulating hormone beta
Tyr/Y	tyrosine
U	units
UV	ultraviolet
V	Volt

v/v	volume per volume
VMH	ventromedial nucleus of the hypothalamus
VO ₂	volume of oxygen
w/v	weight per volume
WAT	white adipose tissue
WHO	World Health Organisation
ZnSO ₄	zinc sulfate
β-M	β-mercaptoethanol
μ	micro

1 Introduction

1.1 The obesity pandemic and associated diseases

The worldwide increase in obesity has reached pandemic proportions, as indicated by more than 1.6 billion people being overweight and 400 million being obese (1). Approximately 50% of American citizens have a body mass index (BMI = weight/size in meters²) higher than 25 and are thus considered overweight; a steady increase of average BMI has also been reported in Europe, Asia and even Africa (2, 3). In Germany, more than 20% of adult men and women are obese as indicated by an BMI greater than 30 (4). Importantly, increases in BMI are not only seen in people already overweight or obese. Analysis of the BMI distribution over the last 60 years indicates a significant shift among lean, normal weight and overweight people of all ages towards an increased BMI, emphasising the reach of the obesity pandemic (5). Obesity is the principal consequence of increased neutral lipid storage in adipocytes in the white adipose tissue due to either increased energy intake, reduced energy expenditure, or both (6-8). In addition to psychosocial effects such as stigmatisation and social isolation, obesity increases the risk for contracting a variety of diseases such as cancer, atherosclerosis, dyslipidemia, retinopathy, renal failure, neuropathy and especially diabetes mellitus (DM), establishing the “metabolic syndrome” (9-14). Economic costs are immense; estimated 20% of the US health care budget is spent on patients with DM (15). Chronic obesity shortens life span; being obese at the age of 40 reduces the predicted life time by up to 7 years (16). Furthermore, there is evidence that maternal obesity during pregnancy has profound effects on body weight of newborns during their adult life, underlining the necessity to combat obesity (17-20). In light of these alarming epidemiological findings, considerable efforts have been undertaken to understand how body weight and glucose homeostasis are regulated in humans.

1.2 Energy homeostasis

In healthy humans and mice, a specific body weight is perpetuated, since both experimental underfeeding and overfeeding will lead to compensatory changes in food intake and energy expenditure (21-24). Therefore, physiological signals exist which contain fat mass gain during overabundance, or increase feeding in case of depleted energy stores. These physiological signals and circuits are therefore responsible for maintaining energy homeostasis. Owing to the obesity pandemic, it has been deduced that body weight gain

indicates malfunctioning of these counterregulatory systems, possibly due to genetic predisposition, environmental factors or most likely, both (25-27). From an evolutionary point of view, the ability to sustain body weight in a scarce environment has been very important, since energy surplus was ultimately very rare until the middle of the 20th century (the “thrifty gene” hypothesis) (28). The hypothesis that signals, for example hormones, secreted by peripheral tissues might have an effect on central/neuronal circuits to control body weight has been highlighted by findings from the late 20th century. These studies indicated that multiple feedback loops between the brain and peripheral tissues regulating energy homeostasis exist, with the hormones insulin and leptin implicated as the most important regulators of body weight and glucose metabolism (29-32).

1.3 The adipokine leptin

The gene of the critical regulator of energy homeostasis, leptin, was cloned in 1995 (33). Leptin is expressed mainly in the adipose tissue in relation to the stored fat content, and released into the circulation (34). It was identified after genetic screening of a mouse strain called the obese/obese (*ob/ob*) mouse, which was revealed to completely lack leptin protein due to a homozygous mutation (33). Later on, human patients were identified which also lack circulating leptin and hence show early-onset morbid obesity, underscoring the importance of leptin in human physiology (35). The leptin receptor (ObR) was subsequently cloned, and mice lacking the signalling isoform of the leptin receptor (ObRb) show massive obesity, and develop early onset DM, and are thus called *db/db* mice (from diabetic) (36, 37). Application of recombinant leptin to *ob/ob* mice or human patients lacking leptin rapidly normalises body weight and glucose homeostasis (33). Nonetheless, the overwhelming majority of obese patients cannot be treated by leptin, since obese patients (and obese animal models) show increased levels of leptin in the circulation, indicating a leptin resistant state. So far, the search for an leptin sensitizing drug with efficacy in patients has been fruitless (38).

1.4 Leptin signalling

Leptin signals by activation of its receptor which is expressed at high levels in several brain regions, especially the hypothalamus (36, 39). It has been demonstrated that the weight-reducing effects of leptin are predominantly mediated by its action on neurons (40). Activation of its receptor leads to recruitment of janus kinases (JAK) 2, which phosphorylate the intracellular domain on specific residues (41). JAK2 is able to phosphorylate the

transcription factor signal transducer and activator of transcription (STAT) 3, which after homodimerisation enters the nucleus to activate or inactivate transcription of leptin-regulated genes by recruitment of histone acetylases or deacetylases, respectively (37, 42). Besides several phosphatases implicated in dephosphorylation of leptin signalling cascade proteins (43), suppressor of cytokine signalling (SOCS) 3 has been shown to be crucial for leptin signalling. Its expression is positively regulated by leptin stimulation, thus leptin increases expression of its own negative regulator, which subsequently reduces interaction of STAT3 with the ObRb and thus enables a new round of stimulation (41, 43). Importantly, it has been shown that a chronic hyperleptinemic state induces a disproportional increase in SOCS3 expression, possibly indicating that chronic leptin signalling by itself induces leptin resistance (44). In addition to JAK2/STAT3 signalling, leptin is able to activate insulin's main signalling cascade phosphatidyl-inositol-3-kinase (PI3K) through the adapter protein SH2-B (45), although duration and signal strength of PI3K activation is considerably lower compared to insulin (46-50).

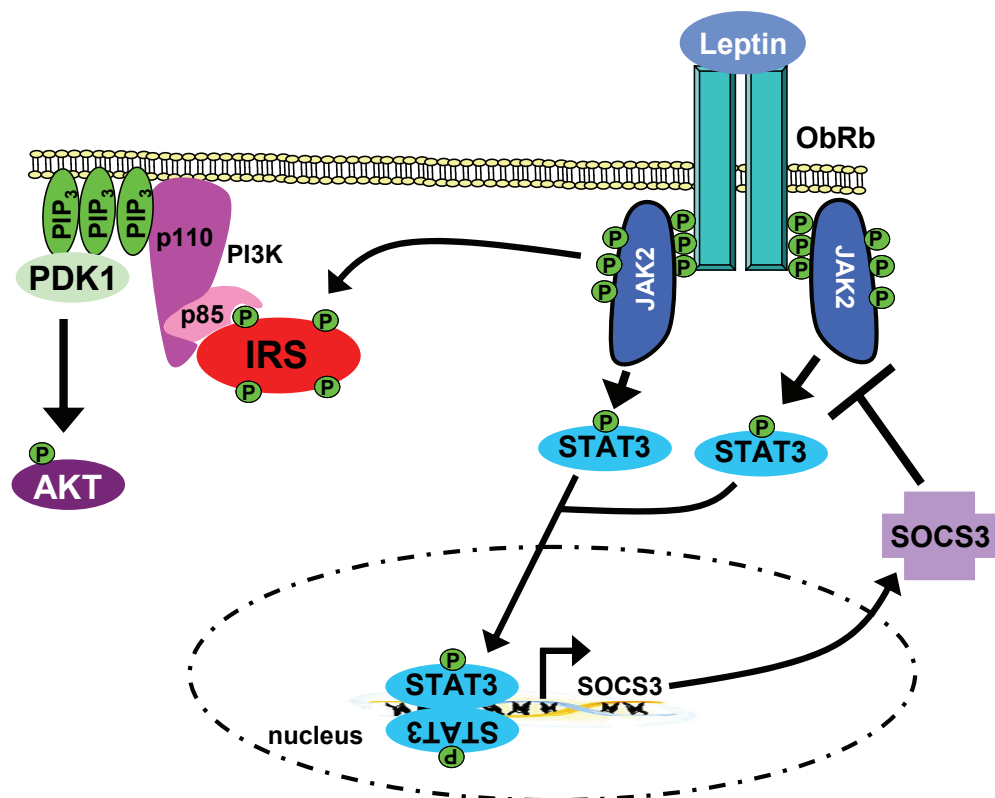


Figure 1: Canonical leptin signalling.

Binding of leptin leads to recruitment of Jak2, autophosphorylation and phosphorylation of ObRb. After Jak2-mediated phosphorylation of STAT3, pSTAT3 dimers activate transcription of target genes by recruitment of histone acetylases. One of these genes is *SOCS3*, and the *SOCS3* protein in a feedback loop binds to JAK2 and thereby inhibits STAT3 phosphorylation. In addition, JAK2 is able to directly activate IRS/PI3K signalling, leading to AKT activation. IRS, insulin receptor substrate; JAK2, Janus kinase 2; ObRb, long form of leptin receptor; PDK1, 3-phosphoinositide-dependent protein kinase 1; PI3K, phosphatidylinositol-3-kinase; PIP2, phosphatidyl-inositol-4,5-bisphosphate; PIP3, phosphatidylinositol-3,4,5-triphosphate; *SOCS3*, suppressor of cytokine signalling 3; STAT3, signal transducer and activator of transcription 3.

1.5 The pancreatic hormone insulin

The notion that a pancreatic hormone is able to acutely reduce glucose concentration in the blood has been known for more than 80 years, following extraction of insulin from dog pancreas by Banting and Best (51). In pancreatic β -cells, insulin is translated as a 51 amino acid preproprotein, which after cleavage of a signalpeptide as well as generation of disulfide bridges in the endoplasmatic reticulum (ER), is stored in cytoplasmatic vesicles (52, 53). If ambient glucose concentrations rise, glucose enters the cell via glucose transporter (GLUT) 2 and is metabolised into adenosine triphosphate (ATP). Rising intracellular ATP concentrations are sensed by ATP-dependent potassium (KATP) channels, which close at a certain ATP concentration threshold. Closure of KATP channels depolarises the membrane of the β -cell, resulting in the opening of calcium channels, allowing Ca^{2+} ion influx. The increasing intracellular Ca^{2+} concentrations induce vesicle exocytosis and thus release of insulin into the bloodstream (52, 54).

1.6 Insulin signalling

The insulin signalling cascade is activated by binding of insulin to the insulin receptor (IR), which is almost ubiquitously expressed in mammalian tissues, including hepatocytes, myocytes, adipocytes, pancreatic cells, several lineages of the immune system, and the brain (55-60). It consists of two heterodimers of the α - and β -chain, wherein the α -chain is located extracellular, while the β -chain spans from the extracellular through the membrane into the intracellular space (61). Binding of insulin to the IR elicits a conformational change, which activates the tyrosine kinase activity of the β -chain (61). After *trans* phosphorylation of the β -chains at seven tyrosine residues, maximal kinase activity is achieved (61). Insulin receptor substrates (IRS) bind to the IR via their phosphotyrosine binding domains (PTB) (62-64). Most of the IRS proteins also contain a pleckstrin homology (PH) domain, which allows interaction with phospholipids in the membrane, ensuring co-localization of the IR and its downstream targets (62). There are at least five known IRS proteins, although the role of IRS1 and IRS2 is best described (65). After phosphorylation, IRS proteins serve as docking platforms for proteins containing a Rous sarcoma virus (Src)-homology (SH) 2 domain, for example growth factor receptor-bound protein (Grb), the SH2 domain containing protein tyrosine phosphatase 2 (Shp2), and importantly, the regulatory subunit p85 of PI3K (66-68). While Grb subsequently mediates activation of the mitogen activated protein kinase (MAPK) pathway which regulates cell growth and mitosis (69), PI3K activation mediates the majority of insulin's effects on glucose and lipid metabolism (68, 70, 71). Activity of the catalytic

subunit p110 is inhibited by the regulatory subunit p85, until p85 binds to phosphorylated tyrosine residues of IRS protein by its SH2 domain (68, 70). This leads to conformational changes, allowing activation of the p110 subunit. Subsequently, PI3K mediates the conversion of the membrane lipid phosphatidyl-inositol-4,5-bisphosphate (PIP₂) to phosphatidyl-inositol-3,4,5-trisphosphate (PIP₃) (68). Accumulation of PIP₃ in the plasma membrane leads to recruitment of 3-phosphoinositide-dependent protein kinase (PDK) 1, which binds to PIP₃ by its PH domain (72). PDK1 phosphorylates protein kinase B (PKB, also known as AKT) isoforms, which regulates the activation of downstream targets such as glycogen-synthase-kinase (GSK) 3, tuberin, S6 and mouse double minute (mdm) 2, which are themselves crucial regulators of glycogen synthesis, translation and cell survival, respectively (72-76).

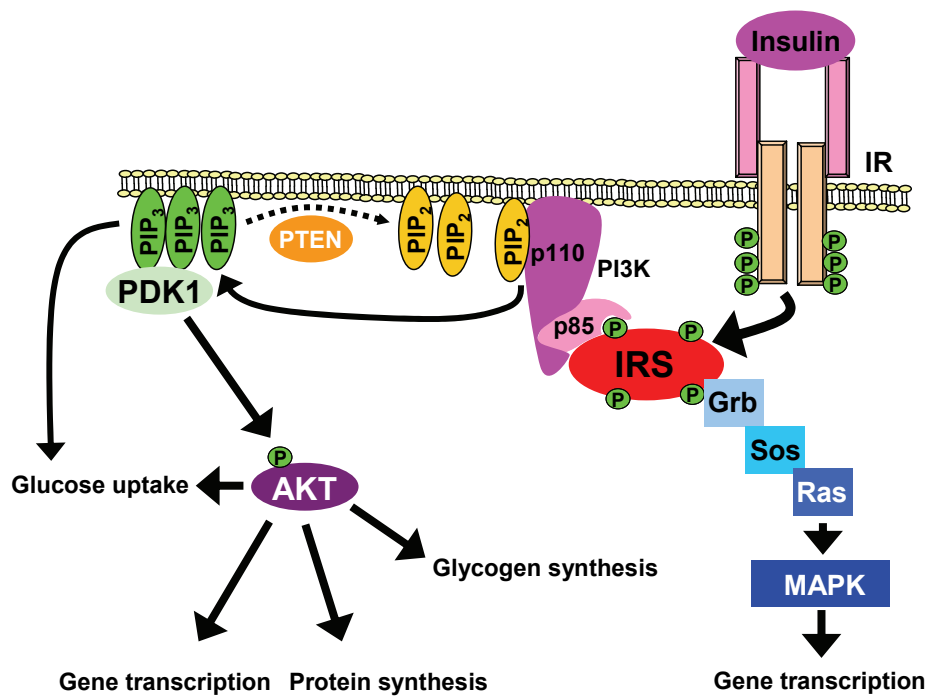


Figure 2: Canonical insulin signalling.

Binding of insulin leads to a conformational change of the IR, ending in activation of the endogenous kinase ability. After autophosphorylation of the IR, IRS proteins bind to the phosphorylated residues by their SH2 domains, and are themselves phosphorylated by the IR. Grb binds via its SH2 domain, eliciting activation of the Ras-Raf-MAPK signalling pathway, which mediates some of insulin's effects on growth. Phosphorylation of IRS proteins allows binding of p85, the regulatory subunit of the PI3K complex. This de-inhibits p110, the catalytic subunit of PI3K, which subsequently phosphorylates the membrane lipid PIP₂ to generate PIP₃. PIP₃ accumulation in turn will recruit and allow binding of both PDK1 and AKT via their PH domains. After co-localisation induced by PIP₃ binding, PDK1 phosphorylates and thereby activates AKT, which mediates most of insulin's effect on glucose and glycogen metabolism, as well as activating protein translation and gene transcription. Grb, growth factor bound; IR, insulin receptor; IRS, insulin receptor substrate; MAPK, mitogen-activated protein kinase; P, activating phosphorylation at threonine or tyrosine residues; PDK1, 3-phosphoinositide-dependent protein kinase 1; PI3K, phosphatidylinositol-3-kinase; PIP₂, phosphatidyl-inositol-4,5-bisphosphate; PIP₃, phosphatidylinositol-3,4,5-triphosphate; Ras, Rat sarcoma protein; Sos, son of sevenless.

Besides the important role in activation of AKT, PDK1 has been shown to be essential for maturation and activation of several kinases, including protein kinase C (PKC) isoforms (72, 77). The crucial role for PDK1 in development and cell cycle control is highlighted by the finding that unlike mice null for any one of the AKT isoforms, PDK1 null mice are embryonic lethal (78-81).

Insulin signalling plays a critical role for glucose and lipid dispersal into adipose tissue and skeletal muscle. In white adipose tissue (WAT) and muscle, insulin stimulates translocation and merge of vesicles containing GLUT4 with the plasma membrane, and increases expression of GLUT1 expression in WAT (58, 82). Insulin has a very prominent anti-lipolytic effect; it decreases activity of hormone sensitive lipase (HSL) and expression of adipocyte triglyceride lipase (ATGL) in WAT (83, 84). In parallel to this anti-lipolytic effect, insulin increases expression of key regulators of lipogenesis and lipid uptake, such as fatty acid synthase (FAS), and lipoprotein lipase (LPL) (85, 86).

Besides increasing glucose uptake, insulin also stimulates muscle glycogen synthesis, protein synthesis, and inhibits protein breakdown, which is in line with its potent anabolic effect on muscle mass (73, 74, 87).

The transcription factor forkhead box 01 (FOXO1) is a key target of insulin signalling (88). FOXO1 directly controls hepatic expression of genes important for gluconeogenesis, such as glucose-6-phosphatase (G6P) and phosphoenolpyruvate carboxykinase (PEPCK) (89-92). Besides glucose homeostasis, FOXOs modulate expression of genes involved in apoptosis, cell cycle progression, oxidative stress response, and DNA repair (88). In line with a conserved role of FOXO1, forkhead transcription factors were originally found in *Drosophila melanogaster*, and homologues also exist in *Caenorhabditis elegans* (93-95). In all of these animals as well as in humans, insulin or insulin-like peptides regulate forkhead/FOXO localisation by phosphorylation, inducing nuclear export of these proteins (88, 93, 94). Interestingly, FOXO homologues also regulate life span in invertebrates (94, 96). Here, FOXO homologues induce a transcriptional program which limits growth, increases life span and oxidative stress resistance (88). In turn, it has been shown that multiple stressors such as starvation activate stress kinases, e.g. JNKs, which positively modulate FOXO function by assuring nuclear localisation (88, 97, 98). Importantly, it has been reported, that FOXO1 signalling in mice is also important for control of energy homeostasis (see below).

1.7 The brain as a regulator of energy homeostasis

Each physiological activity is directly or indirectly controlled by neuronal circuits. Experiments including retrograde tracers studies have demonstrated, that organs involved in

regulation of energy homeostasis, such as liver, muscle, adipose tissue, gut or the pancreas, are under direct control of the central nervous system (CNS) (99-104). Since the advent of the obesity and diabetes pandemic, considerable efforts are underway to understand where homeostatic signals such as leptin or insulin act in the CNS to influence feeding behaviour and glucose metabolism. Extensive experimental evidence points to a crucial role for the hypothalamus in regulation of energy homeostasis (30, 32, 105). Additionally, neurons in other brain centers (and neuropeptides/neurotransmitters expressed therein) such as in the ventral tegmental area (dopamine) or the raphe nucleus (serotonin) regulate feeding and feeding-related behaviour, such as foraging or the rewarding effects of food (106-110). It should be noted that all of these neuronal circuits are not isolated from each other, but instead are connected by direct synaptic input or via inter-neurons (111-114).

1.8 The hypothalamus as a regulator of energy homeostasis

The finding that neuronal populations located in the hypothalamus regulate food intake and energy expenditure stems from historical experiments, in which different hypothalamic nuclei were disrupted by chemical agents or mechanical destruction (115). Besides introduction of lesions, the effect of electrical stimulation in different hypothalamic nuclei was also studied in animal models (116, 117). These studies defined the lateral hypothalamus as a “hunger center” and the ventromedial hypothalamus as a “satiety center”, since stimulation of the first increases and of the latter decreases food intake (118-120). In addition to regulation of body weight, lesion experiments in rabbits demonstrated that the hypothalamus also controls blood glucose levels (121). Nonetheless, it has been noted that in these experiments, during the introduction of the chemicals or electrodes into the hypothalamus, brain regions located above the hypothalamus may be damaged, chemicals may diffuse into other brain nuclei, and cell types apart from neurons are potentially affected (122).

Although it was then noted that hypothalamic neurons are regulators of feeding, the exact efferent and afferent signals to peripheral tissues were still unknown. Following cloning of leptin and its receptor, it was established that the hypothalamus shows very high levels of ObRb expression (123, 124), and the same is true for insulin receptor mRNA (125, 126). In line with this, application of leptin, insulin or insulin mimetics into the hypothalamus or intracerebroventricular (icv) injection into the adjacent third ventricle acutely reduced food intake and body weight, whereas ablation of the leptin or insulin receptor in this region

increased body weight (46, 127-129). Henceforth, it was attempted to identify the neuron population(s) involved in mediating insulin's and leptin's effect on energy homeostasis.

The hypothalamus consists of several nuclei, including the arcuate nucleus (Arc), the ventromedial nucleus of the hypothalamus (VMH), the dorsomedial nucleus (DMH), and the paraventricular nucleus (PVN). The Arc located next to the third ventricle is privileged among these nuclei due to its close contact with the median eminence, a site characterized by an incomplete blood brain barrier (BBB) (130). Thus, this location allows neurons to sense acute fluctuations of hormones or other signals in the blood. Accordingly, peripheral injection of hormones induces rapid (<10 minutes) activation of their signalling cascades in the Arc.

Possibly the most extensively studied neuronal populations in the Arc are the proopiomelanocortin (POMC) and agouti-related protein (AgRP) / neuropeptide Y (NPY) expressing neurons. Several human patients have been found to have mutations in the POMC gene, which inhibit normal expression or processing of the preproprotein (131-133). These patients suffer from massive early-onset obesity. Conventional POMC knockout mice demonstrated the same phenotype, which suggested a conserved role in control of energy homeostasis both in animal models and humans (132-135). In the hypothalamus, POMC is expressed in ~3000 neurons in the Arc (with very few in the PVN), which are consequently called POMC neurons. In these neurons, the POMC pro-protein is cleaved to generate the neuropeptide alpha-melanocyte stimulating hormone (α -MSH), which after secretion binds to and activates the melanocortin receptor 4 (MC4R), which is expressed on secondary neuronal populations, located in the PVN of the hypothalamus, among other nuclei (136, 137). Thus, electrical stimulation leads to membrane depolarisation of POMC neurons, α -MSH release, MC4R activation and ultimately decreases food intake and increases energy expenditure. In line with these findings, mutations in all proteins involved in processing, release or signalling of the so-called melanocortin pathway have been found in humans, which usually lead to early-onset obesity (138-140). However, both the downstream pathways and the nature of the MC4R expressing neurons are only incompletely understood.

POMC is also expressed in two cell types of the pituitary, namely corticotrophs and melanotrophs. Upon stress stimuli, PVN neurons release corticotrophin releasing hormone (CRH) onto pituitary corticotrophs, which produce and secrete the POMC cleavage product adrenocorticotrophic hormone (ACTH). ACTH stimulates release of glucocorticoids, i.e. corticosterone (in rodents) or cortisol (in humans) by the adrenal gland (141-143). Glucocorticoids have profound effects on physiological circuits which include antagonistic effects on insulin signalling and immune cell function. Importantly, glucocorticoids are

necessary to prevent exaggerated stress response (144). In turn, human patients (and mice) without circulating glucocorticoids will die from extreme stressors such as surgery (144).

Melanotroph-released α -MSH modulates hair and skin pigmentation (145). Since POMC null mice show only very faint changes in skin color, the relative importance of melanocortins in mice with regard to pigmentation appears to be smaller compared to the situation in humans (134).

In contrast to the anorexigenic effect of melanocortin neuropeptides, NPY and AgRP release by AgRP/NPY neurons procure orexigenic effects. As the name suggests, these neurons co-express AgRP/NPY and are located in close vicinity to POMC neurons in the Arc (146). While NPY binds to one of five different receptors on target neurons and thus can indirectly counteract the anorexigenic action of leptin or insulin, AgRP as an inverted agonist directly blocks α -MSH mediated activation of the MC4R, thus inhibiting α -MSH action (147, 148). Supporting the critical role of AgRP/NPY on food intake, acute ablation of AgRP/NPY neurons in adult mice leads to starvation (149, 150). Many hormones implicated in control of energy homeostasis such as leptin and insulin have been shown to affect POMC and AgRP neuron function, for example by modulating POMC/AgRP mRNA expression or POMC/AgRP neuron excitability (48, 151-154).

1.9 Leptin, insulin and the melanocortin circuit

In 1979, Woods and colleagues demonstrated insulin's ability to decrease food intake and body weight in baboons when injected icv, and 21 years later mice lacking insulin receptors only in the central nervous system were found to develop diet-sensitive obesity (56, 155). When it was demonstrated that insulin's ability to decrease food intake was dependent on the melanocortin system, attention was directed to the molecular underpinnings of insulin's regulation of neurons and neuropeptides in the melanocortin circuit (156). Icv injection of insulin increases POMC mRNA expression levels in fasted animals, while mice lacking IRS2 show a decrease in hypothalamic POMC expression (156-158). Moreover, insulin negatively modulates NPY mRNA expression (159). In line with these findings, insulin activates PI3K signalling in identified POMC and AgRP neurons (154). Kitamura and colleagues suggested, that FOXO1 is a negative regulator of POMC and a positive regulator of AgRP expression, and that PI3K activation led to FOXO1 phosphorylation and nuclear export, therefore allowing POMC transcription to take place and blocking AgRP expression *in vitro* (42). Another group independently presented the same results, but also provided evidence for a modulating role of FOXO1 in expression of NPY (50). Additionally, it has

been reported that FOXO1 negatively regulates the expression of Carboxypeptidase E (CPE), which is involved in POMC cleavage into α -MSH (160). Nonetheless, most of these findings were based on either short-term studies following icv injections, or on cell line-based *in vitro* experiments.

Könner and colleagues therefore decided to ablate the insulin receptor in POMC (denoted as IR ^{Δ POMC} mice) or AgRP neurons (IR ^{Δ AgRP} mice) using the Cre/loxP system. Interestingly, mice lacking IR on POMC or on AgRP neurons did not show differences in body weight, food intake, leptin levels, hypothalamic POMC mRNA expression or glucose tolerance, possibly due to compensation for the lack of insulin input by unknown mechanisms (151). On the other hand, the authors demonstrated an important role for IR signalling in AgRP neurons in control of glucose metabolism, since IR ^{Δ AgRP} mice showed incomplete suppression of HGP under hyperinsulinemic conditions (151). This effect was not detected in glucose tolerance tests because of compensation by an increase in adipose tissue glucose uptake (151). The considerable effect of hypothalamic insulin action on hepatic glucose output and peripheral glucose uptake has been independently demonstrated several times, although species differences concerning direct hepatic effects and indirect CNS effects of insulin on glucose production might exist (161-166).

Plum and colleagues decided to further examine the role of insulin-activated, PI3K-mediated signalling by generating mice lacking the negative regulator of PI3K signalling, the phosphatase and tensin homologue (PTEN) in POMC neurons (PTEN ^{Δ POMC} mice). PTEN dephosphorylates PIP3 to generate PIP2 (167). These mice demonstrated increased PIP3 levels in identified POMC neurons, even under conditions of starvation when circulating insulin concentration was low (168). In line with previous results which suggested PI3K signalling in control of POMC expression, POMC mRNA levels were increased in young PTEN ^{Δ POMC} mice (168). Surprisingly, these mice unexpectedly developed sex-dimorphic, diet-dependent obesity (168). Further analysis revealed that POMC neurons from PTEN ^{Δ POMC} mice were electrically silent, which was due to potassium outflow mediated by KATP channels (168). Previously, it had been shown that these KATP channels are sensitive to adjacent PIP2/PIP3 concentrations, with PIP3 increasing the probability of KATP channels to open (169, 170). The physiologic role of insulin in KATP channel opening was further demonstrated by insulin's ability to hyperpolarize POMC neurons *ex vivo* (168). This effect is not specific to POMC neurons, as AgRP neurons and neuronal cell lines also show hyperpolarisation after insulin stimulation (47, 151). Therefore, it was deduced that chronic, high level insulin stimulation might lead to hyperpolarisation and electrical silencing of both

POMC and AgRP neurons, which challenged the role of these two neuron populations in control of energy homeostasis (105, 171). Taken together, although the effect of chronic high levels of PI3K activation has thus been studied in a mouse model, the contribution of signalling components acting downstream of PI3K, e.g. PDK1 has not been analysed.

Concurrent with the finding that insulin stimulation leads to nuclear export of FOXO1, leptin stimulation was found to increase STAT3 localisation on the POMC promoter, and FOXO1 and STAT3 were found to compete for binding on adjacent sites on the POMC promoter (42, 50). The physiologically relevant role of leptin signalling on POMC, AgRP and NPY expression is well established (48, 152, 172). Interestingly, leptin's ability to regulate energy homeostasis was shown to be dependent on CNS PI3K signalling, and leptin has been shown to be able to activate neuronal PI3K signalling (47, 129, 173).

Experiments on leptin's effect on electrical activity have led to conflicting results. Leptin was originally shown to induce POMC firing, whereas others have found no effect or inhibition of leptin on neuronal firing (47, 49, 173-175). Adding to the confusion, it was demonstrated that leptin's ability to increase firing of POMC neurons was dependent on PI3K signalling (173). It is unknown how activation of the same signalling pathway (PI3K) either leads to hyperpolarisation (KATP channel activation, by insulin) or depolarisation (channel(s) unknown, by leptin), although magnitude or duration of PI3K stimulation might play into this phenomenon (105). Nonetheless, insulin's ability to hyperpolarise POMC neurons appears to be specific to the postnatal adolescent period in mice, since insulin-induced hyperpolarisation cannot be detected in POMC neurons of adult mice (A. Husch & P. Kloppenburg, unpublished observation). Since virtually all electrophysiological experiments so far have been performed on brain slices derived from mice before the time of weaning, the effect of leptin and insulin on neuronal excitation in adult mice remains unresolved (105).

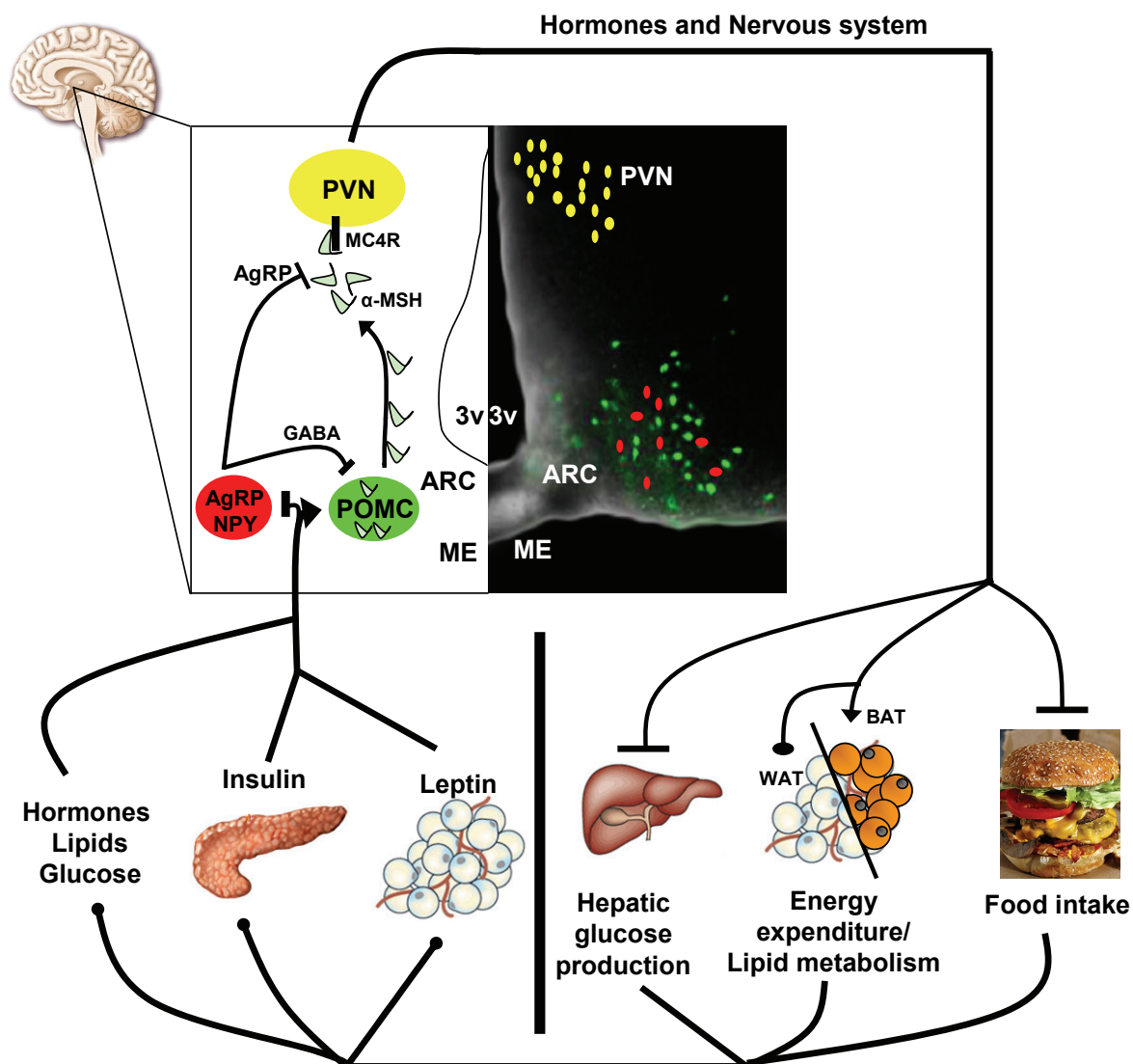


Figure 3: The melanocortin system regulates energy homeostasis.

Adiposity signals such as insulin and leptin signal to proopiomelanocortin neurons in the arcuate nucleus of the hypothalamus to enhance expression of POMC and/or induce release of α -MSH onto second-order neurons, some of which are located in the PVN. α -MSH binds to and activates these neurons via its receptor MC4R. At the same time, activation of orexigenic neurons such as AgRP/NPY neurons is inhibited. This de-inhibits POMC neurons by a reduction of inhibitory GABAergic input by AgRP/NPY neurons. Hormone and nerve outflow of circuits activated by PVN neurons and other second-order neurons inhibits hepatic glucose production, increases energy expenditure in BAT, reduces food intake and modulates lipid metabolism in WAT. This leads to fat mass loss, which subsequently affects circulating concentrations of the adiposity signals. 3v, third ventricle; α -MSH, α -melanocyte stimulating hormone; AgRP, agouti-related protein; ARC, arcuate nucleus of the hypothalamus; BAT, brown adipose tissue; GABA, γ -aminobutyric acid; MC4R, melanocortin receptor 4; ME, median eminence; NPY, neuropeptide Y; POMC, proopiomelanocortin; PVN, paraventricular nucleus of the hypothalamus; WAT, white adipose tissue. Green, POMC neurons; red, AgRP/NPY neurons; yellow, PVN neurons.

1.10 Lipid-induced insulin and leptin resistance

During analysis of leptin's and insulin's role in control of neuronal excitation and expression of neuropeptides, it has become clear that during conditions of high-energy

feeding such as high-fat diet, both signalling cascades show decreased efficacy. Hence, high-fat feeding for five days leads to a decrease in hypothalamic phospho-STAT3 immunoreactivity after leptin stimulation (176). In line with this, chronic leptin signalling has been shown to induce high levels of SOCS3 expression, which will further exacerbate leptin resistance (177, 178). Elevated expression of the phosphatase PTP-1B by high-fat feeding have also been implicated in inducing leptin and insulin resistance (179, 180). Although there is currently no pharmacological agent known to act as an leptin sensitiser, experimental evidence ascribes a high lipid-containing diet to cause CNS leptin and insulin resistance, and in turn, a reduction in dietary lipid content is thought to be beneficial for leptin and insulin sensitivity in the CNS (181-184). Here, especially saturated fatty acids such as palmitate may activate several signalling cascades to reduce leptin and insulin signalling. Several isoforms of protein kinase C (PKC) have been shown to negatively modulate insulin sensitivity, which are directly activated by diacylglycerols, and hypothalamic diacylglycerol concentration is aggravated by a high-fat diet (182, 185). Besides PKC activation, the ability of fatty acids to induce leptin and insulin resistance in the CNS and the periphery has been shown to be mediated by toll-like receptor (TLR) 2 and 4 signalling. Fatty acids are thought to bind to TLRs, although an indirect activation has also been described (186, 187). The evolutionary conserved role of TLRs is the recognition of pathogen-associated molecular patterns (PAMPS) such as bacterial lipopolysaccharides, and thus TLRs are crucial sensors of the innate immune system (188, 189). Mice with loss-of-function mutations in TLR4 have been shown to be protected from diet-induced glucose intolerance, and although protection from diet-induced obesity has also been reported, some find increased obesity (190-195). Of note, activation of TLRs will lead to activation of nuclear factor κ -light chain enhancer of B cells (NF κ B) as well as c-Jun N-terminal kinase (JNK) signalling (192, 194, 195).

1.11 The role of NF κ B and JNK signalling in energy homeostasis

The transcription factor NF κ B plays an integral part in cells of the immune system (196). Consisting of two subunits, the NF κ B complex is bound to the inhibitor of NF κ B (I κ B) and thus sequestered in the cytoplasm. Upon divergent stimuli such as cytokines, foreign substances or UV irradiation, I κ B is phosphorylated by the I κ B kinase (IKK) complex, which subsequently leads to degradation of I κ B. The NF κ B complex will now translocate to the nucleus, where it regulates transcription of hundreds of genes (196). Under obese conditions, NF κ B signalling is mildly, but chronically activated (197, 198). IKK signalling can induce insulin resistance by serine phosphorylation of IRS proteins, but NF κ B activation will also

lead to increased production of cytokines such as tumor necrosis factor (TNF) α (197). In line with this, mice with increased activation of NF κ B signalling in the liver develop glucose intolerance and insulin resistance (197). Importantly, NF κ B signalling in the hypothalamus is a negative regulator of insulin and leptin sensitivity, partially by inducing SOCS-3 expression (184, 198).

Besides NF κ B signalling, the JNK signalling cascade has been shown to be activated by diet-induced obesity (199). There are three known JNK homologues, denominated JNK1, JNK2 and JNK3 (200). Whereas JNK1 and JNK2 are ubiquitously expressed, JNK3 is most abundant in the brain and less in peripheral tissues (200). JNKs are able to regulate transcription, survival, apoptosis and other cellular events in response to diverse stimuli such as UV irradiation or cytokine stimulation (200). Interestingly, JNK1 plays a role in obesity-associated pathologies, since conventional JNK1 but not JNK2 knockout mice are protected from obesity-induced hyperglycemia, hyperinsulinemia and insulin resistance (199). In this context, insulin resistance is caused by JNK1-mediated phosphorylation of specific serine residues of IRS proteins (199, 201). These inhibitory phosphorylation events block recruitment of IRS proteins to the insulin receptor and thereby activation of downstream signalling, causing insulin resistance (202, 203). In addition to protection against diet-induced obesity, several physiologic processes are altered in JNK1 null mice, including bone remodelling and breeding efficiency, and the outward phenotype of JNK1 mice is likely a combination of all of these phenotypes, with most of them unexplored yet (200, 204)

Several groups have aimed to define the peripheral tissues in which JNK1 ablation is crucial for the protection from high-fat diet (HFD)-mediated impairment of glucose metabolism. Recently, mice with JNK1 ablation in the hematopoietic compartment were shown to be resistant to diet-induced insulin resistance due to reduced inflammation (205). In contrast, other investigators could not find any improvement in systemic glucose homeostasis in mice with JNK1 ablation in the hematopoietic compartment or specifically in the myeloid lineage (206, 207). Strikingly, fat cell-specific disruption of JNK1 provided evidence for a crucial role of adipose tissue JNK1 in systemic glucose metabolism (207). In the light of these findings, a role for JNK1 signalling in not yet defined tissues in control of glucose homeostasis seems likely, as neither adipose tissue nor myeloid cell-specific JNK1-deficient mice exhibit a phenotype comparable to conventional JNK1 knockout mice.

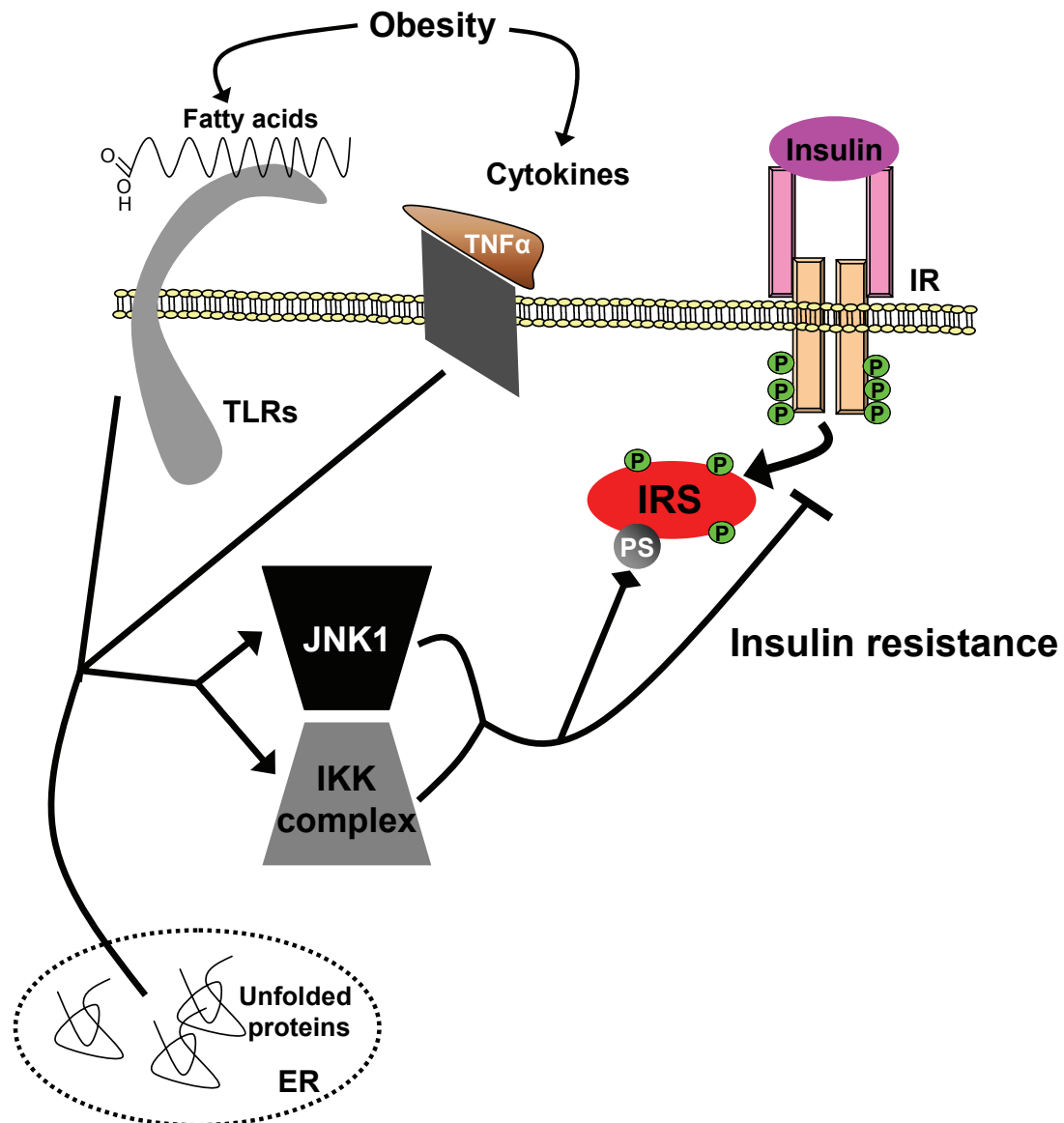


Figure 4: Multiple pathomechanisms of insulin resistance.

Obesity induces hyperlipidemia and chronic, low-level inflammation. This leads to fatty acid-mediated activation of TLRs and activates cytokine signalling. In addition, overabundance of lipids and glucose as well as the physiologic response to obesity will increase protein synthesis. When the folding capacity of the ER is surpassed, unfolded proteins will aggregate, thereby inducing ER stress. These stress response pathways eventually lead to activation of JNK1 and IKK signalling, which act as stress sensors. Both JNK and IKK have been shown to phosphorylate serine residues on IRS proteins, blocking IR/IRS binding and downstream signalling, thus inducing insulin resistance. ER, endoplasmic reticulum; IKK, I κ B kinase; IR, insulin receptor; IRS, insulin receptor substrate; JNK1, c-Jun n-terminal kinase 1; TLR, toll-like receptor; $\text{TNF}\alpha$, tumor necrosis factor α .

1.12 Central and peripheral inflammation and energy homeostasis

Obesity induces a chronic, low-grade state of inflammation both in animal models and in human patients. Levels of cytokines such as TNF α , interleukin (IL) 6, or acute phase proteins such as C-reactive protein (CRP) are increased in the circulation of obese rodents and humans (202, 203, 208). WAT and WAT-invading immune cells such as macrophages have been shown to be responsible for this low-grade inflammation (203, 208). It is thought that at a certain stage during obesity, adipocytes are overloaded with lipids, and activate programmed cell death (apoptosis). This attracts circulating macrophages into WAT, which can be visualised as so-called crown-like structures in adipose tissue biopsies (209). These activated macrophages are distinct from resident macrophages, as indicated by a more pro-inflammatory expression pattern (210). Cytokine signalling has been shown to induce insulin resistance in tissues crucial for energy homeostasis such as liver and adipose tissue, resulting in hyperglycemia and hyperlipidemia, which in a feed-forward loop can induce expression of pro-inflammatory cytokines (211, 212).

Cytokines can pass the BBB (213). Moreover, certain brain nuclei such as the Arc lack a dense blood brain barrier, which might imply that circulating cytokines engage pro-inflammatory signalling in these regions (130). Therefore, it has been investigated if increased inflammatory signalling can be detected in hypothalamic tissue from obese animal models. These experiments have shown that hypothalamic pro-inflammatory cytokine content is increased in diet-induced obesity, although it was not determined if these cytokines are produced in an endocrine or paracrine fashion or both (214). In line with this, NF κ B signalling is increased in the hypothalamus of diet-induced obese mice, and ablation of IKK2 ameliorates diet-induced obesity (184, 198). Nonetheless, it has not been reported if local expression of pro-inflammatory cytokines is increased, for example by microglia, resident immune cells akin to macrophages (215).

Analysis of the effects of centrally applied TNF α on energy homeostasis has shown conflicting results; whereas some investigators find an anorexigenic effect, some do not (216, 217). It has been noted that during infection, TNF α levels rise by several magnitudes, and that this increase might signal in unknown brain regions to induce infection-associated anorexia (216-218).

The role of IL6 in control of energy homeostasis appears to be highly complex. Several groups have reported that IL6, which is released by macrophages/microglia, adipocytes, during/after physical activity by muscle tissue, and at very low levels by neurons, induces hepatic insulin resistance *in vivo* and *in vitro*, while others report a crucial role for

hepatic IL6 signalling in improving whole body glucose dispersal (151, 219, 220). Nonetheless, conventional IL6 knockout mice show adult-onset obesity, which might indicate a role for IL6 in central regulation of body weight control, although CNS-specific IL6 or IL6-receptor knockout mice have not been generated yet (221).

1.13 ER stress and energy homeostasis

Hotamisligil and colleagues first reported that obesity induces hepatic ER stress (222). During normal cellular function, protein folding in the endoplasmic reticulum is assisted by chaperones such as glucose-regulated protein (Grp) 78 (223). Under conditions of cellular stress, the amount of misfolded and unfolded proteins in the ER rises, which activates the unfolded protein response (UPR), an indicator of ER stress (224, 225). At least three different signalling pathways are activated by ER stress: the Protein kinase-like Endoplasmic Reticulum Kinase (PERK), the endoribunuclease/kinase inositol-requiring (IRE) 1 α , and the activating transcription factor (ATF) 6 (226). Under normal conditions, these sensors are located in the ER membrane and held in an inactive state by bound chaperones. When unfolded proteins aggregate in the ER, the chaperones are sequestered into the ER lumen, which allows activation of the ER stress sensors. Activation of the UPR signalling pathways leads to a reduction in total protein translation, and transcription factors such as C/EBP-homologous protein (CHOP) and x-box binding protein (XBP) 1 are activated, which increase expression of chaperones and enzymes required for protein folding (227). If ER stress persists, the UPR can induce apoptosis (227). ER stress can be caused by viral infections, protein misfolding diseases such as Huntingtons, toxic chemical agents, and as previously mentioned, by obesity (203). Mechanical insight into how obesity induces ER stress is limited, although oversupply of amino acids, glucose and lipids as well as hyperinsulinemia are known to stimulate transcription and translation, which might overwhelm the protein folding capacity of the ER (228-230). Tissues such as liver, pancreas and WAT, which are crucial for lipid and glucose metabolism and are directly affected by rising glucose and lipid levels, have repeatedly been shown to show high levels of ER stress under obese conditions (202, 203, 223). Importantly, hepatic ER stress was shown to induce insulin resistance by activation of JNK and NF κ B signalling (201, 203, 223, 231, 232).

Ozcan and colleagues reported, that partial ablation of neuronal UPR signalling cascades leads to severe leptin resistance and in turn, icv injection of chemical chaperones ameliorates diet-induced obesity (233). In line with this, NF κ B signalling is activated by neuronal ER stress, whereas ablation of NF κ B signalling also reduces neuronal ER stress by

unknown mechanisms (184). Taken together, neuronal ER stress induces insulin and leptin resistance, although the specific signalling cascades both upstream as well as downstream of ER stress in the CNS are poorly understood.

1.14 Objectives

The first aim of this study was to analyse the role of PI3K downstream signalling in a defined neuronal population critical for energy homeostasis (POMC neurons) under both ND and HFD conditions. The second aim of this study was to understand the role of inflammatory mediators such as cytokines and lipids partially acting through the stress kinase JNK1 on PI3K signalling in the hypothalamus as well as on a pan-neuronal level.

Besides wild type C57BL/6 mice, the following mutant mouse models were used in this study:

- Mice with POMC cell-specific PDK1 deletion
- Mice with POMC cell-specific PDK1 deletion and overexpression of FOXO1^{Δ256}
- Mice with Nestin cell-specific JNK1 deletion

2 Materials and Methods

2.1 Chemicals and Biologicals

Size markers for agarose gel electrophoresis (Gene Ruler DNA ladder mix) and for SDS-PAGE (Prestained protein ladder Mix) were purchased from Fermentas, St. Leon-Rot, Germany. For polymerase chain reactions, RedTaq polymerase (Sigma-Aldrich, Seelze, Germany) or DreamTaq (Fermentas, St. Leon-Rot, Germany) were used. Chemicals and enzymes used in this work are listed in Table 1 and 2, respectively.

Table 1: Chemicals

β -Mercaptoethanol (β -M)	AppliChem, Darmstadt, Germany
ϵ -aminocaproic acid	Sigma-Aldrich, Seelze, Germany
0.9% saline, sterile	Delta Select, Pfullingen, Germany
2,2,2-Tribromethanol (Avertin)	Sigma-Aldrich, Seelze, Germany
Acrylamide	Roth, Karlsruhe, Germany
Agarose (Ultra Pure)	Invitrogen, Karlsruhe, Germany
Ammoniumpersulfat	Sigma-Aldrich, Seelze, Germany
Aprotinin	Sigma-Aldrich, Seelze, Germany
Avidin Biotin Complex – Vectastain Elite	Vector, Burlingame, USA
Bacillol	Bode Chemie, Hamburg, Germany
Benzamidine	Sigma-Aldrich, Seelze, Germany
Bovine serum albumin (BSA)	Sigma-Aldrich, Seelze, Germany
Bromphenol blue	Marck, Darmstadt, Germany
Calcium chloride	Merck, Darmstadt, Germany
Chloroform	Merck, Darmstadt, Germany
Diaminobenzidin (DAB)	Dako, Denmark
Dimethylsulfoxide (DMSO)	Merck, Darmstadt, Germany
di-Natriumhydrogenphosphat	Merck, Darmstadt, Germany
Enhanced chemiluminescence (ECL) kit	Perbio Science, Bonn, Germany
Ethanol, absolute	Appllichem, Darmstadt, Germany
Ethidium bromide	Sigma-Aldrich, Seelze, Germany

Ethylendiamide tetracetate (EDTA)	Applichem, Darmstadt, Germany
Forene (Isoflurane)	Abbot GmbH, Wiesbaden, Germany
Glucose 20%, sterile	DeltaSelect, Pfullingen, Germany
Glycerol	Serva, Heidelberg, Germany
HEPES	Applichem, Darmstadt, Germany
Hydrochlorid acid (37%)	KMF Laborchemie, Lohmar, Germany
Hydrogen peroxide	Sigma-Aldrich, Seelze, Germany
Insulin (human)	Novo Nordisk, Basvaerd, Denmark
Insulin (porcine)	Sigma-Aldrich, Seelze, Germany
Isopropanol	Roth, Karlsruhe, Germany
Kaisers Glycerin Gelatine	Merck, Darmstadt, Germany
Magnesium chloride	Merck, Darmstadt, Germany
Methanol	Roth, Karlsruhe, Germany
Nitrogen (liquid)	Linde, Pullach, Germany
Octenisept	Schülke & Mayr, Norderstedt, Germany
Paraformaldehyde (PFA)	Fluka, Sigma-Aldrich, Seelze, Germany
Phenylmethylsulfonylfluoride (PMSF)	Sigma-Aldrich, Seelze, Germany
Phosphate buffered saline (PBS)	Gibco, Eggenstein, Germany
Potassium hydroxide	Merck, Darmstadt, Germany
Sodium chloride	Applichem, Darmstadt, Germany
Sodium dodecyl sulfate (SDS)	Applichem, Darmstadt, Germany
Sodium fluoride	Merck, Darmstadt, Germany
Sodium hydroxide	Applichem, Darmstadt, Germany
Sodium orthovanadate	Sigma-Aldrich, Seelze, Germany
Sodium pyruvate (cell culture tested)	Sigma-Aldrich, Seelze, Germany
Tetramethylethylenediamine (TEMED)	Sigma-Aldrich, Seelze, Germany
Tissue freezing medium	Jung, Heidelberg, Germany
Tramadolhydrochlorid (Tramal)	Grünenthal, Aachen, Germany
Trishydroxymethylaminomethane (Tris)	AppliChem, Darmstadt, Germany
Triton X-100	Applichem, Darmstadt, Germany
Vectashield Mounting Medium with DAPI	Vector, Burlingame, USA
Western Blocking Reagent	Roche, Mannheim, Germany
Zinc sulphate	Fluka, Sigma-Aldrich, Seelze, Germany

Table 2: Enzymes

DNase, RNase-free	Promega, Madison, WI, USA
Euroscript Reverse Transcriptase	Eurogentec, Seraing, Belgium
Proteinase K	Roche, Basel, Switzerland
RedTaq DNA Polymerase	Sigma-Aldrich, Seelze, Germany
RNase Inhibitor	Eurogentec, Seraing, Belgium

2.2 Molecular Biology

Standard methods of molecular biology were performed according to protocols described by J. Sambrook, unless otherwise stated (234).

2.2.1 Isolation of genomic DNA

Mouse tail biopsies were digested overnight in lysis buffer (100mM Tris pH 8.5, 5mM EDTA, 0.2% (w/v) SDS, 0.2M NaCl, 500mg/ml Proteinase K) in a thermomixer (Eppendorf, Hamburg, Germany). DNA was precipitated by adding an equivalent volume of 2-Propanol (100%). After washing with 70% (v/v) ethanol and subsequent centrifugation, the DNA pellet was dried and redissolved in double distilled water (ddH₂O).

2.2.2 Quantification of nucleic acids

DNA and RNA concentrations were quantified by measuring the sample absorption at 260nm and 280nm with a NanoDrop ND-1000 UV-Vis Spectrophotometer (Peqlab, Erlangen, Germany). An optical density of 1 corresponds to approximately 50µg/ml of double stranded DNA and to 38µg/ml of RNA. A ratio greater than 2 of absorptions at 260nm (DNA/RNA) divided by the absorption at 280nm (protein) was used as an index of purity of DNA/RNA.

2.2.3 Polymerase chain reaction

PCR was used to detect loxP flanked exons and various transgenes with primers described in table 3. Reactions were performed in a Thermocycler iCycler PCR machine (BioRad, München, Germany) or in a Peltier Therman Cycler PTC-200 (MJ Research, Waltham, USA). All amplifications were performed in a total reaction volume of 30µl,

containing a minimum of 50ng template DNA, 25pmol of each primer, 25 μ M dNTP mix, polymerase buffer and 1.1 unit of polymerase. Standard PCR programs started with 5min of denaturation at 95°C, followed by 35 cycles consisting of denaturation at 95°C for 45 seconds (sec), annealing at oligonucleotide-specific temperatures for 30sec and elongation at 72°C for 30 sec, and a final elongation step at 72°C for 7min.

Table 3: Primer sequences

All primer sequences are displayed in 5'→3' order. Primer orientation is designated "sense" when coinciding with transcriptional direction. All primers were purchased from Eurogentec, Belgium.

Primer	Sequence	T _{annealing} °C	direction
POMC-Cre 1	TGGCTCAATGTCCTTCCT GG	55	sense
POMC-Cre 2	CACATAAGCTGCATCGTTAAG	55	antisense
POMC-Cre 3	CACATAAGCTGCATCGTTAAG	55	antisense
PDK1 1	ATCCCAAGTTACTGAGTTGTGTTGGAAG	55	sense
PDK1 2	TGTGGACAAACAGCAATGAACATACACGC	55	antisense
PDK1 Δ	CAGTTCATCATTGCAAGAGTC	54	sense
CAGS 1	AAAGTCGCTCTGAGTTGTTATC	55	sense
CAGS 2	GATATGAAGTACTGGGCTCTT	55	antisense
CAGS 3	TGTCGCAAATTAAGTGAATC	55	antisense
LACZ 1	ATC CTC TGC ATG GTC AGG TC	60	sense
LACZ 2	CGT GGC CTG ATT CAT TCC	60	antisense
GFP 1	CTG GTC GAG CTG GAC GGC GAC G	62	sense
GFP 2	CAG GAA CTC CAG CAG GAC CAT G	62	antisense
Nestin-Cre 1	CGC TTC CGC TGG GTC ACT GTC G	58	sense
Nestin-Cre 2	TCG TTG CAT CGA CCG GTA ATG CAG GC	58	antisense
JNK1 1	ACATGTACCATGTACTGACCTAAG	54	sense
JNK1 2	CATTACTCTA CTCACTATAG TAACA	54	antisense
JNK1 Δ	GATATCAGTA TATGTCCTTA TAG	54	antisense

2.2.4 RNA extraction, RT-PCR and Quantitative Real-Time PCR

Tissues were homogenized using an Ultra Turrax homogenizer (IKA, Staufen, Germany). RNA was extracted using the Qiagen RNeasy Kit (Qiagen, Hilden, Germany).

When exon-spanning probes were not available to quantify RNA expression of target genes, on-column DNA digestion was performed (RNAse-free DNase, Qiagen, Hilden, Germany). 200ng RNA was reverse-transcribed into cDNA using the Eurogentec RT KIT (Eurogentec, Belgium). For quantitative Real-Time PCR, 100ng cDNA was amplified using Taqman Universal PCR-mastermix, NO AmpERASE UNG with Taqman assay on demand kits (Applied Biosystems, Foster City, USA) (see Table 4) with the exception of genes for which no commercial probes were available. For these genes, custom probes were designed as depicted in Table 5. Relative expression of genes was adjusted for total RNA content by glucuronidase β (GUSB) and hypoxanthine guanine phosphoribosyl transferase (HPRT) 1 RNA quantitative Real-Time PCR. Real-Time PCR analysis was performed on an ABI-PRISM 7700 Sequence detector (Applied Biosystems, Foster City, USA). Assays were linear over 4 orders of magnitude.

Table 4: Real-Time analysis probes

POMC	Mm00435874_m1	Bax	Mm00432050_m1
CART	Mm00489086_m1	Bak	Mm00432045_m1
AgRP	Mm00475829_g1	Zac1	Mm00494250_m1
NPY	Mm00445771_m1	GHRH	Mm00439100_m1
CRH	Mm01293920_s1	Somatostatin	Mm00436671_m1
TRH	Mm01963590_s1	GHRHR	Mm01326479_m1
BDNF	Mm01334042_m1	TRHR	Mm00443262_m1
GUSB	Mm00446953_m1	PIT-1	Mm00476852_m1
HPRT	Mm03024075_m1	Orexin	Mm01185778_m1
MCH	Mm01242886_g1	LPL	Mm00434770_m1
HSL	Mm00495359_m1	UCP1	Mm00494069_m1
UCP2	Mm00627599_m1	UCP3	Mm00494077_m1
TNF α	Mm99999068_m1	IL6	Mm99999064_m1
F4/80	Mm00802530_m1	MCP1	Mm99999056_m1
MAC2	Mm00802901_m1	LysM	Mm00769128_m1
IL10	Mm00439614_m1	PPAR γ	Mm00440945_m1
JNK2	Mm00444231_m1	JNK3	Mm00436518_m1

Table 5: Custom Real-Time analysis probes

target RNA	5` primer	3` primer	probe
GH (custom)	GCCCTTGTCCAGTC TGTTTTTC	GATGGTCTCTGAGAA GCAGAAAG	GTTCGAGCGTGCCTAC ATTCC
POMC (custom)	GACACGTGGAAGA TGCCGAG	CAGCGAGAGGTCGA GTTTGC	CAACCTGCTGGCTTGC ATCCGG
JNK1 (custom)	ATTGGAGATTCTAC ATTCACAGTCCTA	CATTCTGAAATGGCC GGCT	AGTGTGTGCAGCTTAT GATGCC

2.3 Cell Biology

2.3.1 Histological analysis and immunohistochemistry

POMC-Cre^{+/-} were mated with RosaArte1 mice or Z/EG mice to generate lacZ^{ΔPOMC} and GFP^{ΔPOMC} mice which served as controls for the immunohistochemistry studies (168). PDK1^{ΔPOMC} mice were mated with RosaArte1 mice to generate lacZ:PDK1^{ΔPOMC} mice which lack PDK1 in POMC-expressing cells but in these cells express lacZ.

To determine efficiency of PDK1 ablation in PDK1^{ΔPOMC} mice, PDK1/lacZ double stainings were performed. LacZ control and lacZ KO reporter mice were perfused transcardially with physiologic saline solution, frozen in tissue freezing medium (Jung, Leica Instruments, Germany), and sectioned on a cryostat. Tissues were stained with goat anti-β-galactosidase (4600-1409, Biogenesis) and rabbit anti-PDK1 (#1624-1, Epitomics, Burlingame, CA, USA), and double-fluorescence immunostaining was performed using donkey serum for blocking (#S30, Chemicon, Temecula, CA, USA), donkey anti-goat FITC-coupled secondary antibody (#sc-2024, Santa Cruz Biotech., Santa Cruz, CA, USA) and donkey anti-rabbit secondary MFP antibody (#a2207, MoBiTec, Goettingen, Germany) as previously described (151).

For GFP stainings, mice were perfused with saline solution followed by 4% paraformaldehyde (PFA) in 0.1 M phosphate-buffered saline (PBS; pH 7.4). Hypothalami and pituitaries were dissected, postfixed in 4% PFA at 4°C, transferred to 20% sucrose for 6 hr, and frozen in tissue freezing medium. Then, 25 μm thick free-floating coronal sections were cut through the ARC using a freezing microtome (Leica, Germany). The sections were collected in PBS/azide (pH 7.4) and washed extensively to remove cryoprotectant. The

sections were stained as previously described, using rabbit anti-GFP antibody at a 1:10000 dilution (#A6455 from Invitrogen/Molecular Probes, Karlsruhe, Germany) (235).

For pituitary stainings of ACTH, GH or TSH β , sections were attained as described above, and stainings were performed using the ACTH and TSH β antibody kindly provided by A.F. Parlow from the National Hormone and Peptide Program or GH antibody (#A0570) from DAKO, USA.

Slides were viewed through a Zeiss Axioskop equipped with a Zeiss AxioCam for acquisition of digital images using Spot Advanced 3.0.3 software or through a digital camera attached to a binocular (for low magnifications). Please note that 25% less slides from 4 week old GFP reporter mice compared to 12 week old GFP reporter mice were counted, therefore absolute numbers of 4 and 12 week old mice cannot be compared.

2.4 Biochemistry

2.4.1 Enzyme-linked Immunosorbent Assay (ELISA)

Serum insulin, leptin, plasma corticosterone, growth hormone (GH), insulin-like growth factor (IGF) I, free thyroxin 3 (T3) and adiponectin were measured by ELISA using mouse standards according to the manufacturer's guidelines (Mouse Leptin ELISA, #90030, Crystal Chem., Downers Grove, IL, USA; Rat Insulin ELISA, #INSKR020, Crystal Chem., Downers Grove, IL, USA; Corticosterone EIA Kit, #900-097, Assay Designs, Ann Arbor, MI, USA; Mouse Growth hormone ELISA, #EZRMGH-45K, Millipore, St. Charles, MI, USA; Mouse IGF-1 ELISA, #MG100, R&D Systems, Minneapolis, MN, USA; free T3 ELISA, Alpha Diagnostics International. Inc, San Antonio, Texas, USA; mouse adiponectin, #MRP300, R&D Systems).

2.4.2 Protein extraction

Tissues were snap-frozen in liquid nitrogen until protein extraction. Tissues were homogenized in lysis buffer (50 mM HEPES (ph 7.4), 1% Triton X-100, 0.1 M NaF, 10 mM EDTA, 50 mM NaCl, 0.1% SDS, proteinase and phosphatase inhibitor cocktail tablets (Roche, Mannheim, Germany)). Lysates were cleared by centrifugation for 45 min at 13000rpm. Protein concentration of the resulting supernatant was analysed using a NanoDrop ND-1000 UV-Vis spectrophotometer (Peqlab, Erlangen, Germany). Protein supernatant was diluted with 4xSDS sample buffer (125 mM Tris-HCl (ph6.8), 5% SDS, 43.5% glycerol, 100

mM DTT, 0.02% bromophenol blue) to an end concentration of 10mg/ml protein. Before loading of samples onto a Western blot gel, proteins were boiled at 95°C for 5 min.

2.4.3 Western Blotting

Samples were separated on 10% (v/v) SDS polyacrylamide gels and blotted onto PVDF membranes (Bio-Rad, München, Germany). Membranes were blocked with 1% blocking reagent (Roche, Mannheim, Germany) for 1h at RT. Subsequently, primary antibodies (Table 5) diluted in 0.5% blocking reagent at a concentration of 1:1000 were applied overnight at 4°C. After 4x washing with 1% TBS-Tween (TBS-T) for 10min each, secondary antibody was applied for 1h at RT. After a repeat wash step, membranes were incubated for 1min in Pierce ECL Western Blocking Substrate (Perbio Science, Bonn, Germany) and exposed to chemiluminescence films (Amersham, Braunschweig, Germany). Films were developed in an automatic developer (Kodak, Germany).

Table 6: Western Blotting antibodies

Antibody	Catalogue #	Company
β -actin	A5441	Sigma Aldrich
PDK1	#1624-1	Epitomics, Burlingame, CA, USA
IR- β	sc-711	Santa Cruz, San Diego, CA, USA
pS473-AKT	4058	Cell Signalling
pan-AKT	9272	Cell Signalling
JNK1/3	sc-474	Santa Cruz
phospho-S63-c-jun	kit #9810	Cell Signalling

2.4.4 C-jun N-terminal kinase assay

SAPK/JNK assays were performed following the manufacturer's guidelines (#9810, Cell Signalling). Tissues were homogenized in assay buffer, incubated with c-jun fusion protein overnight and after washing, incubated with kinase buffer containing ATP. After the reaction was stopped, samples were loaded onto a 10% polyacrilamide gel. Western blots were performed using the phospho-c-jun antibody supplied in the kit. JNK assays were performed with the kind help of Dr. Jan Mauer, Institute for Genetics, University of Cologne.

2.4.5 Hepatic lipid content analysis

Samples of mouse liver tissue (50 to 150 mg, n = 4) were homogenized with the Homogenisator Precellys 24 (Peqlab, Erlangen, Germany) in 1 ml of water at 6.500 rpm for 30 sec. The protein content of the homogenate was routinely determined using bicinchoninic acid. After addition of 4 ml of methanol and 2 ml of chloroform, lipids were extracted for 24 h at 37 °C. The liquid phase was separated by filtration, and the insoluble tissue residues were further extracted for 24 h at 37 °C in 6 ml of methanol/chloroform 1:1 (v/v) and finally in 6 ml of methanol/chloroform 1:2 (v/v). The extracts were pooled, and the solvent was evaporated in a stream of nitrogen. The residues were purified using a modification of the Bligh-Dyer procedure as previously described (236). Lipids were applied to 20 × 10 cm high performance thin layer chromatography (HPTLC) Silica Gel 60 plates (Merck, Darmstadt, Germany), which were pre-washed twice with chloroform/methanol 1:1 (v/v) and air-dried for 30 min. For quantification of triacylglycerols and cholesteryl esters, each lane of the TLC plate was loaded with the equivalent of 50 µg and 1 mg wet weight of liver tissue, respectively. The TLC solvent system used was hexane/toluene 1:1 (v/v), followed by hexane/diethyl ether/glacial acetic acid 80:20:1 (v/v). For quantification of cholesterol, diacylglycerols and free fatty acids, the equivalent of 2.5 mg of liver tissue was applied to 20 × 20 cm TLC plates, which were developed in hexane/ diethyl ether/ formic acid 30:50:1 (v/v/v). For quantitative analytical TLC determination, increasing amounts of standard lipids (Sigma-Aldrich, Taufkirchen, Germany) were applied to the TLC plates in addition to the lipid samples. For detection of lipid bands, the TLC plates were sprayed with a phosphoric acid/copper sulfate reagent (15.6 g of CuSO₄(H₂O)₅ and 9.4 ml of H₃PO₄ (85 %, w/v) in 100 ml of water) and charred at 180 °C for 10 min. Lipid bands were then quantified by densitometry using the TLC-Scanner 3 (CAMAG, Berlin, Germany) at a wavelength of 595 nm. Lipid analysis was performed by and with Dr. Susanne Brodesser, CECAD, Lipidomics Facility.

2.5 Mouse experiments

General animal handling was performed as described previously (237).

2.5.1 Animal care

Care of all animals was within institutional animal care committee guidelines. All animal procedures were conducted in compliance with protocols and approved by local government authorities (Bezirksregierung Köln, Cologne, Germany) and were in accordance with NIH guidelines. Mice were housed in groups of 3–5 at 22–24°C using a 12-hour light / 12-hour dark cycle. Animals were either fed normal chow diet (Teklad Global Rodent 2018; Harlan) containing 53.5% carbohydrates, 18.5% protein, and 5.5% fat (12% of calories from fat) or a high-fat diet (HFD; C1057; Altromin) containing 32.7% carbohydrates, 20% protein, and 35.5% fat (55.2% of calories from fat). Animals had ad libitum access to water at all times, and food was only withdrawn if required for an experiment. Body weight was measured once a week; body length (naso-anal length) was measured before sacrifice. Mice were sacrificed by lethal CO₂ anaesthesia.

2.5.2 Mice

POMC-Cre mice (152) were mated with PDK1^{flΔneo/flΔneo} (80) and breeding colonies were maintained by mating male POMC-Cre-PDK1^{flΔneo/flΔneo} (PDK1^{ΔPOMC}) mice with female PDK1^{flΔneo/flΔneo} mice. PDK1^{flΔneo/flΔneo} mice were backcrossed three times onto a C57bl/6 background before crossing with POMC-Cre mice.

For analysis of the role of FOXO1-dependent signalling in POMC cells, a mouse was generated with Cre-inducible expression of a dominant-negative FOXO1 mutant protein, which lacks the transactivation and the NLS domain (FOXO1^{Δ256}) (89, 238). In this mouse line, the expression of the FOXO1^{Δ256} mutant and IRES-GFP from the ubiquitously expressed ROSA26 locus is inhibited by a loxP-site flanked Stop-cassette (238). This mouse was originally generated and kindly provided by Marianne Ernst and Dr. F. Thomas Wunderlich in the laboratory of Prof. Dr. Jens C. Brüning in the Institute for Genetics, University of Cologne, Germany (238). All FOXO1^{Δ256}:PDK1^{ΔPOMC} mice were heterozygous for the FOXO1^{Δ256} transgene (238).

Nestin-Cre mice (239) were mated with JNK1^{fl/fl} mice (generated by Dr. F. Thomas Wunderlich and Prof. Dr. Jens C. Brüning in the Institute for Genetics, University of Cologne) and breeding colonies were maintained by mating male Nestin-Cre-JNK1^{fl/fl} (JNK1^{ΔNES}) with female JNK1^{fl/fl} mice. JNK1^{fl/wt} mice were backcrossed on a C57/bl6 background for three additional times before being intercrossed to generate JNK1^{fl/fl} mice.

The backgrounds of experimental animals were unchanged throughout all experiments. Littermates were used for analysis at all times except for reporter mouse studies. Mice were genotyped by PCR using genomic DNA isolated from tail tips. Germline deletion was excluded using primers designed to detect deleted alleles in the tail tip. Additionally, tissues not expressing Cre were used to examine mRNA expression of the various loxP-flanked genes through Real-Time PCR analysis.

2.5.3 Blood collection and determination of glucose levels

Tail bleeding was performed as described before (237). Blood glucose values were determined from whole venous blood using an automatic glucose monitor (GlucoMen; A. Menarini Diagnostics, Florence, Italy). For collection of plasma, EDTA (1.6 mg/1ml serum) was added to prevent clotting. Determination of blood glucose levels and collection of blood samples from control and various conditional knockout mice were performed side-by-side in the morning to avoid intra-group deviations due to circadian variations.

2.5.4 Food intake and indirect calorimetry

Daily food intake was calculated as the average intake of chow from custom made food racks within the time stated. Mice were acclimated to the food intake settings for at least five days. Weight of the racks was determined every day. Calorimetry measurements were performed in a PhenoMaster System (TSE systems, Bad Homburg, Germany), which allows measurement of metabolic performance and activity-monitoring by an infrared light-beam frame. Mice were placed at room temperature (22 °C–24 °C) in 7.1-l chambers of the PhenoMaster open circuit calorimetry. Mice were allowed to adapt to the chambers for at least 24h. Food and water were provided *ad libitum* in the appropriate devices and measured by the build-in automated instruments. Locomotor activity and parameters of indirect calorimetry were measured for at least the following 48 hr. Presented data are average values obtained in these recordings.

2.5.5 Glucose, insulin and pyruvate tolerance test

For glucose tolerance tests (GTT), mice were fasted overnight for 16h. After determination of fasted blood glucose levels, each animal received an intraperitoneal injection of 20% glucose solution (10ml/kg body weight). Blood glucose was determined 15, 30, 60,

and 120min after injection. For insulin tolerance tests (ITT), each random fed animal received an intraperitoneal injection of 0,75U/ml insulin solution (0,75U/kg body weight) after determination of random fed blood glucose concentration. For pyruvate tolerance tests (PTT), mice were fasted for 20h, followed by i.p. injection of 2g/kg sodium pyruvate (Sigma-Aldrich) dissolved in 0.9% saline solution. Blood glucose was determined 15, 30, 60 and 120min after injection, and blood glucose concentrations relative to starting blood glucose levels were calculated.

2.5.6 Analysis of body composition

Body fat content was measured *in vivo* by nuclear magnetic resonance using a minispec mq7.5 (Bruker Optik, Ettlingen, Germany). Radiofrequency pulse sequences are transmitted into mouse tissue, which are retransmitted by hydrogen atoms in the tissue, the signals of which are detected by the minispec. Amplitude and duration of these signals are related to properties of the material.

2.5.7 Restraint stress

Mice were handled at least weekly after weaning. Before the restraint, blood was taken from the tail vein for determination of basal plasma corticosterone levels. Directly after that, mice were subjected to 60 minutes of restraint in a plastic tube with openings for air supply. Directly after the restraint, blood was collected from the tail vein into EDTA-containing tubes for determination of stressed plasma corticosterone levels (from plasma samples).

2.5.8 Intracerebroventricular indwelling catheter implantation

For icv cannula implantation, 10-week-old male C57BL/6 (Charles River Laboratories) mice were anesthetized by intraperitoneal injection of Avertin (650 mg/kg) (2,2,2-tribromoethanol; Sigma) and placed in a stereotactic device (Stoelting; Foehr Medical Instruments GmbH, Germany). A sterile osmotic pump connector cannula (Bilaney Consultants) was implanted into the left lateral brain ventricle (−0.2 mm anterior and 1.0 mm lateral relative to Bregma and 2.3 mm below the surface of the skull). The support plate of the catheter was attached to the skull with Super Glue (Super Glue Corp.). The catheter was prefilled with 0.9% saline and connected to a sealed microrenathane catheter (MRE-025;

Braintree Scientific Inc.). After 5 days of recovery, mice were fasted overnight and the sealed microrenathane catheter was removed. TNF- α (Sigma-Aldrich) dissolved in aCSF or vehicle (aCSF) was injected in a volume of 2 μ l according to the respective experimental set-up. The catheter was subsequently sealed to avoid backflow. Injections were performed in isoflurane anesthesia. Mice were killed after 24h.

For experiments with multiple icv injections into the same mouse, male JNK1^{fl/fl} and JNK1 ^{Δ NES} mice were anesthetized by intraperitoneal injection of avertin (2,2,2-tribromoethanol, 0.2 ml/g). Scalp fur was shaved and prepared using sterile techniques and the mice were then placed into a stereotaxic device (Stoelting; Foehr Medical Instruments GmbH, Germany) with lambda and bregma at the same vertical coordinate. A small midline incision was made over the dorsal scalp to provide access to the cranium and the cranial surface was cleaned by swabbing with hydrogen peroxide and allowed to dry. The lateral ventricle was targeted using coordinates located using a Brain Atlas (coordinates were bregma 1.0mm lateral, 0.2mm caudal, and 2.0mm ventral). A 5 mm² skull window was outlined with a fine dremel bit and removed with forceps; the sagittal sinus was displaced laterally prior to lowering a 26-gauge stainless steel cannula (Plastics One, Roanoke, VA) such that the cannula tip was 4.8 mm below bregma. Dental acrylic was used to secure the cannula to the skull. After 1 week recovery, mice were icv injected with insulin, leptin or aCSF according to the experimental paradigm, and food intake and body weight was measured before and 24h later.

For icv insulin signalling experiments, mice were fasted for 48h, injected with aCSF or insulin, sacrificed 20min later and tissues extracted as necessary.

2.5.9 Intraperitoneal leptin sensitivity tests

For i.p. leptin sensitivity tests, vehicle (0.9% NaCl) or leptin at a dose of 2 mg/kg was injected twice daily over a period of 3 consecutive days. Body weight and food intake was monitored twice daily.

2.5.10 Implantation of osmotic minipumps

To investigate the effect of corticosterone restoration in the hypocorticosteronemic PDK1 ^{Δ POMC} mice, osmotic minipumps filled with corticosterone were implanted. Before surgery, dexamethasone (5 mg/kg BW; Sigma-Aldrich) was injected i.p. to prevent death as a consequence of stress arising from surgery in PDK1 ^{Δ POMC} mice. Osmotic minipumps (Model

2004, Alzet, California, USA) pre-filled with 10µg/µl corticosterone dissolved in PEG400 (Sigma-Aldrich) were implanted in anaesthetized mice according to the manufacturers instructions. Blood was taken every week between 2 and 4 pm. Mice which did not show a significant increase in plasma corticosterone were dismissed from the study.

2.5.11 Behavioural analysis

To control for behavioural differences between control and JNK1^{ΔNES} mice, several experimental paradigms were analysed. To examine locomotor efficacy, Rotarod analysis was performed. Control and JNK1^{ΔNES} mice were mounted on the Rotarod, and total time on the accelerating rotating rod until mouse fell off was measured. To analyze anxiety, the zero maze paradigm was chosen. Control and JNK1^{ΔNES} mice were put on the zero maze, and the time in which the mouse stayed in the closed part of the maze was tracked by an automatic visual system. Additionally, open field analysis of control and JNK1^{ΔNES} mice was performed. Control and JNK1^{ΔNES} mice were put into the open field, and the time in which the mouse stayed close to the wall and total distance travelled was tracked by an automatic computer-based system. To gain insight into potentially impaired spatial memory, Morris water maze analysis was performed. Control and JNK1^{ΔNES} mice were trained daily for 4 days to memorize the location of submerged platform in a water pool using several local markers, and the time taken by each mouse to find the platform was measured by an automatic, software based system. On the fifth day of the Morris water maze analysis, the platform was removed from the pool, and the time the mouse swam in the quadrant in which the platform had been was automatically measured by an automatic, software based system. All experimental setups were purchased from TSE Systems, Bad Homburg, Germany, and the experimental analysis was performed by and with the help of Dr. Hella Brönneke, Cluster of Excellence in aging-associated diseases (CECAD), University of Cologne, Germany.

2.6 Cell culture

GH4C1 cells (240) cells were cultivated in 5% CO₂ at 37°C in DMEM with 10% FCS and Penicillin/Streptomycin. 1x10⁶ cells per 6cm well were fasted for 6h, followed by 16h of stimulation with either control, SP600125, LY294002 or PD98059 (Sigma-Aldrich). All inhibitors were used at a final concentration of 10µM, and were prepared on the day of the experiment. DMSO was present in all wells at a final concentration of 0.1%. The experiments were performed in triplicates, and three independent experiments were analysed with rat

specific Real-Time probes for TRHR (Rn00564882_m1) and GUSB (Rn00566655_m1) as a housekeeping gene (Applied Biosystems).

2.7 Computer analysis

2.7.1 Densitometrical analysis

Western Blot bands were measured in intensity per mm² using the Quantity One Software (Bio-Rad, München, Germany). After background subtraction, each sample was normalized to an internal loading control such as the unphosphorylated protein, IR β or β -actin expression. Average protein expression of control mice was set to 1 or 100% and compared to expression of conditional knockout mice unless stated otherwise.

2.7.2 Statistical methods

Data were analysed for statistical significance by two-tailed unpaired Student's t test unless indicated otherwise. *P* values below 0.05 were considered significant. All displayed values are means +/- SEM. **p*<0.05; ***p*<0.01; ****p*<0.001.

3 Results

3.1 Generation of POMC cell-specific PDK1 knockout mice

To address the effect of kinase signalling downstream of PI3K on energy homeostasis and stress response *in vivo*, we generated mice lacking 3-phosphoinositide-dependent protein kinase-1 (PDK1) selectively in POMC-expressing cells ($PDK1^{\Delta POMC}$) using Cre/loxP-mediated recombination. To this end, mice expressing a Cre recombinase under control of the *POMC*-promoter (152, 241) were crossed with mice carrying a loxP-flanked *PDK1* gene ($PDK1^{fl\Delta neo/fl\Delta neo}$) (Figure 5) (80).

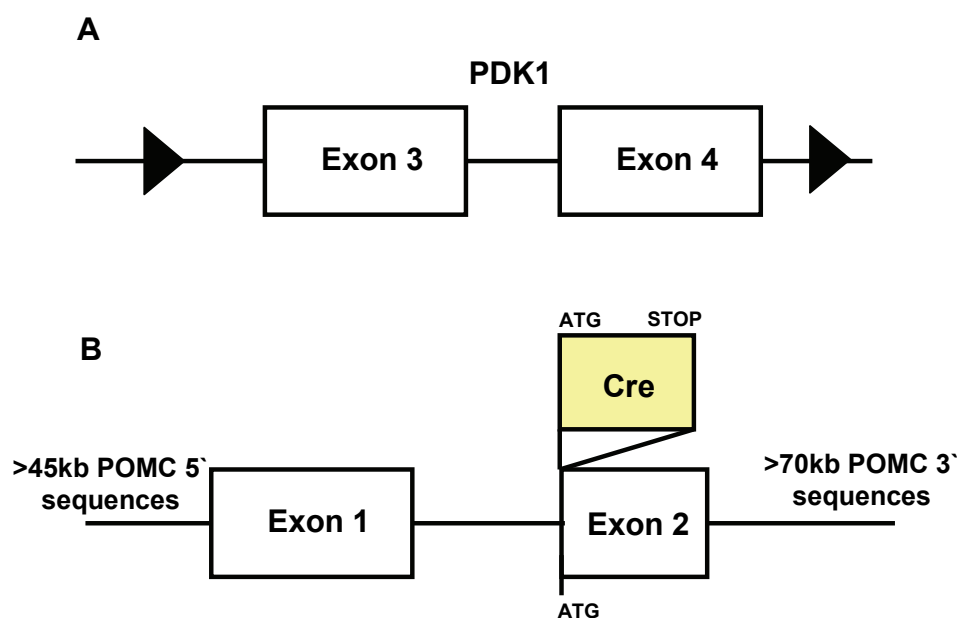


Figure 5: Targeted genomic loci in $PDK1^{fl\Delta neo/fl\Delta neo}$ and POMC-Cre mice.

A) In $PDK1^{fl\Delta neo/fl\Delta neo}$ mice, exon 3 and 4 are flanked by loxP sequences. Cre-mediated excision of these exons will induce a frame-shift, inhibiting translation of the PH and the kinase domain and leading to a premature stop of translation. B) POMC-Cre mice are carriers of a POMC bacterial artificial chromosome (BAC) in which a Cre expression cassette was inserted into the translational initiation site (ATG) of POMC exon 2.

In $PDK1^{fl\Delta neo/fl\Delta neo}$ mice, which served as controls, exons 3 and 4 are flanked by loxP sites which does not impair transcription of the *PDK1* gene or translation of PDK1 mRNA (80, 238, 242). In littermates which inherit the POMC-Cre transgene, exons 3 and 4 are removed in all POMC expressing cells, leading to a frameshift mutation and thus selective inactivation of the PDK1 gene only in POMC cells ($PDK1^{\Delta POMC}$ mice) ((80, 238).

To analyze cell-type specific inactivation of PDK1, Cre-mediated recombination was visualized by crossing POMC-Cre mice and $PDK1^{\Delta POMC}$ mice to a reporter mouse strain

expressing the β -galactosidase gene (*lacZ*) under control of the ubiquitously expressed *ROSA26* promoter only after Cre-mediated removal of a floxed *hygromycin resistance* gene (243). Analysis of *lacZ* immunoreactivity in *lacZ* ^{Δ POMC} mice revealed a pattern of expression in the hypothalamus in agreement with reported localisation of Cre and POMC expression in POMC-Cre mice (152).

Double immunostaining for PDK1 and *lacZ* revealed expression of PDK1 in approximately 70% of *lacZ*-expressing cells. Consistently, PDK1 expression was reduced to less than 10% of *lacZ*-positive hypothalamic neurons in *lacZ:PDK1* ^{Δ POMC} reporter mice (Figure 6).

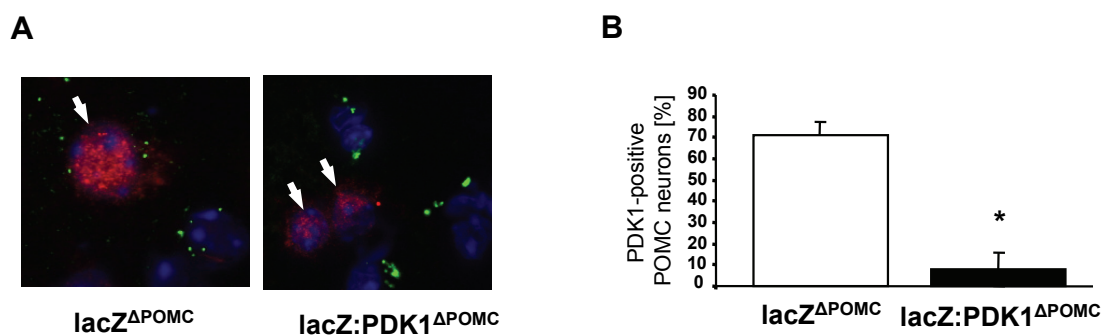


Figure 6: Ablation of the PDK1 protein in POMC neurons.

A) Detection of PDK1 in POMC neurons by immunohistochemistry. Using *lacZ* ^{Δ POMC} and *lacZ:PDK1* ^{Δ POMC} reporter mice, co-immunohistochemistry for β -galactosidase and PDK1 was performed, and the number of POMC cells positive for PDK1 staining was counted for at least 100 neurons from 2 mice for each genotype. red, *lacZ* (POMC neurons), green, PDK1, blue, DAPI. Original magnification, 630x. B) Quantification of PDK1 expression in POMC neurons from *lacZ* ^{Δ POMC} and *PDK1:lacZ* ^{Δ POMC} mice. *, $p \leq 0.05$.

To confirm specificity of recombination, Western blot analysis for PDK1 was performed in peripheral tissues from control and *PDK1* ^{Δ POMC} mice. PDK1 expression was unchanged between control and *PDK1* ^{Δ POMC} mice in brain, liver, skeletal muscle and pancreas (Figure 7). Since the POMC neuron population is very small compared to total neuron number in the hypothalamus, there was also no change observable in hypothalamic PDK1 expression between control and *PDK1* ^{Δ POMC} mice, which is in agreement with other reports using POMC-Cre animals (151, 235) (Figure 7).

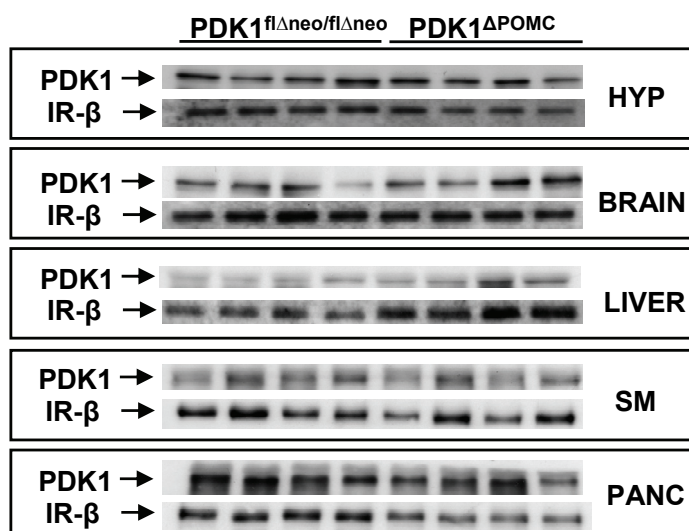


Figure 7: Unchanged PDK1 protein content in peripheral tissues and total brain.

Western blot analysis of PDK1 and IR- β subunit expression (loading control) in hypothalamus (HYP), whole brain (BRAIN), liver (LIVER), skeletal muscle (SM) and pancreas (PANC) of PDK1^{flΔneo/flΔneo} and PDK1^{ΔPOMC} mice (n= 4 of each group).

The *POMC* gene is also expressed in corticotrophs and melanotrophs of the pituitary, where the POMC protein is cleaved to generate ACTH or α -MSH, respectively (130, 238, 244, 245). Since the POMC-Cre transgene also targets Cre expression to these two cell types of the pituitary, PDK1 deletion in hypothalamus and pituitary was detected by PCR-based analysis (Figure 8).

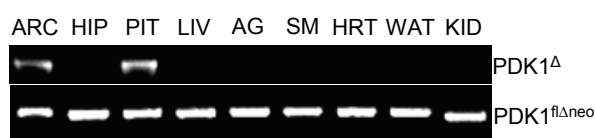


Figure 8: PDK1 deletion follows endogenous POMC expression.

Detection of deletion of the PDK1 allele in PDK1^{ΔPOMC} mice. DNA was extracted from the arcuate nucleus (ARC), hippocampus (HIP), pituitary (PIT), liver (LIVER), adrenal gland (AG), skeletal muscle (SM), heart (HRT), white adipose tissue (WAT) and kidney (KID) from a PDK1^{ΔPOMC} mouse. Using a PCR strategy, the deleted allele could only be detected in the arcuate nucleus and the pituitary, but not in the other tissues (upper bands).

PI3K and PDK1 signalling is involved in regulation of development, mitosis, apoptosis, and cell size in several cell types (78, 80, 246-248). To exclude the possibility that PDK1 deficiency leads to POMC neuron apoptosis and/or developmental changes, POMC-Cre and PDK1^{ΔPOMC} mice were crossed to a second reporter line, which expresses enhanced green fluorescent protein (GFP) only after Cre-mediated recombination of a transcriptional stop cassette (249). Quantification of GFP immunoreactive cells in hypothalami of GFP^{ΔPOMC}

and GFP:PDK1^{ΔPOMC} mice revealed unaltered cell numbers at the time of weaning and in adult mice (Figure 9).

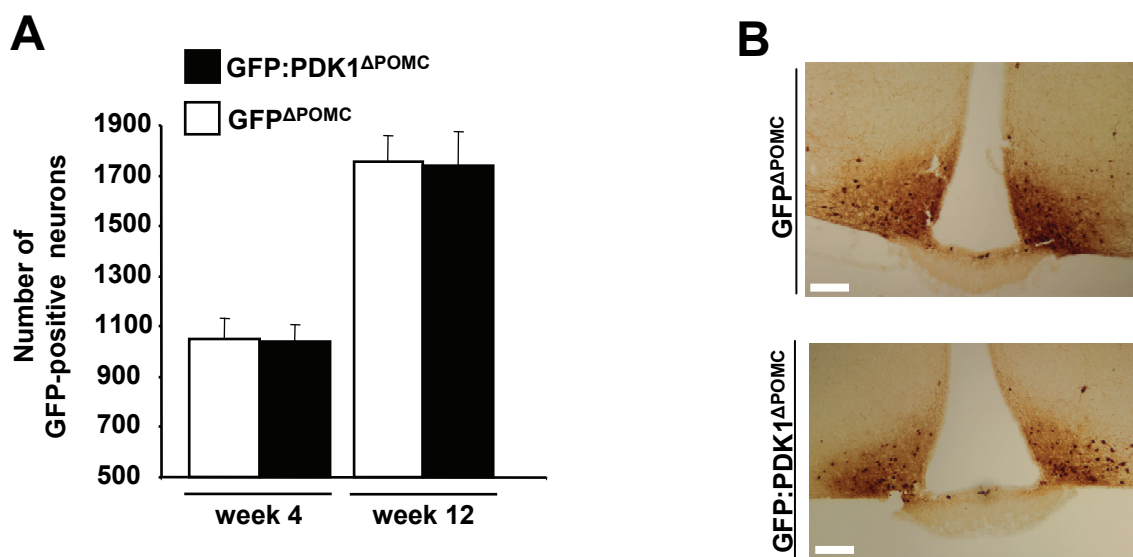


Figure 9: PDK1 deletion does not affect generation and survival of POMC neurons.

A) POMC cell counts in the arcuate nucleus of GFP reporter mice showed no difference between GFP^{ΔPOMC} and PDK1:GFP^{ΔPOMC} reporter mice at the age of 4 and 12 weeks (n= 3 of each genotype at each age). Results are expressed as number of neurons positive for GFP staining +/- SEM. B) Cre-mediated recombination was visualized by immunohistochemistry for GFP in brains of GFP^{ΔPOMC} and PDK1:GFP^{ΔPOMC} mice. Representative sections for GFP^{ΔPOMC} and PDK1:GFP^{ΔPOMC} mice are shown. Scale bars, 50μm.

Taken together, PDK1^{ΔPOMC} mice are a viable tool to analyze the role of PDK1-dependent signalling in hypothalamic POMC neurons and pituitary melanotrophs and corticotrophs.

3.2 Increased body weight and hyperphagia in young PDK1^{ΔPOMC} mice

To investigate whether the role of the PI3K signalling cascade in energy homeostasis in POMC neurons is PDK1-dependent, body weight of control and PDK1^{ΔPOMC} mice fed either normal chow diet (ND) or high-fat diet (HFD) was monitored. Shortly after weaning, PDK1^{ΔPOMC} mice exhibited slightly but significantly increased body weight independently of diet. However, body weight of control and PDK1^{ΔPOMC} mice converged over time (Figure 10A, B). Consistent with the increased body weight of young PDK1^{ΔPOMC} mice, these animals also exhibited elevated serum leptin and glucose concentrations at the age of 8 weeks (Figure 10C, D). To address whether initially increased body weight of PDK1^{ΔPOMC} mice resulted from increased energy intake, we determined food intake in these mice at 8 weeks of age, which revealed significant hyperphagia in PDK1^{ΔPOMC} mice (Figure 10 F).

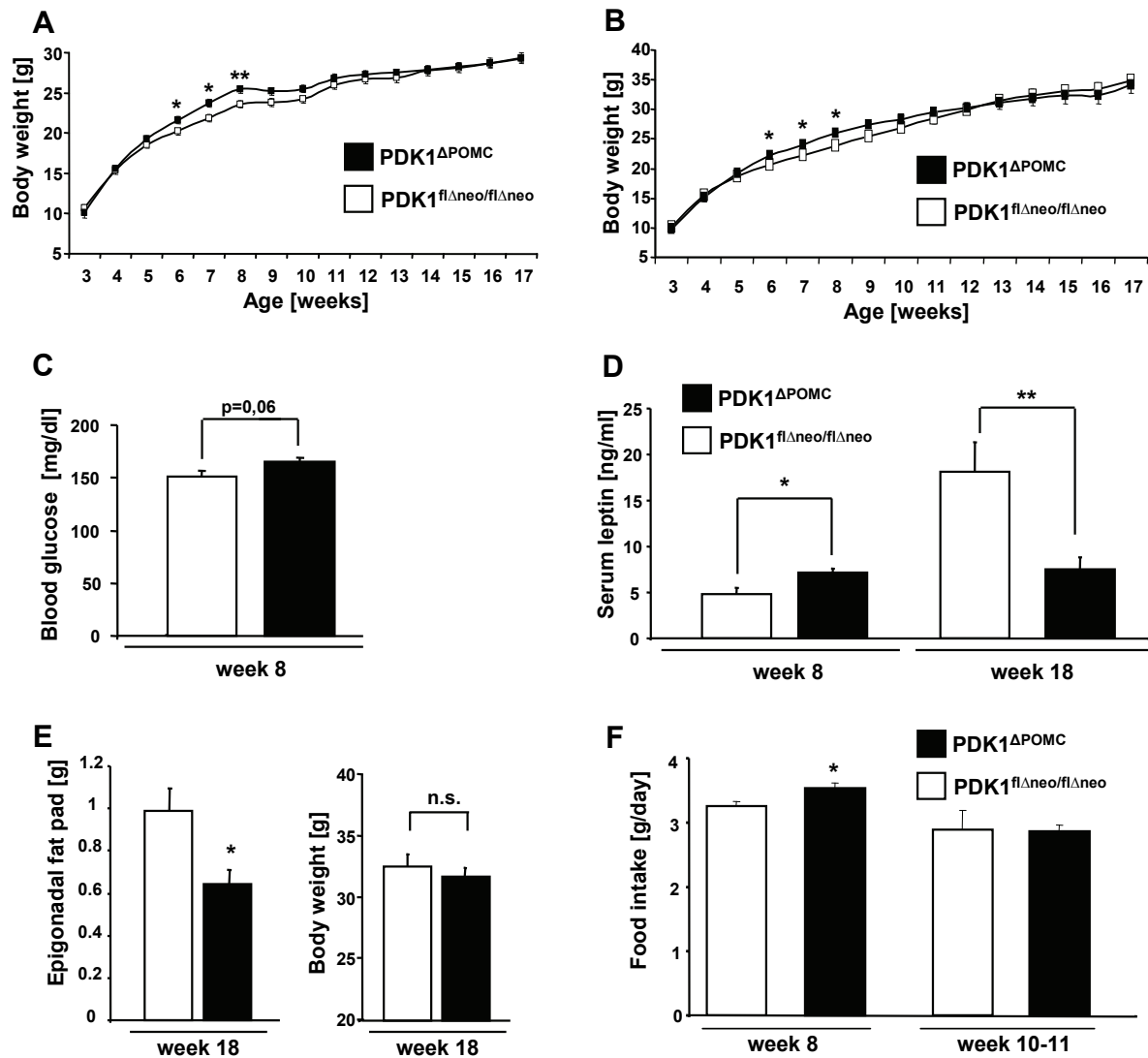


Figure 10: Increased body weight and hyperphagia in young PDK1^{ΔPOMC} mice.

A) Average body weight of PDK1^{flΔneo/flΔneo} and PDK1^{ΔPOMC} mice on ND (n= 16-20). B) Average body weight of PDK1^{flΔneo/flΔneo} and PDK1^{ΔPOMC} mice on HFD (n= 12-24). C) Blood glucose levels in 8 week old PDK1^{flΔneo/flΔneo} (n= 21) and PDK1^{ΔPOMC} (n= 16) mice. D) Serum leptin concentrations of PDK1^{flΔneo/flΔneo} (n=17-20) and PDK1^{ΔPOMC} (n= 10-13) mice at 8 and 18 weeks of age. E) Epigonadal fat pad weight and body weight in PDK1^{flΔneo/flΔneo} (n=21) and PDK1^{ΔPOMC} (n= 13) mice on ND at the age of 18 weeks. F) Daily food intake in PDK1^{flΔneo/flΔneo} (n=13;5) and PDK1^{ΔPOMC} (n= 7;4) mice on ND at 8 weeks and at 10-11 weeks of age. *, p ≤ 0.05; **, p ≤ 0.01.

Analysis of hypothalamic neuropeptide expression in PDK1^{flΔneo/flΔneo} and PDK1^{ΔPOMC} mice revealed a significant reduction in POMC expression in the absence of any alteration in the expression of the orexigenic neuropeptides agouti-related protein (AgRP) (Figure 11). Thus, PDK1^{ΔPOMC} mice initially develop transiently increased body weight as a consequence of hyperphagia caused by reduced hypothalamic POMC expression.

Since the body weights of male PDK1^{ΔPOMC} mice were not distinguishable from PDK1^{flΔneo/flΔneo} mice starting from 10 weeks of age, we next determined parameters of energy homeostasis in older mice. Surprisingly, food intake of PDK1^{ΔPOMC} mice was not significantly

different from controls at 10 weeks of age (Figure 10F). Strikingly, at 18 weeks of age, $PDK1^{\Delta POMC}$ mice exhibited significantly reduced epigonadal fat pad mass and lower serum leptin concentrations but unchanged body weight (Figure 10D, E). Hypothalamic expression of NPY, AgRP and TRH was again unchanged (Figure 18) also at 18 weeks of age, while hypothalamic POMC expression was still reduced by 80% in $PDK1^{\Delta POMC}$ mice compared to controls (Figure 11A). Thus, progressive reduction of body weight, food intake, serum leptin concentrations and epigonadal fat pad mass occurred in the presence of constantly reduced hypothalamic POMC expression.

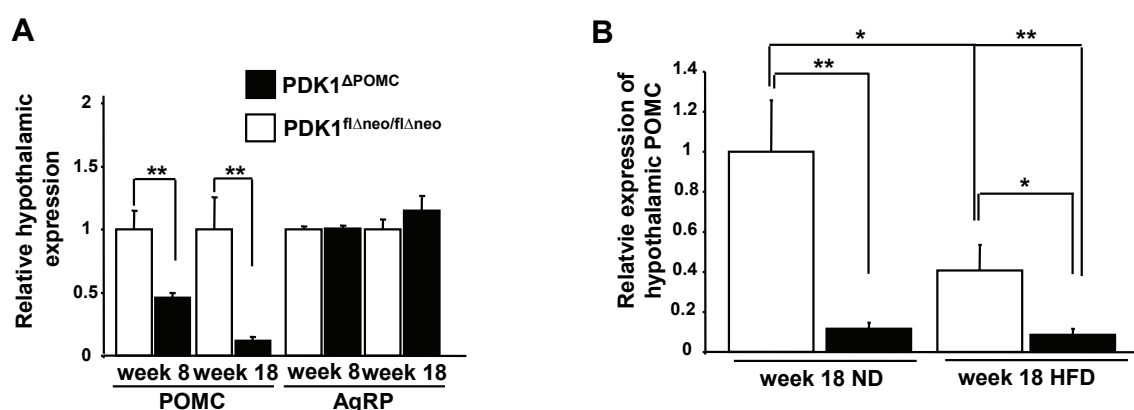


Figure 11: POMC mRNA expression is impaired in $PDK1^{\Delta POMC}$ mice.

A) Neuropeptide expression in male $PDK1^{fl\Delta neo/fl\Delta neo}$ and $PDK1^{\Delta POMC}$ mice on normal diet at the age of 8 and 18 weeks as measured by Real-Time PCR (n= 5-11 per group). B) Hypothalamic POMC expression in male $PDK1^{fl\Delta neo/fl\Delta neo}$ and $PDK1^{\Delta POMC}$ mice on ND or HFD at the age of 18 weeks as measured by Real-Time PCR (n= 4-5 per group). *, $p \leq 0.05$; **, $p \leq 0.01$.

3.3 Secondary hypocortisolism in $PDK1^{\Delta POMC}$ mice

Given the paradoxical decline of initially increased body weight and hyperphagia in the presence of constantly repressed POMC transcription, possible mechanisms underlying this phenotype were investigated. Old $PDK1^{\Delta POMC}$ mice showed significantly increased insulin sensitivity during insulin tolerance tests (Figure 12A). Moreover, analysis of glucose-stimulated insulin secretion (GSIS) revealed that although insulin secretion was lower compared to $PDK1^{fl\Delta neo/fl\Delta neo}$ mice, blood glucose concentrations were significantly lower than in control groups, further supporting that $PDK1^{\Delta POMC}$ mice exhibit dramatically increased peripheral insulin sensitivity and subsequent compensatory reduction of insulin secretion (Figure 12B, C).

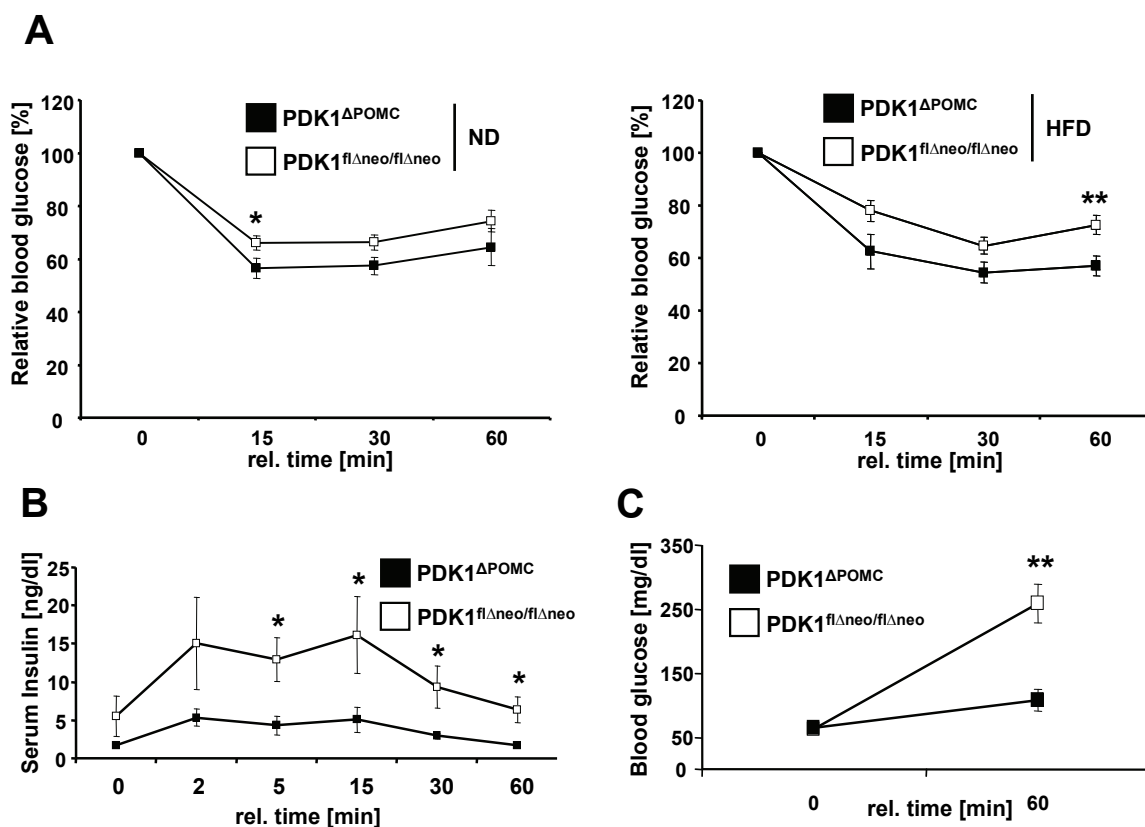


Figure 12: Elevated insulin sensitivity in PDK1^{ΔPOMC} mice.

A) Relative blood glucose during an insulin tolerance test of PDK1^{flΔneo/flΔneo} and PDK1^{ΔPOMC} mice on ND (left panel) or HFD (right panel) at the age of 15 weeks (n= 7-15 per group). B) Serum insulin levels during glucose-stimulated insulin secretion (GSIS) of female PDK1^{flΔneo/flΔneo} (n= 5) and PDK1^{ΔPOMC} (n= 5) mice at the age of 22 weeks. C) Blood glucose levels at the beginning and the end of the glucose-stimulated insulin secretion experiment of female PDK1^{flΔneo/flΔneo} (n= 5) and PDK1^{ΔPOMC} (n= 5) mice. *, p ≤ 0.05; **, p ≤ 0.01.

Taken together, relative body weight loss and dramatically increased insulin sensitivity in older mice resembled key clinical features of severe hypocortisolism, since corticosterone/cortisol is a positive regulator of food intake and a negative regulator of insulin sensitivity (250, 251).

To elucidate if PDK1^{ΔPOMC} mice suffer from reduced circulating corticosterone concentrations, blood samples from control and PDK1^{ΔPOMC} mice at different ages were taken. Analysis of plasma corticosterone concentrations revealed a significant reduction in PDK1^{ΔPOMC} mice compared to control mice already at the age of 3 weeks and corticosterone concentrations further decreased over time in PDK1^{ΔPOMC} mice (Figure 13A, B). Moreover, analysis of stress-induced corticosterone release revealed that PDK1^{ΔPOMC} mice exhibited a dramatic impairment in stress-induced corticosterone production (Figure 13A). Similarly, injection of an ACTH analogue (Synacthen) resulted in a largely blunted raise in plasma corticosterone concentrations in PDK1^{ΔPOMC} mice, consistent with adrenal insufficiency

(Figure 13C). Taken together, this indicates that PDK1^{ΔPOMC} mice exhibit critically reduced circulating corticosterone with further progressive loss into adulthood.

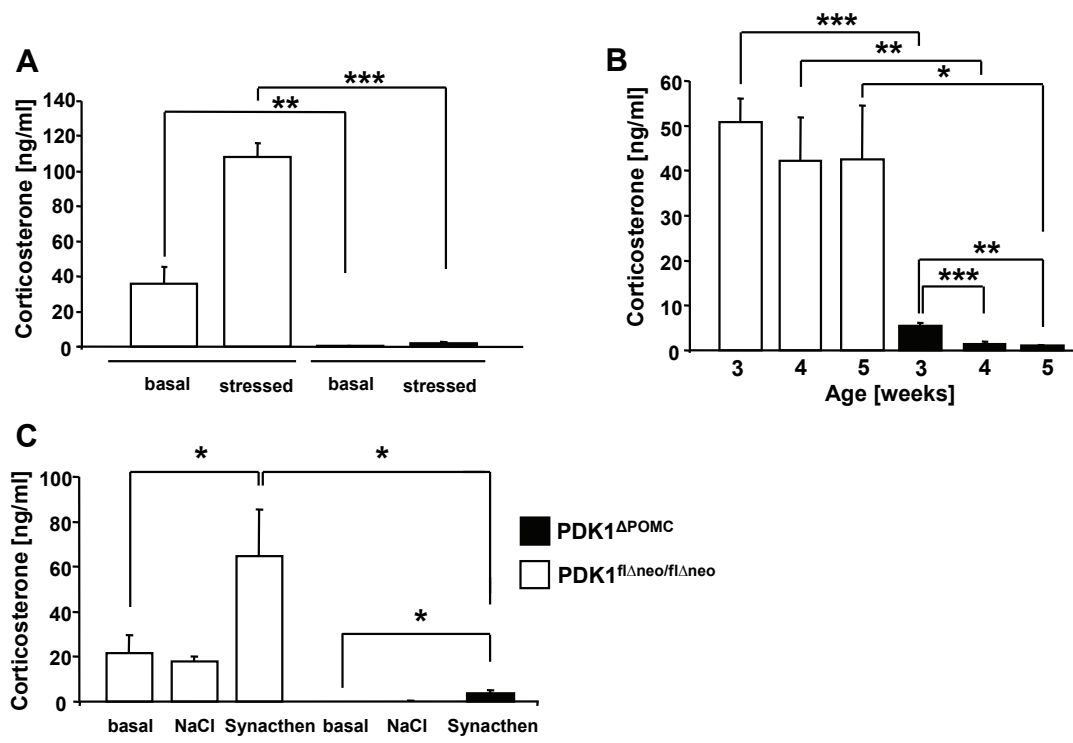


Figure 13: Reduced plasma corticosterone and adrenal ACTH insensitivity in PDK1^{ΔPOMC} mice.

A) Plasma corticosterone levels of PDK1^{flΔneo/flΔneo} and PDK1^{ΔPOMC} mice on ND before and after a stress test at the age of 12 weeks (n= 5-6 per group). B) Basal plasma corticosterone levels in PDK1^{flΔneo/flΔneo} and PDK1^{ΔPOMC} mice at the age of 3, 4 and 5 weeks (n= 5-10 per group). C) Plasma corticosterone levels in PDK1^{flΔneo/flΔneo} and PDK1^{ΔPOMC} mice after intraperitoneal injection of saline or an ACTH analogue (Synacthen) at the age of 12 weeks (n= 5 per group). *, p ≤ 0.05; **, p ≤ 0.01; ***, p ≤ 0.001.

Hypothalamic CRH is partially responsible for POMC expression and ACTH release from the pituitary after stress stimuli but not under basal conditions, as CRH knockout mice do not show any change in basal pituitary POMC expression (244). There was no difference in hypothalamic CRH expression between PDK1^{flΔneo/flΔneo} and PDK1^{ΔPOMC} mice at any age or diet, indicating that hypothalamic circuits are not responsible for the loss of circulating corticosterone in PDK1^{ΔPOMC} mice (Figure 18).

Since changes in the function of corticotrophs of the pituitary were possibly responsible for hypocortisolism in PDK1^{ΔPOMC} mice, the pattern of GFP expression in the pituitary of GFP^{ΔPOMC} mice and GFP:PDK1^{ΔPOMC} mice was investigated. This analysis revealed a more than 90% reduction in GFP-positive corticotroph cells in GFP:PDK1^{ΔPOMC} mice compared to GFP^{ΔPOMC} mice (Figure 14A, B). In the same vein, cells immunoreactive for ACTH were drastically reduced in PDK1^{ΔPOMC} mice (Figure 14C). Consistent with the dramatic reduction in corticotroph number, Real-time PCR analysis of POMC mRNA

expression revealed a ~80% reduction of pituitary POMC mRNA expression in $PDK1^{\Delta POMC}$ mice compared to $PDK1^{fl\Delta neo/fl\Delta neo}$ mice (Figure 14 D).

Melanotroph numbers in the intermediate lobe of the pituitary were also reduced, but in accordance with the notion that even POMC knockout mice have a relatively faint change in pigmentation and fur color, we did not notice any obvious change in fur color or skin pigmentation of $PDK1^{\Delta POMC}$ mice (134).

Taken together, these findings demonstrate that PDK1 is essential for survival of corticotrophs and that POMC cell-restricted PDK1 deficiency results in secondary hypocortisolism: while PDK1 deficiency in hypothalamic POMC neurons affects POMC transcription and not cell survival, it primarily controls cell survival of corticotrophs and melanotrophs in the pituitary.

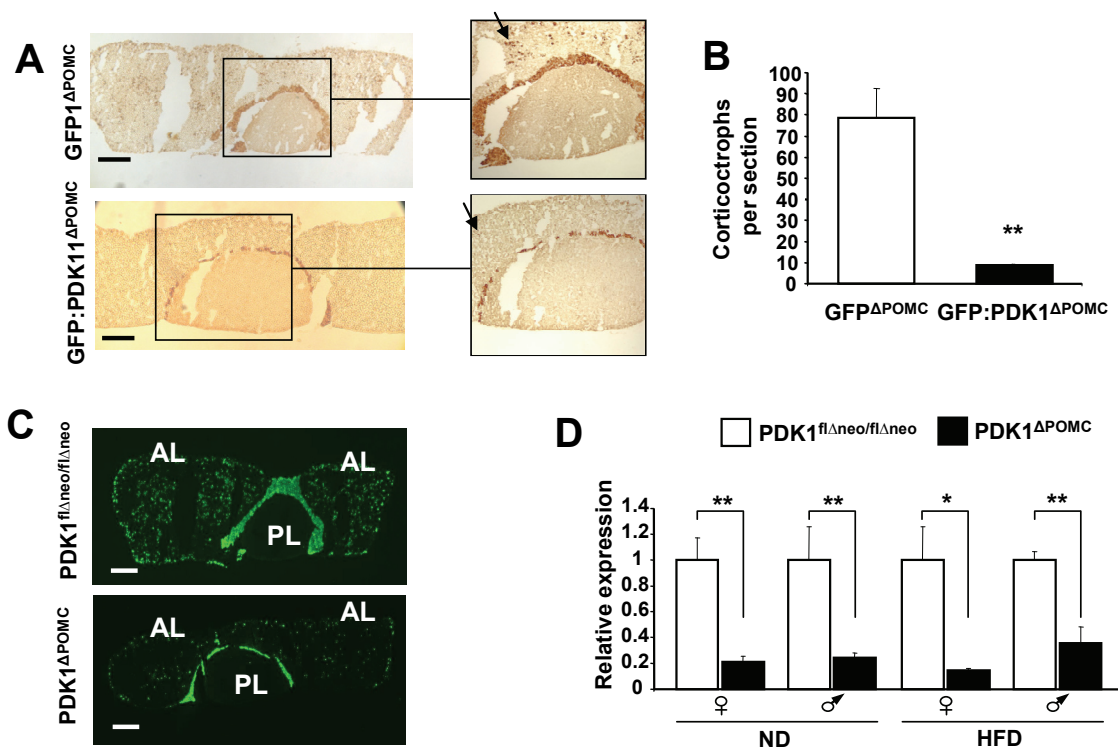


Figure 14: Loss of POMC cells in pituitaries of $PDK1^{\Delta POMC}$ mice.

A) Immunohistochemistry for GFP from pituitary sections of $GFP^{\Delta POMC}$ and $GFP:PDK1^{\Delta POMC}$ mice at approximately 12 weeks of age. Brown, horseradish peroxidase (GFP). Single corticotrophs are marked by arrows. Scale bar, 100 μ m. B) Quantification of GFP-positive corticotrophs from pituitary sections of $GFP^{\Delta POMC}$ (n= 2) and $GFP:PDK1^{\Delta POMC}$ (n= 3) mice. C) Immunohistochemistry for ACTH from pituitary sections of $PDK1^{fl\Delta neo/fl\Delta neo}$ and $PDK1^{\Delta POMC}$ mice at approximately the age of 8 weeks. Green, ACTH. At least 3 mice of each genotype were analysed. Scale bar, 100 μ m. AL, anterior lobe; PL, posterior lobe. D) Pituitary POMC expression in female and male $PDK1^{fl\Delta neo/fl\Delta neo}$ (n= 5-6) and $PDK1^{\Delta POMC}$ (n= 4-6) mice on normal or high-fat diet at 18 weeks of age as measured by Real-Time PCR. *, $p \leq 0.05$; **, $p \leq 0.01$.

3.4 Corticosterone replacement prolongs hyperphagia and increased body weight in PDK1^{ΔPOMC} mice

To directly address, whether progressive hypocortisolism contributes to the normalization of hyperphagia and increased body weight of PDK1^{ΔPOMC} mice, circulating corticosterone concentrations were restored in PDK1^{ΔPOMC} mice. Therefore, osmotic mini pumps filled with corticosterone were implanted in 8 week old mice and corticosterone concentrations, body weight and food intake were subsequently monitored. Circulating corticosterone levels were similar one week after surgery between PDK1^{flΔneo/flΔneo} mice and PDK1^{ΔPOMC} mice (Figure 15A) Two weeks after surgery, food intake and body weight was significantly increased in PDK1^{ΔPOMC} mice, at a time where there is no significant difference between un-restored PDK1^{ΔPOMC} mice and control mice (Figure 15B, C). Moreover, epigonadal fat pad mass was significantly increased in PDK1^{ΔPOMC} mice three weeks after surgery (Figure 15 D).

Taken together, corticosterone restoration aggravates positive energy balance in PDK1^{ΔPOMC} mice, indicating that in un-restored PDK1^{ΔPOMC} mice the effect of reduced hypothalamic POMC expression is ameliorated by progressive loss of circulating corticosterone.

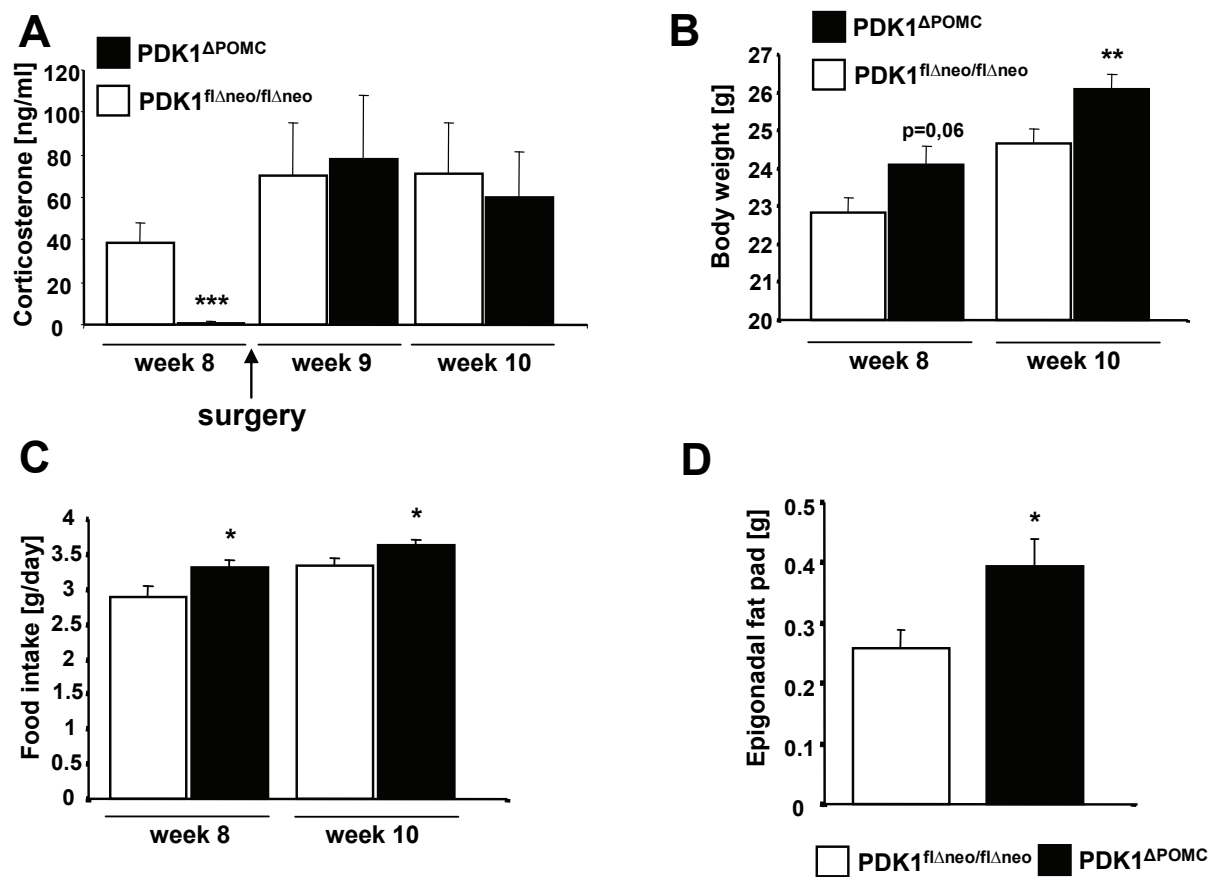


Figure 15: Corticosterone restoration maintains hyperphagia and increased body weight in PDK1^{ΔPOMC} mice.

A) Plasma corticosterone concentration in PDK1^{flΔneo/flΔneo} and PDK1^{ΔPOMC} mice before and after implantation of a corticosterone mini pump. Animals were bled at the age of 8 weeks, and surgery was performed immediately afterwards. Corticosterone levels were measured one and two weeks after surgery (n= 7-12 per genotype). B) Body weight of PDK1^{flΔneo/flΔneo} and PDK1^{ΔPOMC} mice before and after corticosterone minipump implantation (n= 7-12 per genotype). C) Daily food intake of PDK1^{flΔneo/flΔneo} and PDK1^{ΔPOMC} mice before and after corticosterone minipump implantation (n= 7-12 per genotype). D) Epigonadal fat pad mass of PDK1^{flΔneo/flΔneo} and PDK1^{ΔPOMC} mice at the end of corticosterone restoration (three weeks after surgery, n= 7-10). *, p ≤ 0.05; **, p ≤ 0.01; ***, p ≤ 0.001.

3.5 Restoration of energy homeostasis in PDK1^{ΔPOMC} mice by FOXO1 inhibition *in vivo*

Next, experiments were designed to define the pathways acting downstream of PDK1 to regulate hypothalamic POMC expression and/or corticotroph survival in the pituitary. Many kinases and transcription factors act downstream of PDK1, notably AKT, mTOR, S6K1, SGK1 and PKC isoforms and thus could contribute to the observed phenotype (247). Yet, one of the major mediators of PI3K signalling is the transcription factor FOXO1, which controls both expression of pro-apoptotic genes and has also been implicated in the control of POMC transcription (42, 50, 252, 253). As FOXO1 phosphorylation and exclusion from the nucleus is AKT-dependent, cells lacking PDK1 have increased FOXO1 activity. Therefore, a mouse line for Cre-inducible expression of a dominant negative FOXO1 (FOXO1^{Δ256}) mutant

was generated, which lacks the transactivation domain and the nuclear export signal (Figure 16) (89). Expression of FOXO1^{Δ256} leads to its accumulation in the nucleus, where it binds to FOXO1 cis elements and inhibits binding of endogenous FOXO1 protein, thus precluding transactivation or -repression. FOXO1^{Δ256} mice were crossed with PDK1^{ΔPOMC} mice to generate FOXO1^{Δ256}:PDK1^{ΔPOMC} mice, which specifically in POMC-expressing cells lack PDK1, but at the same time express FOXO1^{Δ256}.

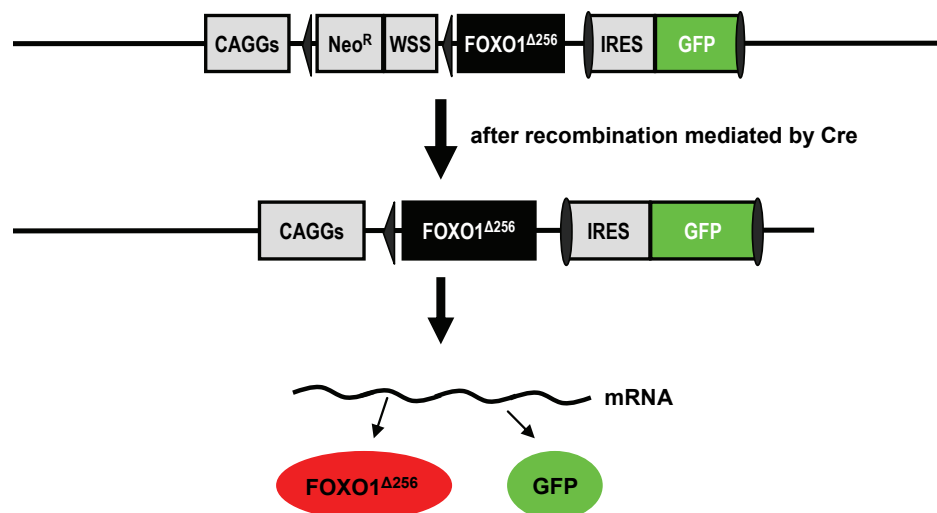


Figure 16: Generation of mice with inducible FOXO1^{Δ256} expression.

Depicted is the knockin at the ROSA26 locus in mice with inducible FOXO1^{Δ256} expression. Note that Cre-mediated recombination of the Neomycin resistance (Neo)/Westphal Stop sequence (WSS) cassette leads to expression of the FOXO1^{Δ256} protein but also to expression of GFP via an internal ribosome entry site (IRES), therefore GFP can be used for detection of FOXO1^{Δ256} expression. As only mice with one targeted allele were used, GFP expression is weaker than GFP expression from transgenic GFP reporter mice, which carry multiple integrations of the GFP transgene. CAGGS, chicken beta actin promoter/enhancer coupled with the cytomegalovirus immediate-early enhancer.

Since the mRNA encoding the FOXO1^{Δ256} mutant also codes for GFP protein which is translated from an internal ribosome entry site (IRES), GFP immunohistochemistry can identify cells expressing the FOXO1^{Δ256} mutant (Figure 16).

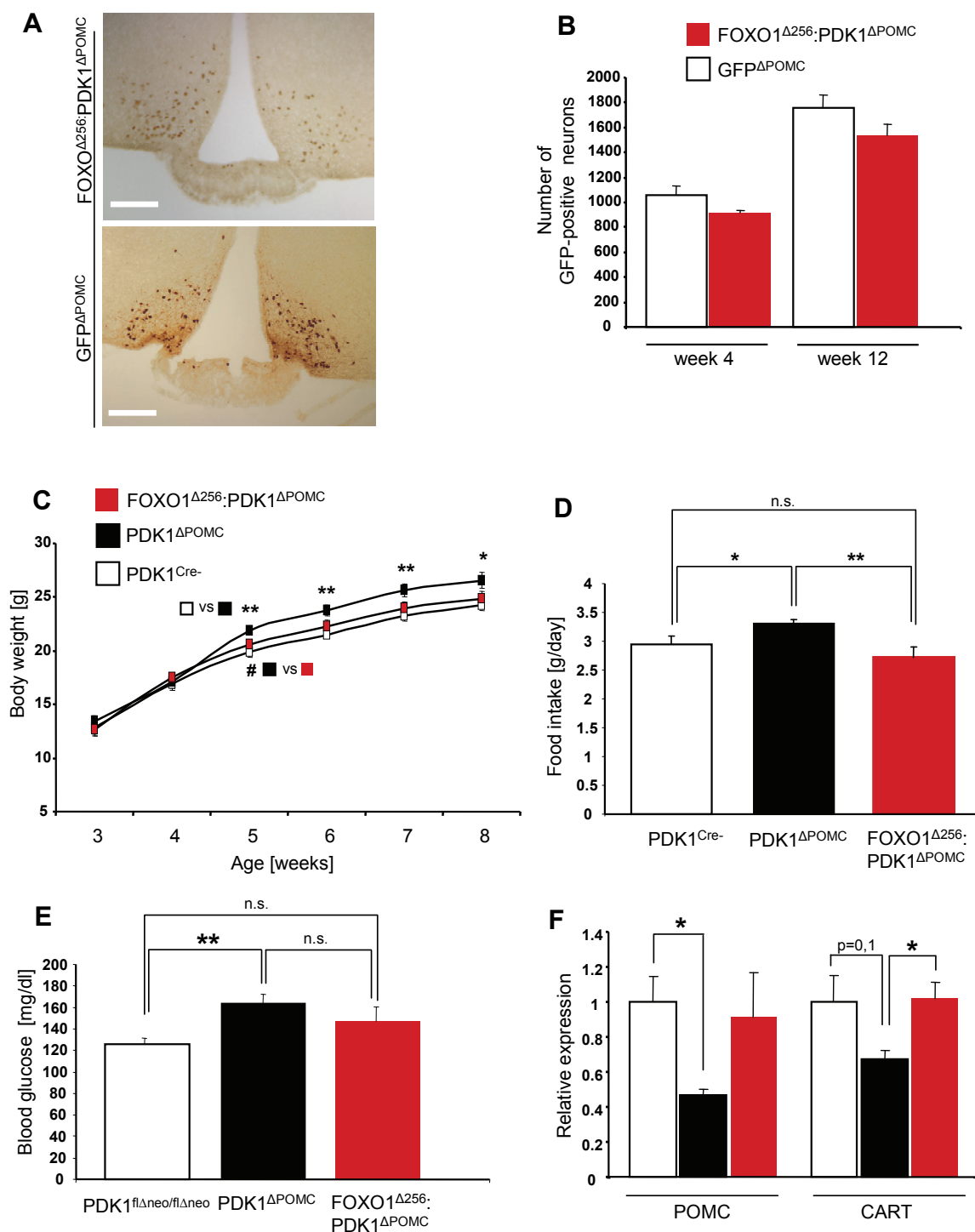


Figure 17: Expression of FOXO1^{Δ256} rescues the hypothalamic phenotype of PDK1^{ΔPOMC} mice.

A) Cre-mediated recombination was visualized using immunohistochemistry for GFP in brains of GFP^{ΔPOMC} and FOXO1^{Δ256};PDK1^{ΔPOMC} mice. Brown, horseradish peroxidase (GFP). Scale bar, 100μm. B) POMC cell counts in the Arc of GFP reporter mice showed no difference between GFP^{ΔPOMC} and FOXO1^{Δ256};PDK1^{ΔPOMC} reporter mice at the age of 4 and 12 weeks (n= 3 per group). C) Average body weight of male PDK1^{Cre-} (n= 19), PDK1^{ΔPOMC} (n= 15) and FOXO1^{Δ256};PDK1^{ΔPOMC} (n= 8) mice on ND until 8 weeks of age. *p<0.05 between control and PDK1^{ΔPOMC}; **p<0.01 between PDK1^{Cre-} and PDK1^{ΔPOMC}; #p<0.05 between PDK1^{ΔPOMC} and FOXO1^{Δ256};PDK1^{ΔPOMC}. D) Food intake of male PDK1^{Cre-} (n= 9) and PDK1^{ΔPOMC} (n= 10) and FOXO1^{Δ256};PDK1^{ΔPOMC} (n= 7) mice on normal diet at 8 weeks of age. E) Blood glucose concentration of male PDK1^{flΔneo/flΔneo} (n= 19), PDK1^{ΔPOMC} (n= 15) and FOXO1^{Δ256};PDK1^{ΔPOMC} (n= 8) mice on ND at the age of 8 weeks. F) Relative expression of hypothalamic POMC and CART mRNA in male PDK1^{Cre-} (n= 17), PDK1^{ΔPOMC} (n= 15) and FOXO1^{Δ256};PDK1^{ΔPOMC} (n= 7) mice on normal diet at 8 weeks of age as measured by Real-Time PCR. *, p ≤ 0.05; **, p ≤ 0.01.

Hypothalamic GFP-positive cell counts between FOXO1^{Δ256}:PDK1^{ΔPOMC}, GFP:PDK1^{ΔPOMC} and GFP^{ΔPOMC} at the age of 4 or 12 weeks were similar, indicating appropriate expression of the FOXO1^{Δ256} mutant protein without an effect on POMC neuron number (Figure 9 and Figure 17A, B).

Since young PDK1^{ΔPOMC} mice showed increased body weight and hyperphagia, Cre-negative (FOXO1^{Δ256}):PDK1^{flΔneo/flΔneo}, PDK1^{ΔPOMC} and FOXO1^{Δ256}:PDK1^{ΔPOMC} littermates were analysed with regards to energy homeostasis. Body weight of FOXO1^{Δ256}:PDK1^{flΔneo/flΔneo} and PDK1^{flΔneo/flΔneo} mice was indistinguishable, thus animals of both genotypes were combined into the control group (called PDK1^{Cre-}). While PDK1^{ΔPOMC} mice showed significantly increased body weight compared to control littermates, expression of FOXO1^{Δ256} restored normal body weight in FOXO1^{Δ256}:PDK1^{ΔPOMC} mice (Figure 17C). Similarly, FOXO1^{Δ256} expression prevented the hyperphagia in PDK1^{ΔPOMC} mice (Figure 17D). In the same line, mild hyperglycemia in PDK1^{ΔPOMC} mice was ameliorated by FOXO1^{Δ256} expression in POMC cells (Figure 17E).

Strikingly, while hypothalamic POMC expression was significantly decreased in PDK1^{ΔPOMC} mice compared to PDK1^{Cre-} mice, there was no significant difference between control and FOXO1^{Δ256}:PDK1^{ΔPOMC} mice (Figure 17F). Consistent with earlier observations, it was noticed that there was a strong tendency of decreased expression of the anorexigenic neuropeptide cocaine-and-amphetamine-related transcript (CART) in PDK1^{ΔPOMC} mice which was completely rescued in FOXO1^{Δ256}:PDK1^{ΔPOMC} mice (Figure 17F)(50). Similar to findings in PDK1^{ΔPOMC} mice, hypothalamic expression of AgRP, NPY or CRH was not affected in FOXO1^{Δ256}:PDK1^{ΔPOMC} mice (Figure 18).

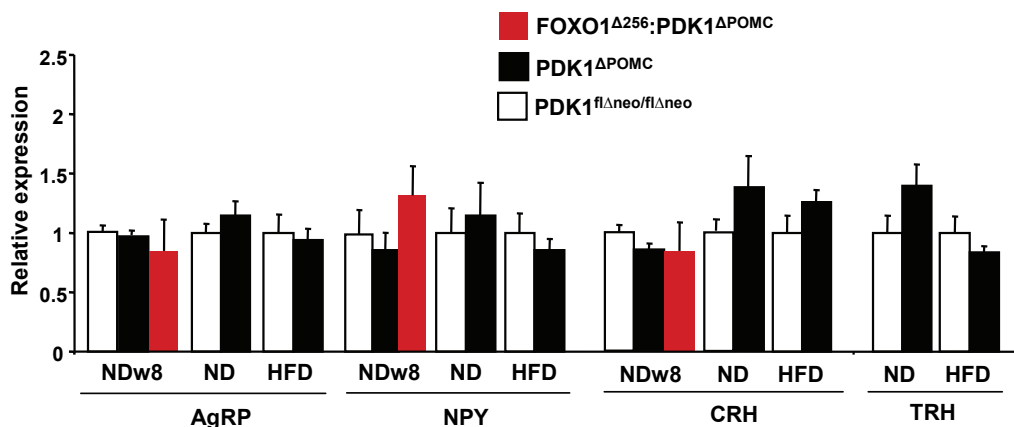


Figure 18: Unchanged orexigenic and PVN neuropeptide expression in PDK1^{ΔPOMC} mice.

Analysis of hypothalamic expression of the orexigenic neuropeptides AgRP, NPY as well as CRH and TRH in male PDK1^{flΔneo/flΔneo}, PDK1^{ΔPOMC} and FOXO1^{Δ256}:PDK1^{ΔPOMC} mice fed normal diet at the age of 8 weeks (NDw8), 18 weeks (ND), and at the age of 18 weeks fed high-fat diet (HFD) (n>= 5 per genotype).

Overall, these *in vivo* findings indicate that regulation of FOXO1 activity in hypothalamic POMC neurons is the principal way by which PDK1 signalling controls energy homeostasis.

3.6 Corticotroph cell loss in PDK1^{ΔPOMC} mice is FOXO1-independent

To investigate the effect of FOXO1^{Δ256} expression in corticotrophs, corticosterone levels in FOXO1^{Δ256}:PDK1^{ΔPOMC} mice were measured. FOXO1^{Δ256}:PDK1^{ΔPOMC} mice showed very low circulating corticosterone levels, similar to PDK1^{ΔPOMC} mice (Figure 19A). GFP and ACTH stainings of pituitaries from FOXO1^{Δ256}:PDK1^{ΔPOMC} mice showed the same reduction in corticotrophs as seen in PDK1^{ΔPOMC} mice, and POMC expression in the pituitaries was again significantly reduced in 8 week old mice (Figure 19B, C).

To gain insights into the dynamics of corticotroph loss, gene expression patterns in pituitaries of 3 week old mice were analysed. POMC mRNA expression was already critically reduced at this age in both PDK1^{ΔPOMC} and FOXO1^{Δ256}:PDK1^{ΔPOMC} mice (Figure 20). Strikingly, increased pituitary expression of the pro-apoptotic genes Bax and Bak was found in PDK1^{ΔPOMC} mice but not FOXO1^{Δ256}:PDK1^{ΔPOMC} mice (Figure 20). Moreover, only PDK1^{ΔPOMC} mice, but not FOXO1^{Δ256}:PDK1^{ΔPOMC} mice exhibited a tendency for increased expression of the pro-apoptotic gene Zac1, which has been shown to be under negative control of PI3K in pituitary cells *in vitro* (Figure 20) (254). Taken together, while increased expression of several pro-apoptotic genes in pituitaries of PDK1^{ΔPOMC} mice can be rescued by expression of FOXO1^{Δ256}, survival of corticotrophs appears to depend on additional PDK1-dependent, FOXO1-independent pathway(s).

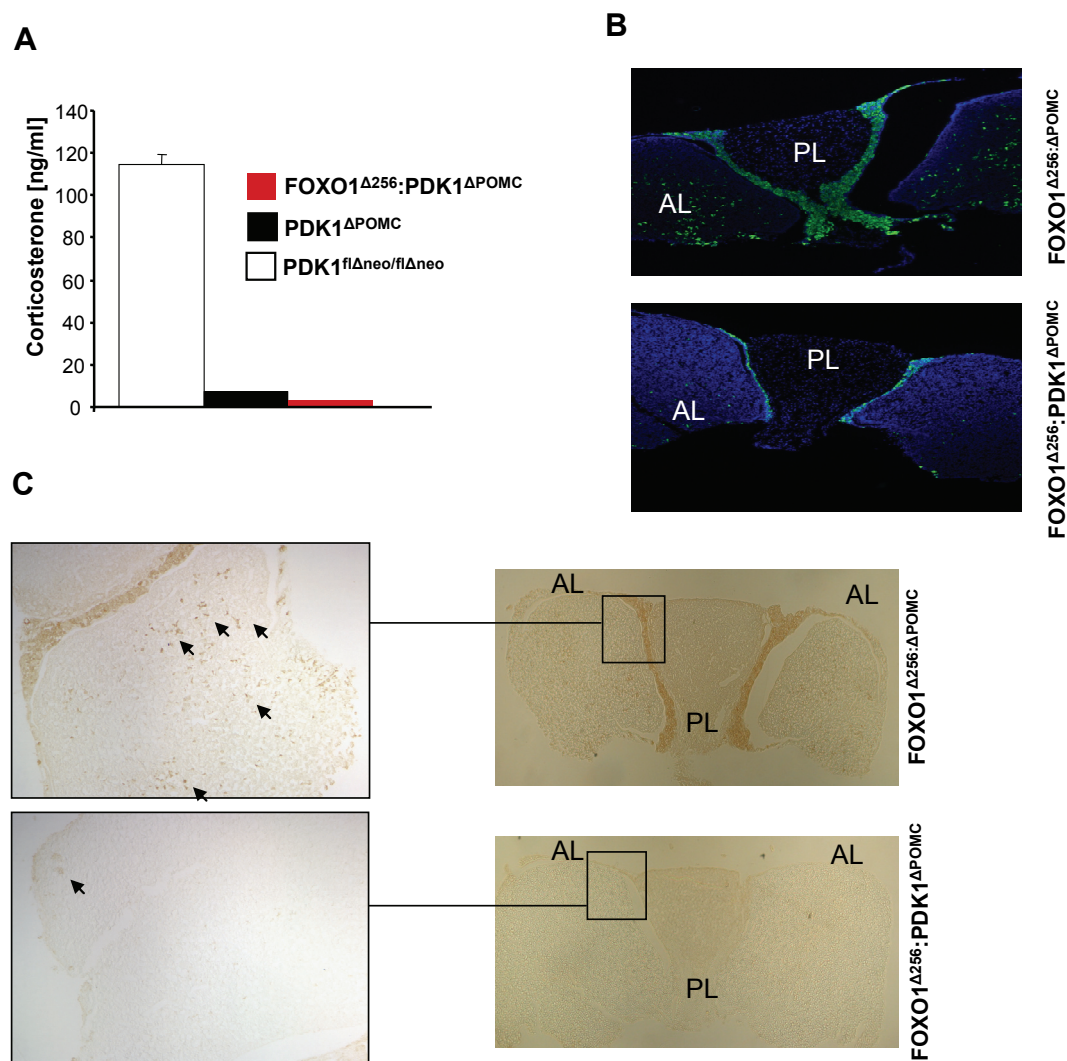


Figure 19: Corticotroph loss is not FOXO1-dependent in PDK1^{ΔPOMC} mice.

A) Serum corticosterone levels in male PDK1^{flΔneo/flΔneo}, PDK1^{ΔPOMC} and FOXO1^{Δ256}:PDK1^{ΔPOMC} mice fed normal diet at the age of 8 weeks (n= 8, 1, 2). B) Expression of ACTH was visualized by immunohistochemistry for ACTH in pituitaries of FOXO1^{Δ256}:PDK1^{ΔPOMC} mice (which served as control) and FOXO1^{Δ256}:PDK1^{ΔPOMC} mice. Shown are representative stainings from 3 mice for each genotype. Blue, DAPI; green, ACTH. Original magnification, 100x. AL, anterior lobe; PL, posterior lobe. C) Expression of the FOXO1^{Δ256}-transgene was visualized by immunohistochemistry for GFP in pituitaries of FOXO1^{Δ256}:PDK1^{ΔPOMC} mice (which served as control) and FOXO1^{Δ256}:PDK1^{ΔPOMC} mice. Shown are representative stainings from 3 mice for each genotype. Brown, horseradish peroxidase (GFP). Single GFP-positive cells are indicated by arrows. Original magnification, 60x. AL, anterior lobe; PL, posterior lobe.

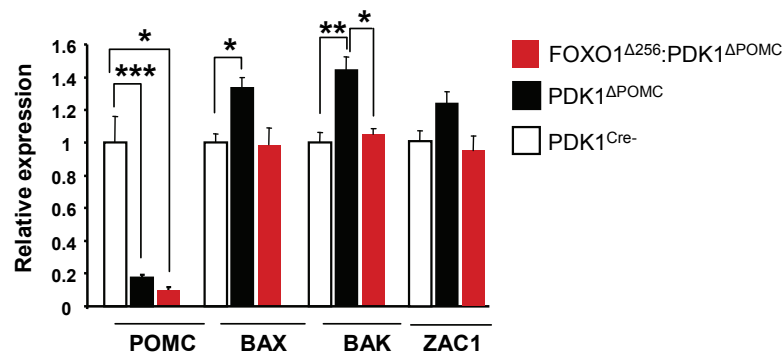


Figure 20: Pituitary pro-apoptotic gene expression in young PDK1^{ΔPOMC} mice

Relative expression of POMC and pro-apoptotic genes in pituitary extracts from male PDK^{Cre-} (n= 8) and PDK1^{ΔPOMC} (n= 11) and FOXO1^{Δ256}.PDK1^{ΔPOMC} (n= 4) mice at the age of 3 weeks as determined by Real-Time PCR. *, p ≤ 0.05; **, p ≤ 0.01; ***, p ≤ 0.001.

3.7 Hypothalamic JNK activity is increased by HFD

Since it was demonstrated that the interaction between FOXO1 and PI3K signalling is a critical regulator of energy homeostasis in the hypothalamus, further signalling pathways potentially impinging on FOXO1 and/or PI3K signalling were investigated. FOXO1 is directly phosphorylated by c-jun N-terminal (JNK) kinases which promotes its nuclear localisation and thus its ability to regulate transcription (88, 97). FOXO and JNK interaction has been shown to be important for life span expectancy, at least in invertebrates (97, 98, 255). Since JNK has been shown to induce insulin resistance at the level of IRS protein through serine phosphorylation, JNK action could potentially negate PI3K activation both proximal (IRS) and distal (FOXO) to IR signalling (199, 256). JNK activation can be induced by hyperlipidemia, oxidative stress or inflammatory cytokine signalling, all of which have been reported to be present in hypothalamic tissue of diet-induced obese rodents (182, 214, 257). To analyse if hypothalamic JNK activity is increased upon HFD feeding in mice, JNK kinase assays were performed. Hypothalamic JNK activity, as assessed by the ability of immunoprecipitated JNK to phosphorylate c-Jun *in vitro*, was significantly increased upon exposure to HFD for 8 weeks (Figure 21).

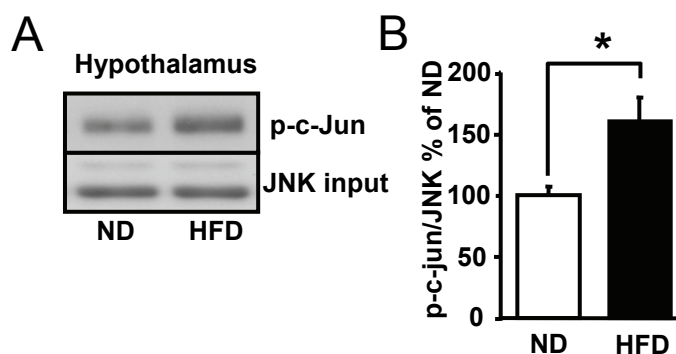


Figure 21: High-fat diet induces hypothalamic JNK activation

A) High-fat diet (HFD) feeding increases hypothalamic JNK activation. C57bl/6 mice were either fed ND or HFD for 8 weeks, and hypothalami were microdissected. Total JNK activity in this tissue was measured by performing JNK kinase assays, and phosphorylation of the JNK target c-Jun was detected by immunoblot. JNK1/3 loading was used as input control. A representative immunoblot from one ND and one HFD animal is shown. B) Quantification of HFD-induced JNK activation in the hypothalamus. The ratio of p-c-Jun to JNK1/3 input was quantified in Western blots of hypothalami from 8 ND and 8 HFD-fed animals as shown in A). *, $p \leq 0.05$.

3.8 HFD induces an inflammatory response in the hypothalamus

Aside from its induction by HFD, JNK is classically activated by stress signals and cytokines and is also capable to mediate cytokine expression itself (184, 198, 258). Therefore, hypothalamic expression of cytokines was determined in control and diet-induced obese mice. After 24 weeks of HFD, hypothalamic expression of TNF α and IL6 mRNA was significantly increased as was a marker of macrophage/microglia activation, lysozyme M (LysM) (Figure 22A, B). Expression of the anti-inflammatory cytokine IL10 was unchanged by HFD, as was the microglia/macrophage marker F4/80 (Figure 22B).

Taken together, local cytokine expression is increased in hypothalami of diet-induced obese mice, indicating that besides increased influx of pro-inflammatory cytokines originating from the periphery, locally expressed cytokines may activate inflammatory signalling, leading to leptin and insulin resistance and thus exacerbating obesity.

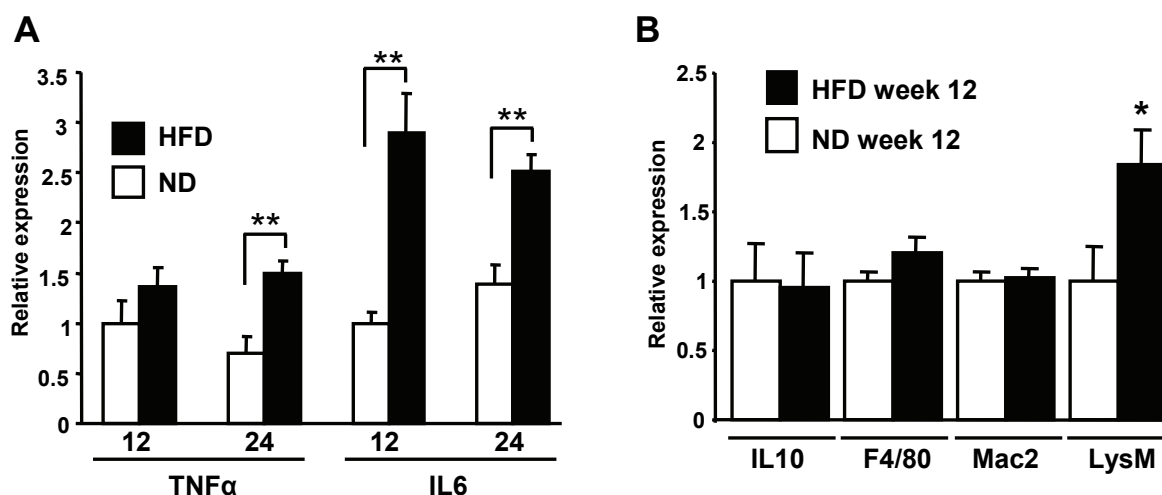


Figure 22: High-fat diet induces hypothalamic transcription of cytokines

A) Relative mRNA expression of TNF α and IL6 in hypothalami taken from wildtype mice fed ND or HFD for 12 and 24 weeks as determined by Real-Time PCR. B) Relative mRNA expression of anti-inflammatory IL10 and the macrophage/microglia marker F4/80 and MAC2, as well as the activation marker LysM in the hypothalami from wildtype mice fed ND or HFD for 12 weeks as determined by Real-Time PCR. *, $p \leq 0.05$; **, $p \leq 0.01$.

3.9 TNF α has both anorexigenic and orexigenic properties in the CNS

Since hypothalamic TNF α expression was increased in diet-induced obese mice, and TNF α is also increased in the circulation of both obese rodent models as well as obese human patients (201, 208), the effect of icv injected TNF α was examined. To this end, vehicle, a low dose (2fMol) or a high dose (2pMol) of TNF α was applied icv into fasted animals, and food intake and body weight upon re-feeding were measured (Figure 23A). These dosages were based on previous work in rats, and also based on the notion, that TNF α concentrations eliciting strong activation of JNK or IKK *in vitro* are in the range of 0.05-2fMol/ μ l (214, 259).

Compared to vehicle, high dose TNF α blunted re-feeding and body weight gain (Figure 23B, C). This is in good agreement with previous reports that high doses of TNF α are involved in mediating fever and sepsis-induced anorexia (216, 218). In contrast, low dose TNF α increased food intake and body weight gain after 4h or 24h refeeding (Figure 23B, C).

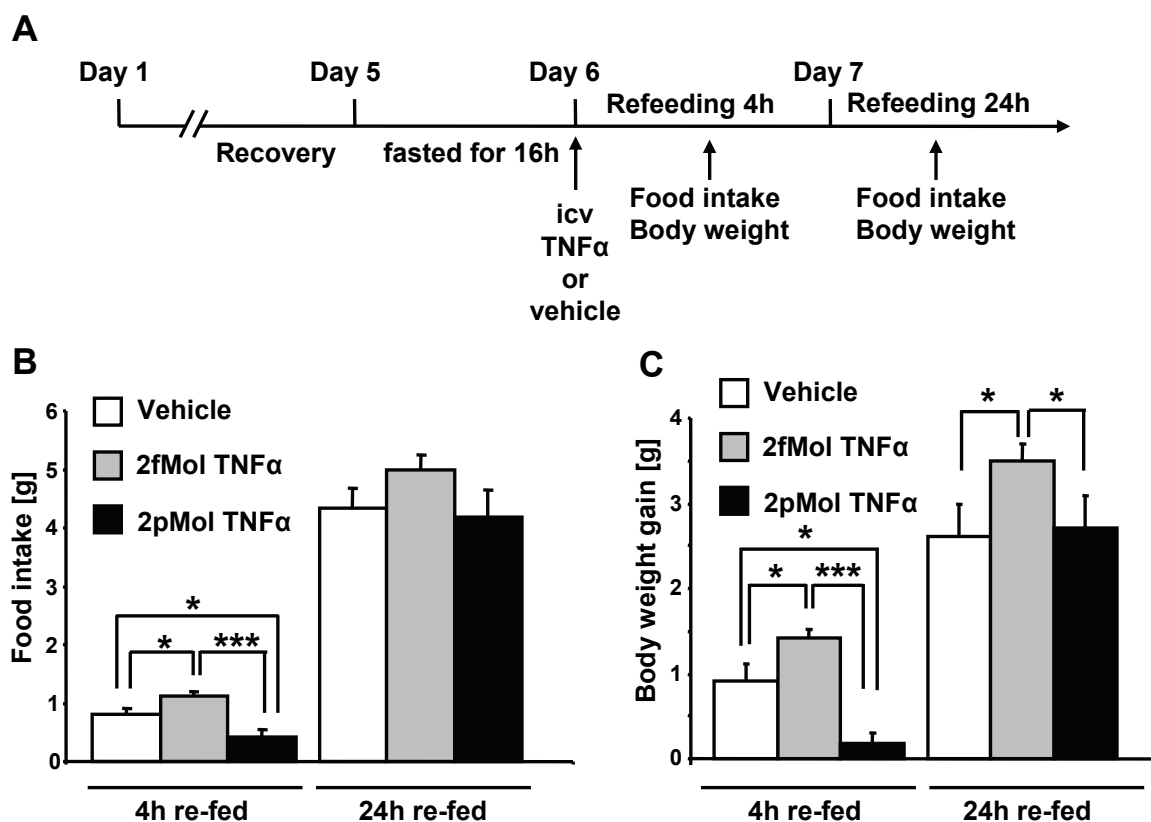


Figure 23: TNF α elicits orexigenic and anorexigenic effects in a dose-dependent manner

A) Scheme of surgery, injection schedule and experimental paradigm. B) Vehicle, low (2fMol) or high (2pMol) TNF α doses were icv injected into 9 week old wild type mice after an overnight fast, and food intake was measured 4 and 24 later. C) Body weight changes in the experimental paradigm depicted in A) and B). (n= 13, 20, 11). *, $p \leq 0.05$; ***, $p \leq 0.001$.

3.10 HFD-induced hypothalamic expression of cytokines is not readily reversible

The increase in hypothalamic cytokine mRNA expression induced by HFD may be caused by hyperlipidemia, hyperglycemia or increased circulating proinflammatory cytokines found in obese animals and patients (190, 211, 260-262). To further define the cause underlying this increased expression of cytokines, an experimental paradigm was designed in which mice were subjected to HFD for 20 weeks, followed by 50% of these mice being subjected to ND (denoted as HFD->ND), whereas all other mice continued to be fed HFD (denoted HFD). After 3 weeks of ND, the HFD->ND group showed significantly decreased body weight and glucose tolerance as measured by GTT (Figure 24A-C). Hypothalamic cytokine expression was evaluated in HFD and HFD->ND mice. Compared to the HFD group, expression of TNF α was even further elevated, whereas expression of the anti-inflammatory cytokine IL10 was reduced compared to the HFD group (Figure 24D). While expression of the macrophage markers F4/80 and Mac2 was unchanged between groups, a

significant decrease in LysM expression was noted, which might indicate decreased activation of local macrophages/microglia cells. Taken together, inflammatory cytokine expression of the hypothalamus is not readily reversed by a reduced uptake of dietary lipids at a time when body weight and glucose homeostasis are significantly improved, but instead shows further up-regulation of TNF α expression.

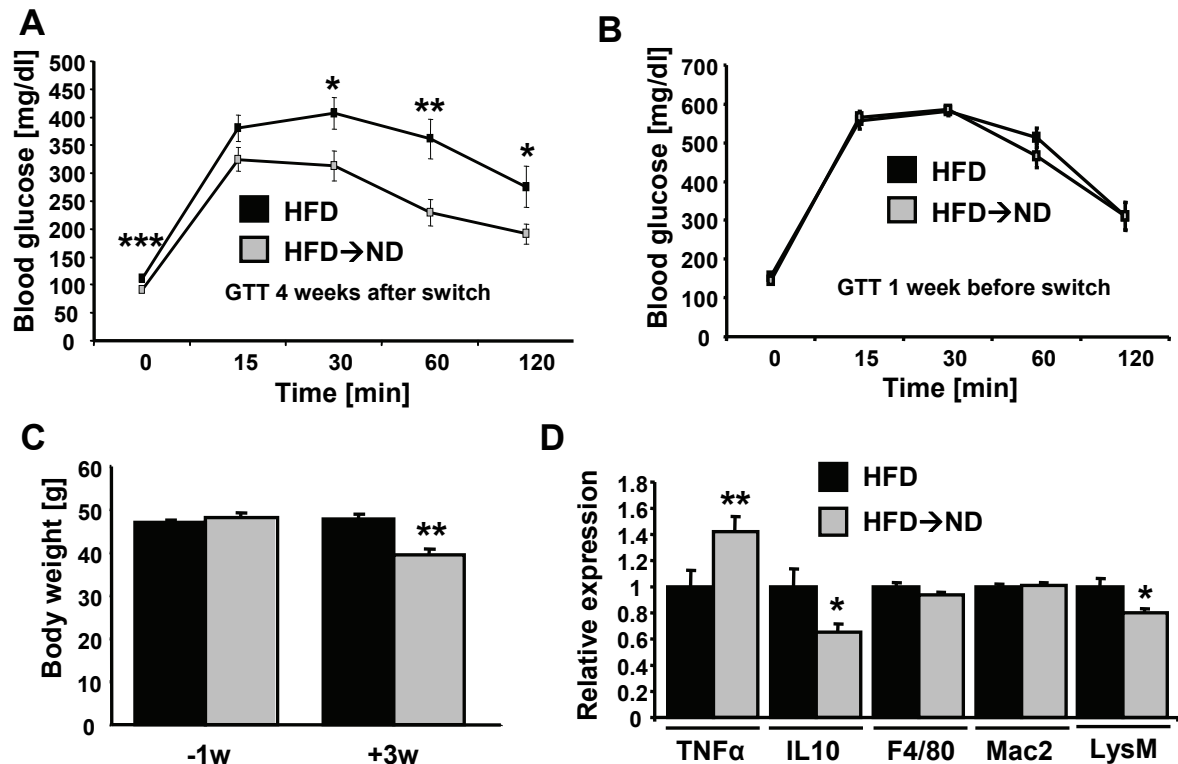


Figure 24: Diet-induced up-regulation of cytokine expression is not readily reversible by diet modulation

A) Wildtype mice were fed HFD for 20 weeks. Half of the group (n= 8) were then fed ND for 4 weeks while the other group continued to feed on HFD, and a GTT was performed. B) GTT in both groups one week before half the group was switched onto ND. C) Body weights of both groups one week before (-1w) and three weeks after the switch (+3w). D) Relative hypothalamic expression of cytokines and macrophage markers was measured by Real-Time analysis in both groups of mice (n= 8 per group). *, p \leq 0.05; **, p \leq 0.01; ***, p \leq 0.001.

3.11 Generation of JNK1^{ANES} mice

Conventional JNK1 knockout animals are protected against diet-induced obesity and glucose intolerance (199). Both saturated lipids as well as inflammatory cytokines are able to activate JNK signalling (205, 260). To further investigate the role of hypothalamic JNK1 signalling, mice with central ablation of JNK1 were created. To this end, mice were generated in which exon 2 of JNK1 is flanked by loxP sites (JNK1^{fl/fl} mice, kindly provided by Dr. T. Wunderlich; Figure 25A). Cre-mediated deletion of exon 2 leads to a frame shift and a premature STOP codon, inhibiting expression of normal JNK1 protein. JNK1^{fl/fl} mice were crossed with Nestin-Cre mice to generate mice homozygous for the loxP flanked exon 2 of the JNK1 gene and heterozygous for the Nestin-Cre transgene (denominated as JNK1^{ANES}

mice) (Figure 25B). Littermates lacking the Nestin-Cre transgene were used as controls (genotype $JNK1^{fl/fl}$, denominated as controls).

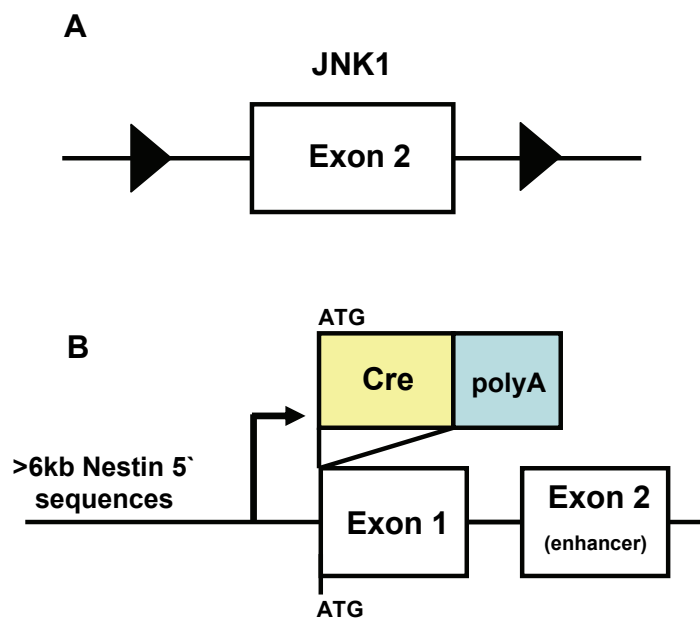


Figure 25: Nestin cell-specific deletion of JNK1

A) In $JNK1^{fl/fl}$ mice, exon 2 is flanked by loxP sequences. Cre-mediated ablation of this exon will induce a frame-shift, leading to a premature stop of translation. B) Nestin-Cre mice are carriers of a Nestin-Cre transgene in which a Cre expression cassette was inserted into the translational initiation site (ATG) of Nestin exon 1. Exon 2 of the Nestin gene contains a known enhancer of Nestin gene expression.

Nestin-Cre mice express the Cre recombinase under control of the *Nestin* promoter, which, at the time of generation of these mice, was thought to be neuron-specific (239). To ascertain that presence of the Nestin-Cre transgene itself has no effect on weight regulation on its own, body weight of mice with and without the transgene was monitored. In accordance with previous reports, there was no difference in body weight between mice with or without the transgene (Figure 26A) (56, 263). Efficient JNK1 protein ablation and severely decreased JNK1 mRNA expression was detected in the brain of $JNK1^{\Delta NES}$ mice, whereas JNK1 expression was unchanged in peripheral tissues such as liver and skeletal muscle (Figure 26B, C). In addition to neurons, the *Nestin* gene is also expressed in a subset of pituitary stem cells, allowing deletion of target genes in all cell types of the adult pituitary using Nestin-Cre transgene animals (264). In line with this, deletion of JNK1 was detected in pituitaries of $JNK1^{\Delta NES}$ mice using a PCR-based analysis (Figure 26D). Taken together, $JNK1^{\Delta NES}$ mice are a novel tool to study the role of neuronal and pituitary JNK1 signalling *in vivo*.

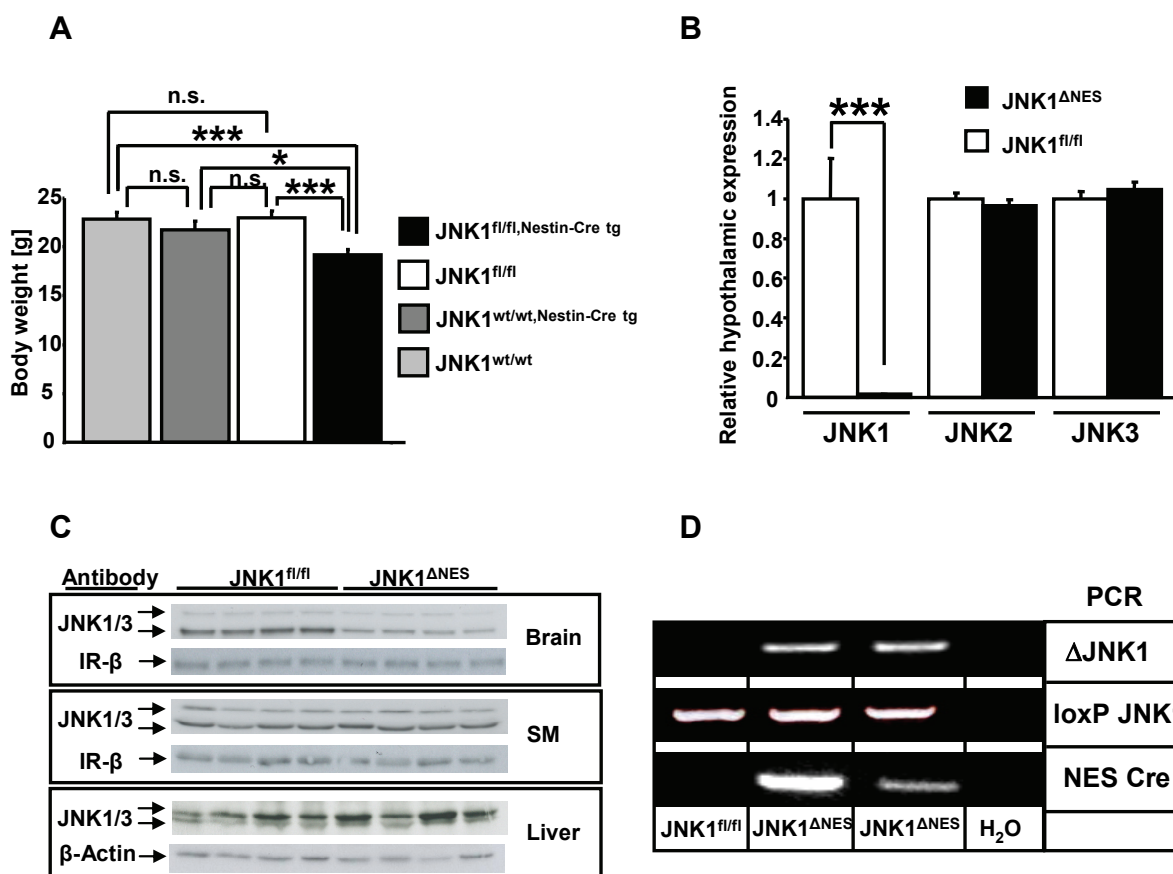


Figure 26: Generation of JNK1^{ANes} mice.

A) Presence of Nestin-Cre construct or the loxP flanked JNK1 exon does not impair body weight control. Body weight of wild type, Nestin-Cre transgenic, control and JNK1^{ANes} mice at the age of 6 weeks is shown (n>= 4 per group). B) Hypothalamic expression of JNK 1, 2 and 3 in JNK1^{fl/fl} and JNK1^{ANes} mice (n=6 per group) as measured by real-Time PCR. C) Western blot analysis of JNK1/3 and IR-β or β-actin expression (loading control) in whole brain, liver and skeletal muscle (SM) of JNK1^{ANes} and JNK1^{fl/fl} mice (n=4 per group). Note that since no JNK1-specific antibody is available, an antibody with dual JNK1 and JNK3 specificity was used. D) Deletion of the JNK1 allele in the pituitary of JNK1^{ANes} mice. After DNA extraction from the pituitary, PCR was used to detect the deleted JNK1 allele (ΔJNK1), the loxP flanked JNK1 alleles as well as presence of the Nestin-Cre transgene. *, p ≤ 0.05; ***, p ≤ 0.001.

3.12 JNK activity is increased in pituitaries of diet-induced obese mice

Since the Nestin-Cre transgene targeted JNK1 ablation also to pituitary stem cells, it was investigated if JNK activity is up-regulated in pituitaries from diet-induced obese mice. Pituitary JNK activity, as assessed by the ability of immunoprecipitated JNK to phosphorylate c-Jun *in vitro*, was significantly increased upon exposure to HFD, mirroring the effect of HFD on hypothalamic JNK activity (Figure 27). Thus, JNK1^{ANes} mice are a suitable tool to analyze the role of HFD-induced activation of JNK signalling in the hypothalamus and pituitary.

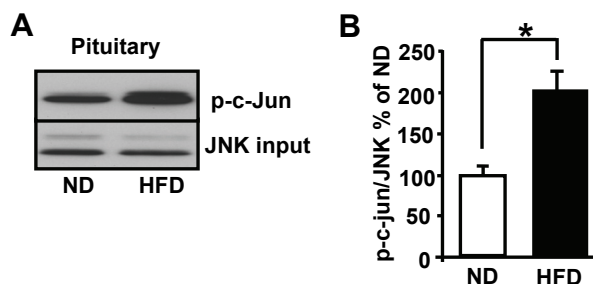


Figure 27: Pituitary JNK activation upon high-fat feeding

A) High-fat diet (HFD) feeding increases pituitary JNK activation. C57BL/6 mice were either fed ND or HFD for 8 weeks, and pituitaries were isolated. Total JNK activity in this tissue was measured by performing JNK kinase assays, and phosphorylation of the JNK target c-Jun was detected by immunoblot. JNK1/3 loading was used as input control. A representative immunoblot from one ND and one HFD animal is shown. B) Quantification of HFD-induced JNK activation in the pituitary. The ratio of p-c-Jun to JNK1/3 input was quantified in Western blots of pituitaries from 4 ND and 4 HFD-fed animals as shown in A). *, $p \leq 0.05$.

3.13 Unchanged behaviour in JNK1^{ΔNES} mice

JNKs are involved in the development of brain structures, since mice lacking 2 out of the three JNK isoforms show severe brain defects (265). To determine if behaviour of JNK1^{ΔNES} mice was affected, which might impair their ability to find food, or increase body weight in case of reduced spontaneous activity, several behavioural tests were performed.

To study locomotor control, control and JNK1^{ΔNES} mice were subjected to the Rotarod setup. In this experiment, mice are put on a at the beginning slowly rotating rod, which accelerates over time. The time on the rod was monitored. Control and JNK1^{ΔNES} mice kept on the rod for the same time, indicating unchanged locomotor control (Figure 28A).

To examine anxiety behaviour, both control and JNK1^{ΔNES} mice were subjected to the elevated zero maze paradigm, in which mice are put on an elevated ring, which has two closed and two open sides. Using an automated video-based system, the time in which the mouse was in the closed or the open part was measured. To avoid predators, mice tend to stay in the closed part of the maze, and accordingly, control mice stayed in the closed part for an average of 90% of the time. JNK1^{ΔNES} mice also strongly preferred to stay in the closed part of the maze, indicating unchanged anxiety behaviour (Figure 28B).

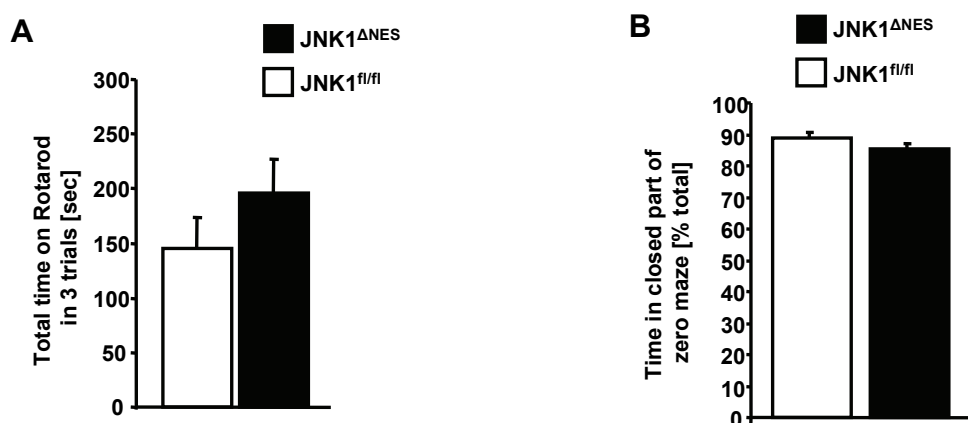


Figure 28: Unchanged locomotor control and anxiety in JNK1^{ΔNES} mice

A) Rotarod analysis of control and JNK1^{ΔNES} mice. Control and JNK1^{ΔNES} mice were mounted on the Rotarod, and total time on the rotating rod until mouse fell from the rotarod was measured (n= 8 per group). B) Zero maze analysis of control and JNK1^{ΔNES} mice. Control and JNK1^{ΔNES} mice were put on the zero maze, and the time in which the mouse stayed in the closed part of the maze was tracked by an automatic visual system. n= 8 per genotype.

Since JNKs are involved in brain development, learning and memory recovery was tested using the Morris water maze paradigm (265). In this test, mice are put into a round pool filled with water which is divided into four quadrants. In one quadrant, a platform is submerged. Mice dislike swimming, therefore search for the platform, on which they come to rest. During daily trials, mice are put into different quadrants of the pool, and learn to find the hidden platform using localisation markers, which are permanently structured around the pool. In line with this, control mice found the platform 50% faster at the end of the trial compared to day 1 (Figure 29A). JNK1^{ΔNES} mice performed similar, indicating unimpaired memory (Figure 29A). On the last day of trials, the platform was removed, and the time each mouse spent in the correct quadrant (searching for the platform) was measured. Control and JNK1^{ΔNES} mice performed similarly, indicating unchanged spatial memory and memory retrieval in JNK1^{ΔNES} mice (Figure 29B). Taken together, JNK1^{ΔNES} mice show normal anxiety, locomotor and learning behaviour.

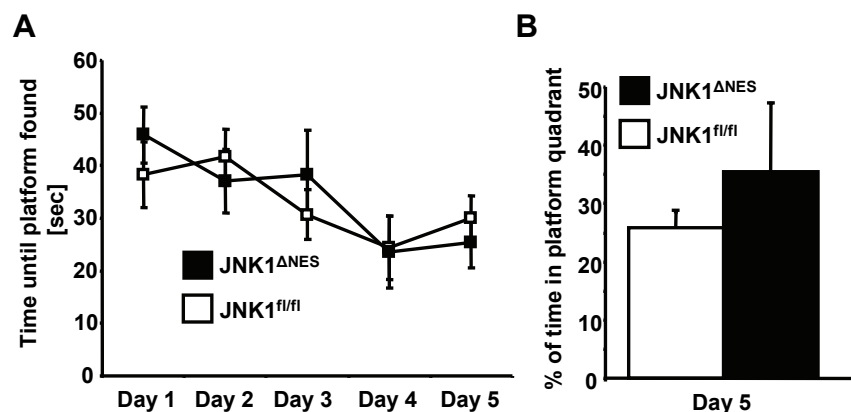


Figure 29: Unchanged water maze performance by JNK1^{ANES} mice

A) Morris water maze analysis of control and JNK1^{ANES} mice. Control and JNK1^{ANES} mice were trained daily for 4 days to memorize the location of the platform, and the time taken by each mouse to find the platform was measured by an automatic, software based system (n= 8 per group). B) On the fifth day of the Morris water maze analysis, the platform was removed from the pool, and the time the mouse swam in the quadrant in which the platform had been was automatically measured by an automatic, software based system (n= 8 per genotype).

3.14 Decreased weight but unchanged body composition in JNK1^{ANES} mice

To gain insight into the effect of neuronal and pituitary JNK1 signalling in the control of energy homeostasis, body weight was monitored in control and JNK1^{ANES} mice. JNK1^{ANES} mice showed reduced body weight at the time of weaning, and continued to show decreased body weight until the end of the study at the age of 16 weeks (Figure 30A). Although body weight was decreased, nuclear magnetic resonance (NMR) analysis revealed unchanged body composition between control and JNK1^{ANES} mice, indicating that the reduction in body weight is not due to loss of fat or lean mass (Figure 30B). In line with this finding, food intake when corrected for lean mass was unchanged (Figure 30C). Calorimetric analysis of control and JNK1^{ANES} mice showed a strong tendency to increased oxygen consumption during the night in JNK1^{ANES} mice, although this did not reach statistical significance (Figure 30D). Fuel preference as determined by respiratory quotient as well as activity was comparable between both groups (Figure 30E, F).

Taken together, JNK1^{ANES} mice show decreased body weight but unchanged body composition and food intake with only minor increases in energy expenditure when fed ND.

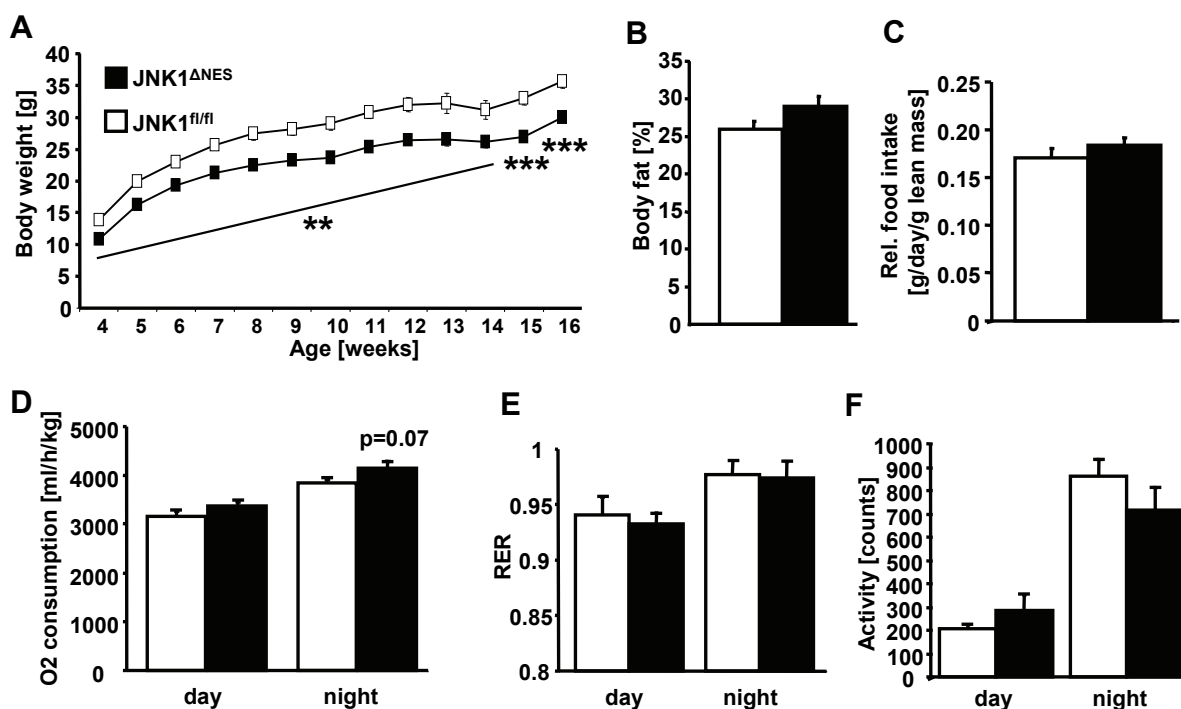


Figure 30: Decreased weight but unchanged body composition in JNK1^{ΔNES} mice on Normal Diet

A) Average body weight of JNK1^{fl/fl} and JNK1^{ΔNES} mice on normal diet (n= 12 per group). B) Body fat content of JNK1^{fl/fl} and JNK1^{ΔNES} mice on normal diet at the age of 16 weeks as measured by nuclear magnetic resonance (NMR) analysis (n= 12 per group). C) Relative food intake of JNK1^{fl/fl} and JNK1^{ΔNES} mice on normal diet at the age of 13 weeks (n= 8 per group). Relation of food intake to body weight was calculated individually for each mouse. D) Daily and nightly oxygen consumption of JNK1^{fl/fl} and JNK1^{ΔNES} mice on normal diet at the age of 13 weeks (n= 8 per group). Oxygen consumption was calculated per gram lean mass of each individual mouse. E, F) Daily and nightly respiratory quotient (RER) and activity of control and JNK1^{ΔNES} mice on normal diet at the age of 13 weeks (n= 8 per group). **, p ≤ 0.01; ***, p ≤ 0.001.

3.15 Improved glucose homeostasis in JNK1^{ΔNES} mice under ND conditions

Hypothalamic insulin signalling regulates peripheral glucose production, uptake and insulin sensitivity (32, 102, 126, 151, 166). Since CNS JNK1 may be a negative regulator of insulin signalling, glucose homeostasis of control and JNK1^{ΔNES} mice was measured. JNK1^{ΔNES} mice showed reduced random and fasted blood glucose levels at all ages tested (Figure 31A). Whereas both control and JNK1^{ΔNES} mice performed as well during GTTs, JNK1^{ΔNES} mice also showed improved insulin sensitivity as measured by ITTs accompanied by reduced circulating insulin concentrations (Figure 31B-D). Taken together, JNK1^{ΔNES} mice show increased insulin sensitivity and improved glycemic control when fed ND.

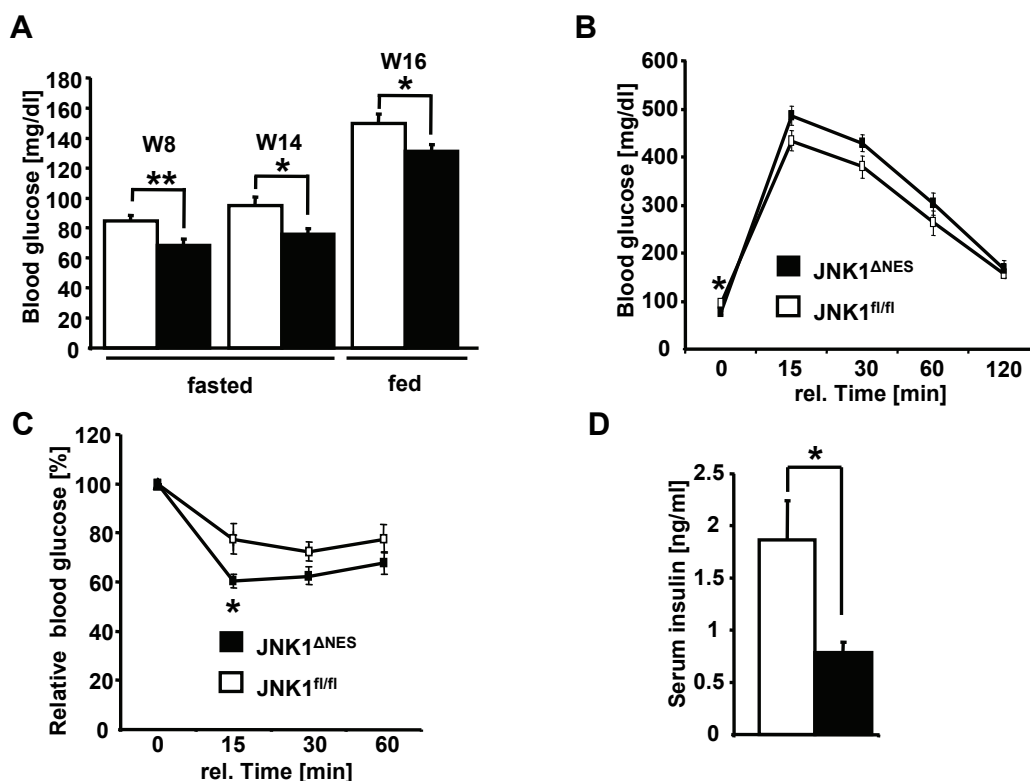


Figure 31: Improved insulin sensitivity and glycemic control in JNK1^{ΔNES} mice on Normal Diet

A) Fasted and fed blood glucose concentration of JNK1^{fl/fl} and JNK1^{ΔNES} mice on normal diet at the indicated ages (n= 10-17 per group). B) Intraperitoneal glucose tolerance test in JNK1^{fl/fl} and JNK1^{ΔNES} mice on normal diet at the age of 14 weeks (n= 9-10 per group). C) Intraperitoneal insulin tolerance test in JNK1^{fl/fl} and JNK1^{ΔNES} mice on normal diet at the age of 15 weeks (n= 9-10 per group). D) Serum insulin concentrations in JNK1^{fl/fl} and JNK1^{ΔNES} mice on normal diet at the age of 8 weeks (n= 8 per group). *, p ≤ 0.05; **, p ≤ 0.01-

3.16 JNK1^{ΔNES} mice show decreased body weight but are not protected from diet-induced obesity

JNK1^{ΔNES} mice demonstrated elevated insulin sensitivity, and mildly reduced glucose levels as well as reduced body weight when fed ND. To examine if JNK1^{ΔNES} mice are protected from diet-induced obesity and the associated glucose intolerance, control and JNK1^{ΔNES} mice were fed HFD after weaning. Again, JNK1^{ΔNES} mice showed significantly decreased body weight compared to controls (Figure 32A). Nonetheless, NMR analysis revealed no differences in fat content compared to controls, indicating that JNK1^{ΔNES} mice are not protected from diet-induced obesity (Figure 32B). Food intake, when normalized for lean mass, was also comparable between control and JNK1^{ΔNES} mice (Figure 32C). Calorimetric analysis revealed significantly increased oxygen consumption in JNK1^{ΔNES} mice even when corrected for lean body mass (Figure 32D), while fuel preference or activity was similar between groups (Figure 32E, F). Taken together, JNK1^{ΔNES} mice are not protected from diet-induced obesity, but show increased energy expenditure during HFD feeding.

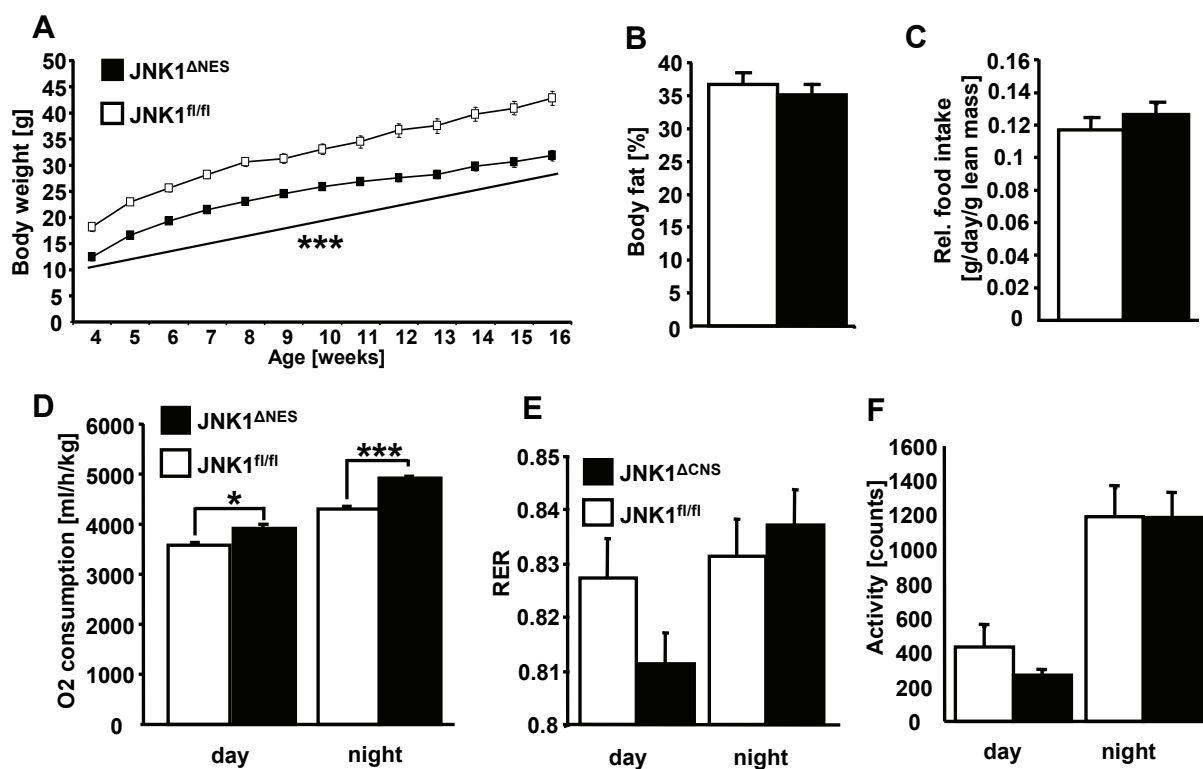


Figure 32: Decreased weight but unchanged body composition in $JNK1^{\Delta NES}$ mice on HFD

A) Average body weight of $JNK1^{fl/fl}$ and $JNK1^{\Delta NES}$ mice on high-fat diet (n= 12 per group). B) Body fat content of $JNK1^{fl/fl}$ and $JNK1^{\Delta NES}$ mice on high-fat diet at the age of 16 weeks as measured by nuclear magnetic resonance (NMR) analysis (n= 12 per group). C) Relative food intake of $JNK1^{fl/fl}$ and $JNK1^{\Delta NES}$ mice on high-fat diet at the age of 13 weeks (n= 8 per group). Relation of food intake to body weight was calculated individually for each mouse. D) Daily and nightly oxygen consumption of $JNK1^{fl/fl}$ and $JNK1^{\Delta NES}$ mice on high-fat diet at the age of 13 weeks (n= 8 per group). Oxygen consumption was calculated per gram lean mass of each individual mouse. E, F) Daily and nightly respiratory quotient (RER) and activity of control and $JNK1^{\Delta NES}$ mice on high-fat diet at the age of 13 weeks. n= 8 per group. *, $p \leq 0.05$; ***, $p \leq 0.001$.

3.17 Improved glucose homeostasis in obese $JNK1^{\Delta NES}$ mice

Since $JNK1^{\Delta NES}$ mice showed improved glucose homeostasis under normal diet conditions, glucose tolerance tests were performed with control and $JNK1^{\Delta NES}$ mice fed HFD. These experiments revealed significantly improved glucose clearance in $JNK1^{\Delta NES}$ mice (Figure 33A). In line with this finding, fasting and random fed glucose concentrations were reduced in $JNK1^{\Delta NES}$ mice compared to controls at all ages tested (Figure 33B). $JNK1^{\Delta NES}$ mice also performed better in ITTs and showed reduced circulating insulin concentrations, indicating improved insulin sensitivity under HFD conditions (Figure 33C, D). Taken together, $JNK1^{\Delta NES}$ mice are protected from obesity-induced glucose intolerance and insulin resistance.

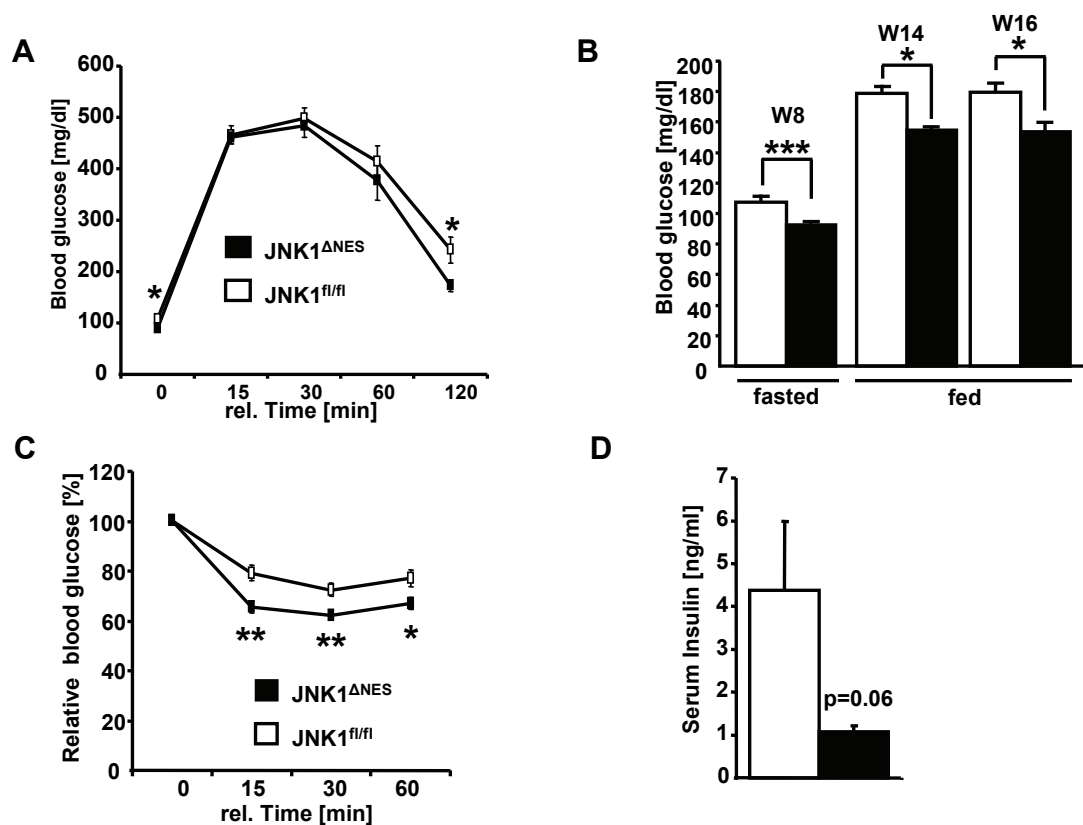


Figure 33: Improved glucose tolerance and insulin sensitivity in obese JNK1^{ANES} mice

A) Intraperitoneal glucose tolerance test in JNK1^{fl/fl} and JNK1^{ANES} mice on high-fat diet at the age of 14 weeks (n= 10 per group). B) Fasted and fed blood glucose concentration of JNK1^{fl/fl} and JNK1^{ANES} mice on high-fat diet at the indicated ages (n= 10-17 per group). C) Intraperitoneal insulin tolerance test in JNK1^{fl/fl} and JNK1^{ANES} mice on high-fat diet at the age of 15 weeks (n= 9-10 per group). D) Serum insulin concentrations in JNK1^{fl/fl} and JNK1^{ANES} mice on high-fat diet at the age of 10 weeks (n= 8 per group). *, p ≤ 0.05; **, p ≤ 0.01; ***, p ≤ 0.001.

3.18 JNK1^{ANES} mice show increased hypothalamic insulin but not leptin sensitivity

Hypothalamic leptin and insulin signalling is able regulate peripheral glucose homeostasis (32, 102, 126, 151, 166, 266, 267). Since JNK1^{ANES} mice showed improved glucose homeostasis under both ND and HFD conditions, improvement of hypothalamic insulin and/or leptin sensitivity might underlie this phenotype. Therefore, intraperitoneal leptin sensitivity tests were performed. Both control and JNK1^{ANES} mice fed HFD reacted to repeated leptin injections with only minor body weight or food intake reductions (Figure 34A, B), indicating leptin resistance in both groups. To further evaluate hypothalamic leptin sensitivity, indwelling cannulas were used to inject leptin into the lateral ventricle (icv), and food intake and body weight was monitored 24h later. Control and JNK1^{ANES} mice fed ND showed similarly reduced body weight and food intake upon leptin treatment, indicating that also under ND conditions, JNK1^{ANES} mice do not show increased leptin sensitivity, which was in line with unchanged serum leptin concentrations under ND conditions (Figure 34C-E).

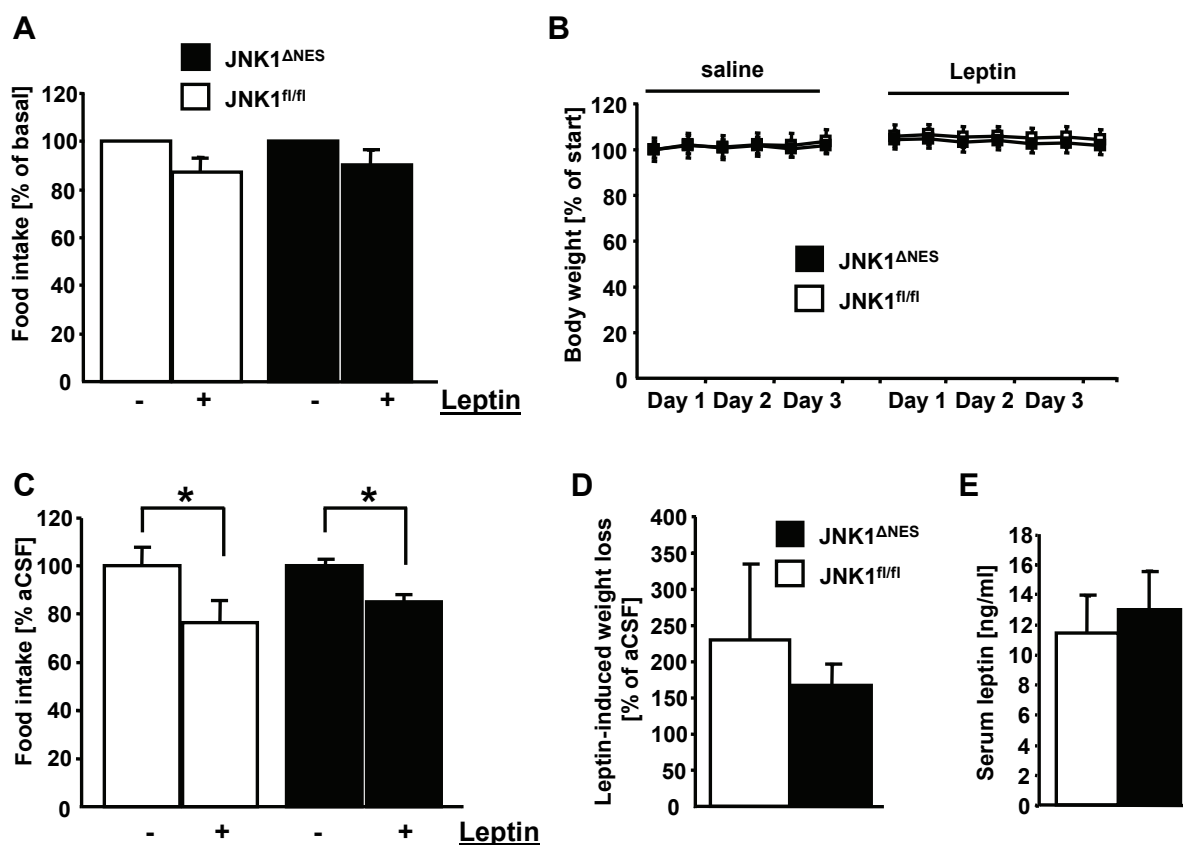


Figure 34: Unaltered leptin sensitivity in JNK1^{ΔNES} mice

A, B) Changes in food intake and body weight after intraperitoneal leptin treatment in control and JNK1^{ΔNES} mice on high-fat diet at the age of 13 weeks (n=8 per group). Data represent daily food intake after a 3-day treatment with twice-daily injections of saline or 2 mg/kg leptin. Body weight was measured twice a day. C) 24h food intake after icv leptin treatment in JNK1^{fl/fl} (n= 5) and JNK1^{ΔNES} mice (n=4) mice on normal diet at the age of 12 weeks. Mice were injected with either vehicle or 2μg leptin immediately before onset of dark phase, and food intake was measured 24h later. D) Body weight loss 24h after icv leptin treatment in JNK1^{fl/fl} (n= 5) and JNK1^{ΔNES} mice (n= 4) mice on normal diet at the age of 12 weeks. Mice were injected with either vehicle or 2μg leptin immediately before onset of dark phase, and body weight was measured 24h later. Shown is fold change of body weight after leptin injection compared to vehicle injection. E) Serum leptin concentration of JNK1^{fl/fl} and JNK1^{ΔNES} mice on normal diet at the age of 12 weeks (n= 8 per group). *, p ≤ 0.05.

In the same experimental paradigm, insulin was applied icv to both control and JNK1^{ΔNES} mice. The specific amount of insulin (2mU on ND/4mU on HFD) was chosen, since earlier observations indicated no effect on food intake and body weight 24h after icv injection of these boluses (Jens C. Brüning, personal communication). In line with these findings, icv insulin injection did not change body weight or food intake compared to vehicle in control animals fed ND or HFD (Figure 35A-D). In contrast, JNK1^{ΔNES} mice fed either ND or HFD showed significantly reduced body weight and food intake even 24h after insulin injection (Figure 35A-D).

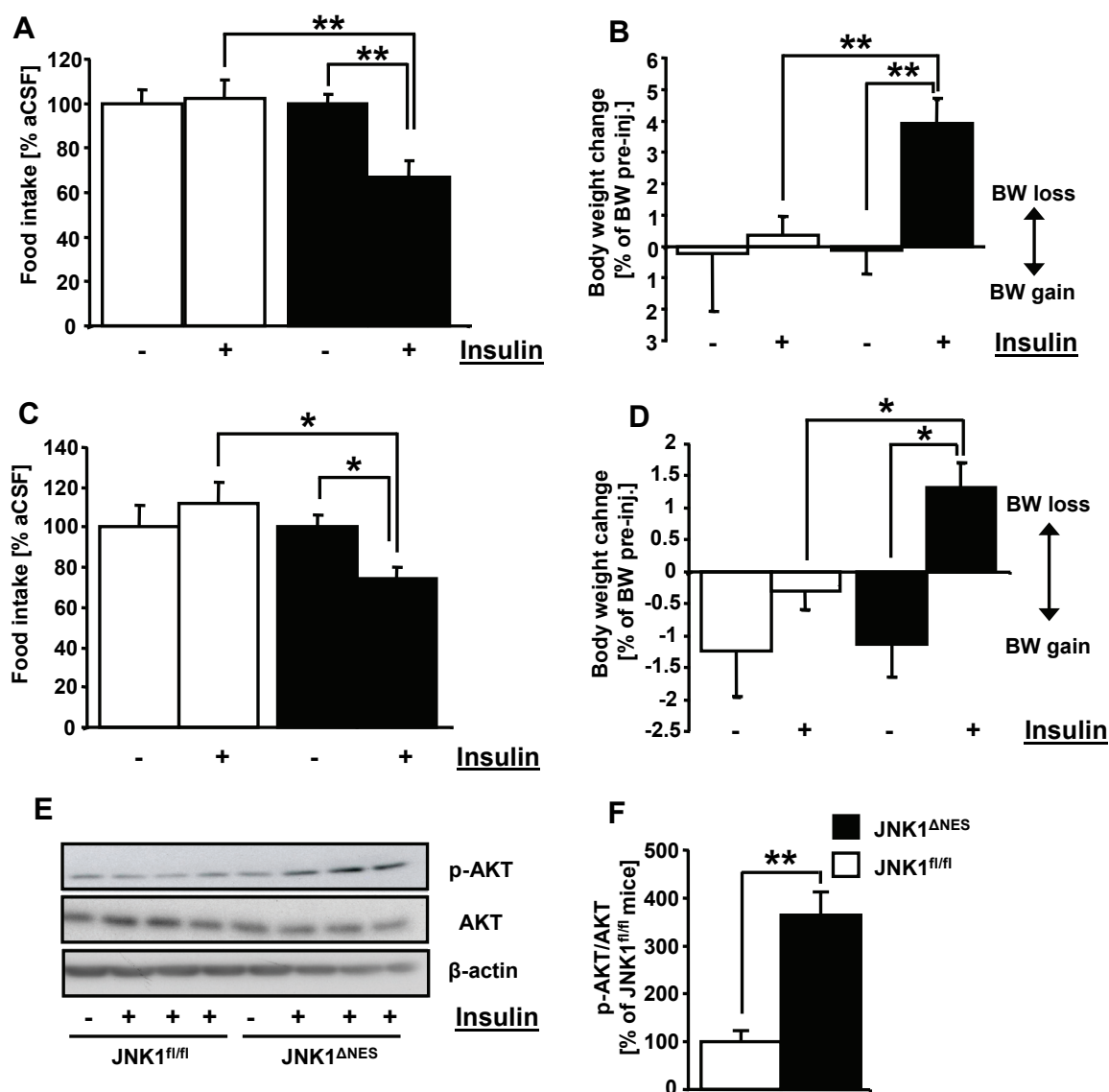


Figure 35: Elevated hypothalamic insulin sensitivity in JNK1^{ANES} mice

A) 24h food intake after icv insulin treatment in JNK1^{fl/fl} (n= 9) and JNK1^{ANES} (n=8) mice on normal diet at the age of 12 weeks. Mice were injected with either vehicle or 2mU insulin immediately before onset of dark phase, and food intake was measured 24h later. B) Body weight loss 24h after icv insulin treatment in JNK1^{fl/fl} (n= 9) and JNK1^{ANES} (n= 8) mice on normal diet at the age of 12 weeks. Mice were injected with either vehicle or 2mU insulin immediately before onset of dark phase, and body weight was measured 24h later. Shown is percent change of body weight after insulin injection compared to vehicle injection. C) 24h food intake after icv insulin treatment in JNK1^{fl/fl} (n= 5) and JNK1^{ANES} (n=5) mice on high-fat diet at the age of 10 weeks. Mice were injected with either vehicle or 4mU insulin immediately before onset of dark phase, and food intake was measured 24h later. D) Body weight change 24h after icv insulin treatment in JNK1^{fl/fl} (n= 5) and JNK1^{ANES} (n= 5) mice on high-fat diet at the age of 10 weeks. Mice were injected with either vehicle or 4mU insulin immediately before onset of dark phase, and body weight was measured 24h later. Shown is percent change of body weight after insulin injection compared to aCSF injection. E) Hypothalamic AKT activation upon icv insulin treatment is improved in JNK1^{ANES} mice. JNK1^{fl/fl} and JNK1^{ANES} mice on high-fat diet at the age of 10 weeks were fasted for 48h, injected with aCSF or 4mU insulin and sacrificed 20min later. Immunoblot was performed for phosphorylated (activated) AKT, total AKT and β-actin protein content. F) Quantification of insulin-induced AKT phosphorylation compared to total AKT content shown in E). *, p ≤ 0.05; **, p ≤ 0.01.

To further assess if hypothalamic insulin action was improved in JNK1^{ANES} mice, control and JNK1^{ANES} mice were fasted for 48h to reduce background AKT phosphorylation,

injected with insulin, and sacrificed 20min later. Western blot analysis revealed improved insulin-mediated AKT phosphorylation in JNK1^{ΔNES} mice (Figure 35E, F). Taken together, JNK1 ablation improves hypothalamic insulin action.

3.19 Unchanged hypothalamic expression of neuropeptides, cytokines and ER stress mediators in JNK1^{ΔNES} mice

To determine if increased hypothalamic insulin sensitivity in concurrence with normal leptin sensitivity had a direct effect on local neuropeptide expression, Real-Time PCR was used to measure neuropeptide mRNA levels. No consistent changes in expression of POMC, AgRP or NPY were detected (Figure 36A). Hypothalamic ER stress has been reported in obese mouse models (233). Similarly, HFD feeding led to increased expression of ER stress markers glucose-regulated protein 78kD (GRP78) and spliced (activated) XBP-1 (XBP-1s) in controls, and to the same extent in JNK1^{ΔNES} mice, while expression of CHOP remained unaltered (Figure 36B). In wild type mice fed HFD for approximately 12-14 weeks, hypothalamic IL6 but not TNF α was elevated (Figure 22A). Accordingly, IL6 expression was increased by trend upon HFD feeding both in control and JNK1^{ΔNES} mice, while TNF α was not altered (Figure 36C). Importantly, TNF α and IL6 expression was similar between genotypes.

Taken together, these findings indicate that hypothalamic ablation of JNK1 improves insulin sensitivity even in the unaltered presence of cytokine expression and ER stress.

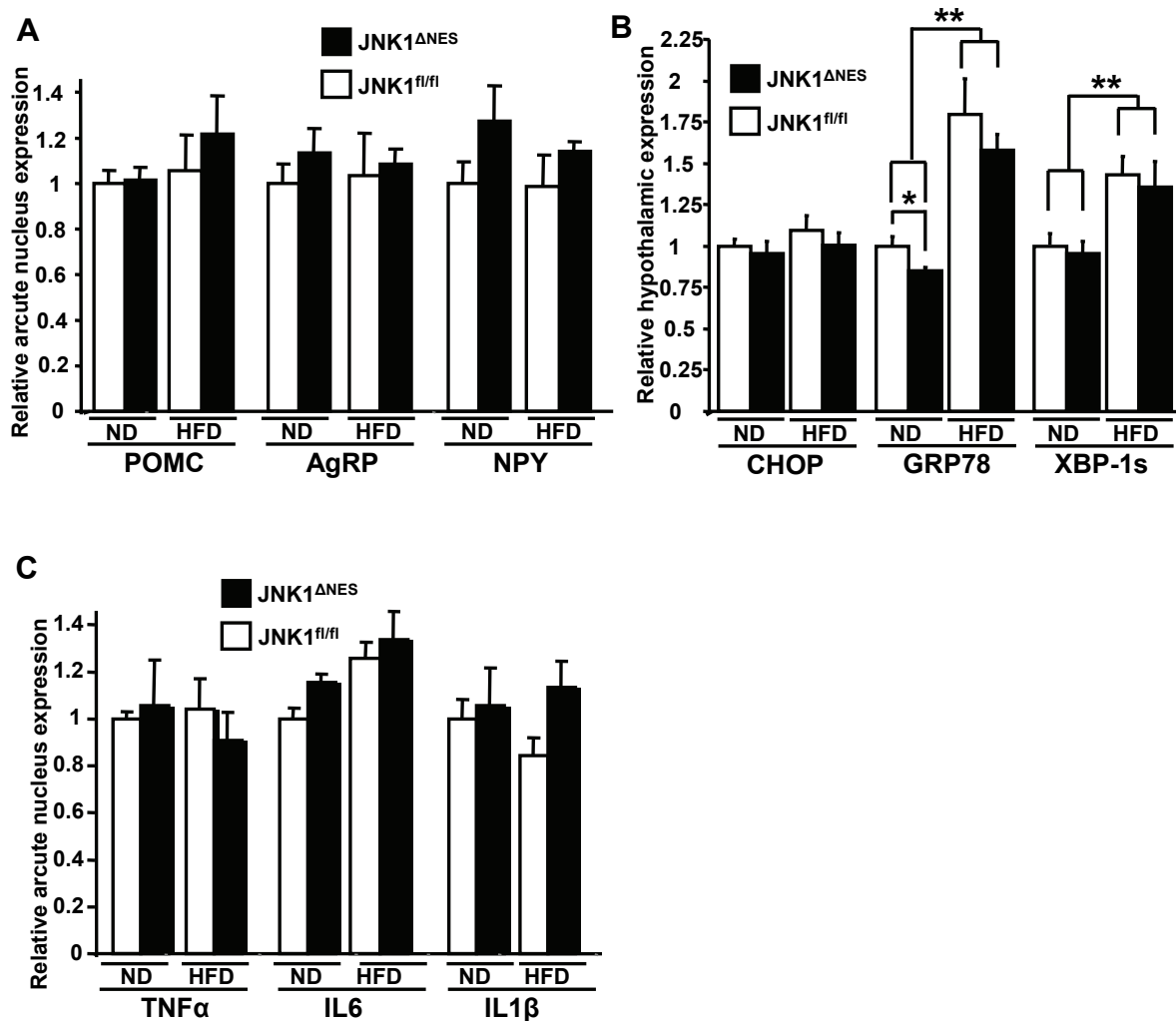


Figure 36: Hypothalamic neuropeptide, cytokine and ER stress marker expression is unchanged in JNK1 Δ NES mice

A) Neuropeptide expression in the arcuate nucleus. Arcuate nuclei of control and JNK1 Δ NES mice either on normal chow or on high-fat diet were microdissected at the age of 16 weeks. Real-Time expression analysis of the anorexigenic neuropeptide proopiomelanocortin (POMC) and the orexigenic neuropeptides Neuropeptide Y (NPY) and Agouti-related protein (AgRP) was performed (n= 6 per group). B) Hypothalamic expression of ER stress markers. Hypothalami of control and JNK1 Δ NES mice either on normal chow or on high-fat diet were microdissected at the age of 16 weeks. Real-Time PCR expression analysis of the ER stress markers CCAAT/enhancer binding protein ϵ (CHOP), the chaperone glucose-regulated protein 78kD (GRP78) and spliced (activated) form of the X-box binding protein 1 (XBP-1s) was performed (n= 6 per group). C) Cytokine expression in the arcuate nucleus. Arcuate nuclei of control and JNK1 Δ NES mice either on normal chow or on high-fat diet were microdissected at the age of 16 weeks. Real-Time expression analysis of the cytokines tumor necrosis factor α (TNF α), Interleukin 6 (IL6) and Interleukin 1 β (IL1 β) was performed (n= 6 per group). *, p \leq 0.05; **, p \leq 0.01.

3.20 HFD induces ER stress in the pituitary in a JNK1-independent manner

Since JNK activation had been shown to take place in the pituitary of diet-induced obese animals, it was asked, if ER stress is induced in parallel. In line with diet-induced ER stress in the hypothalamus, mRNA expression of ER stress markers such as GRP78 and spliced XBP-1 were also increased in pituitaries of HFD-fed control animals (Figure 37).

Interestingly, CHOP, but not GRP78 expression was increased in $JNK1^{\Delta NES}$ mice fed ND. Nonetheless, $JNK1^{\Delta NES}$ mice showed similar expression of ER stress markers under HFD feeding conditions, indicating that JNK1 deficiency does not protect from diet-induced ER stress in the pituitary (Figure 37).

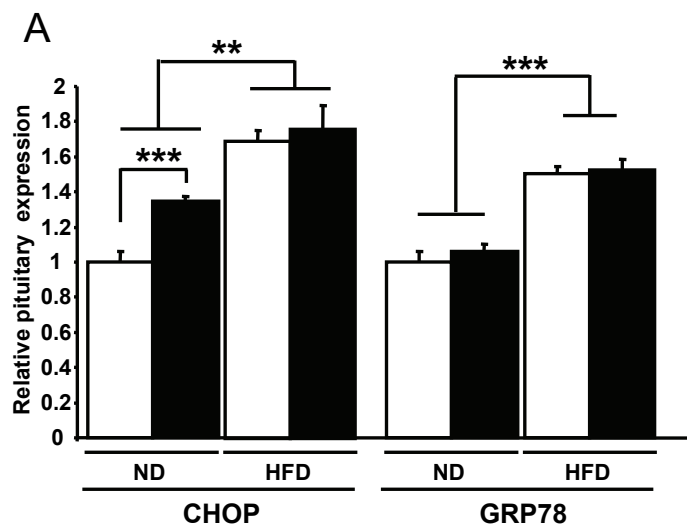


Figure 37: HFD induces ER stress marker expression in the pituitary

A) Pituitary expression of ER stress markers. Pituitaries of control and $JNK1^{\Delta NES}$ mice either on normal chow or on high-fat diet were microdissected at the age of 16 weeks. Real-Time expression analyses of the ER stress markers CHOP and GRP78 was performed (n= 6 per group). **, $p \leq 0.01$; ***, $p \leq 0.001$.

3.21 $JNK1^{\Delta NES}$ mice show decreased activation of the somatotrophic axis

$JNK1^{\Delta NES}$ mice consistently showed decreased body weight both under ND and HFD conditions, although body composition was unchanged. Therefore, to assess if changes in longitudinal growth were responsible for this decrease in body weight, naso-anal length was measured in control and $JNK1^{\Delta NES}$ mice at the age of 16 weeks. $JNK1^{\Delta NES}$ mice showed significantly reduced naso-anal length (Figure 38A). Furthermore, it has been noted that diet-induced obese rodents show increased linear growth compared to ND fed animals, although the mechanism underlying this phenotype is poorly defined (268, 269). While control animals were significantly longer when fed HFD, this increase in body length was blunted in $JNK1^{\Delta NES}$ mice fed HFD, again pointing to differential control of the somatic growth axis (Figure 38A).

In control of somatic growth, hypothalamic neurons release growth hormone releasing hormone (GHRH) which acts on somatotrophs in the pituitary to produce and release growth hormone (GH). Growth hormone in turn acts on GH receptors on the liver, inducing insulin-like growth factor (IGF)-1 transcription and release, which acts on chondrocytes to increase longitudinal growth (for review see (270)). One biomarker of the somatotrophic axis is serum

IGF-1, which was examined by ELISA. IGF-1 levels were decreased by 50% in $JNK1^{\Delta NES}$ mice (Figure 38B).

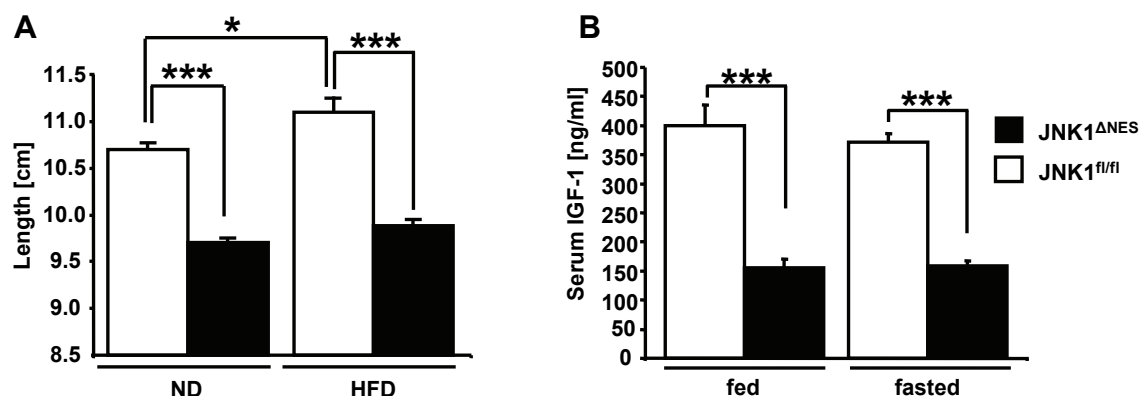


Figure 38: Serum IGF-1 is reduced in $JNK1^{\Delta NES}$ mice

A) Naso-anal length of $JNK1^{fl/fl}$ and $JNK1^{\Delta NES}$ on normal or high-fat diet at the age of 16 weeks (n= 9 per group). B) Serum IGF-1 concentrations of $JNK1^{fl/fl}$ (n= 10) and $JNK1^{\Delta NES}$ (n= 10) on normal diet either random fed or fasted at the age of 10 weeks. *, $p \leq 0.05$; ***, $p \leq 0.001$.

To determine if diminished GH was underlying this phenotype, circulating growth hormone was measured in both groups of mice. Despite considerable variation of GH concentrations in control mice, presumably due to the pulsatile secretion pattern of GH, $JNK1^{\Delta NES}$ mice showed strongly decreased levels of circulating GH (Fig. 39A).

Neuronal JNK1 ablation might potentially regulate expression of hypothalamic neuropeptides regulating the somatotrophic axis, namely GHRH and somatostatin, which can inhibit GH release (271). Nonetheless, hypothalamic mRNA expression of both peptides was unchanged, indicating that JNK1 mediated regulation of the somatotrophic axis does not occur on the hypothalamic level (Figure 39B). Therefore, pituitary GH mRNA expression was measured through Real-Time PCR analysis. In line with decreased GH and IGF-1 levels in circulation, decreased GH mRNA expression was detected in pituitaries of $JNK1^{\Delta NES}$ mice (Figure 39C).

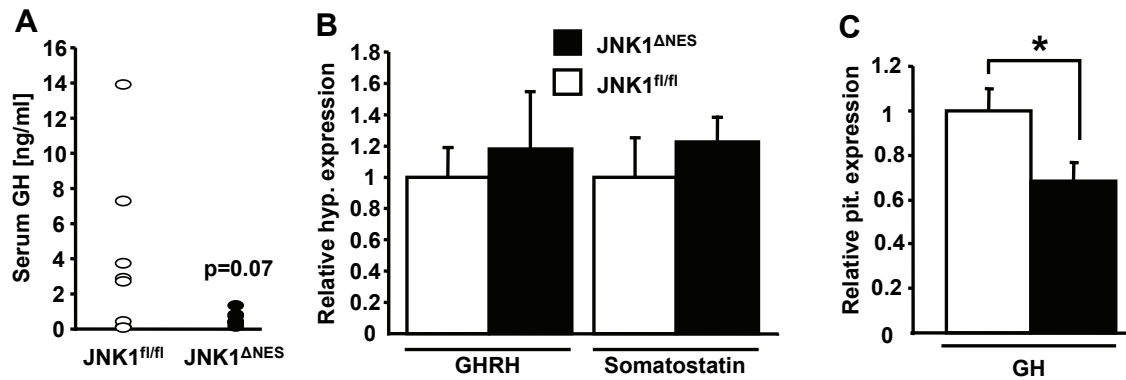


Figure 39: Somatic growth is reduced at the control level of the pituitary in JNK1^{ΔNES} mice

A) Serum GH concentrations of JNK1^{fl/fl} and JNK1^{ΔNES} on ND at the age of 10 weeks (n= 8 per group). B) Hypothalamic expression of GHRH and somatostatin of JNK1^{fl/fl} and JNK1^{ΔNES} mice on ND at the age of 16 weeks as measured by Real-Time PCR (n= 6 per group). C) Pituitary expression of GH of JNK1^{fl/fl} and JNK1^{ΔNES} mice at the age of 16 weeks as measured by Real-Time PCR (n= 6 per group). *, $p \leq 0.05$.

These findings could either be a consequence of reduced transcription, or of reduced survival of somatotrophs due to JNK1 ablation. Immunohistochemical analysis of GH positive cells revealed unaltered pituitary structure, indicating that cell loss does not account for the decrease in GH expression (Figure 40A).

In the face of unchanged GHRH expression but decreased GH production, an intermediate signalling molecule could be regulated in JNK1^{ΔNES} mice. The GHRH receptor (GHRHR) is crucial for the ability of GHRH to stimulate GH expression and release (272-274). Pituitaries from JNK1^{ΔNES} mice showed decreased GHRHR expression compared to control mice fed either ND or HFD, indicating that decreased GHRHR signalling may underlie the decreases in circulating GH and subsequently IGF-1 (Figure 40B). Notably, GHRHR expression was elevated in diet-induced obese controls (Figure 40B).

To further understand regulation of GHRHR expression, mRNA levels of PIT-1, a critical regulator of GHRHR expression was determined (275). PIT-1 expression was reduced by 30% in pituitary of JNK1^{ΔNES} mice (Figure 40C). Taken together, JNK1^{ΔNES} mice show decreased somatotrophic GHRHR expression, and subsequently reduced GH and IGF-1 serum levels and ultimately impaired somatic growth, indicating an unexpected critical role for pituitary JNK1 signalling in control of somatic growth and body length.

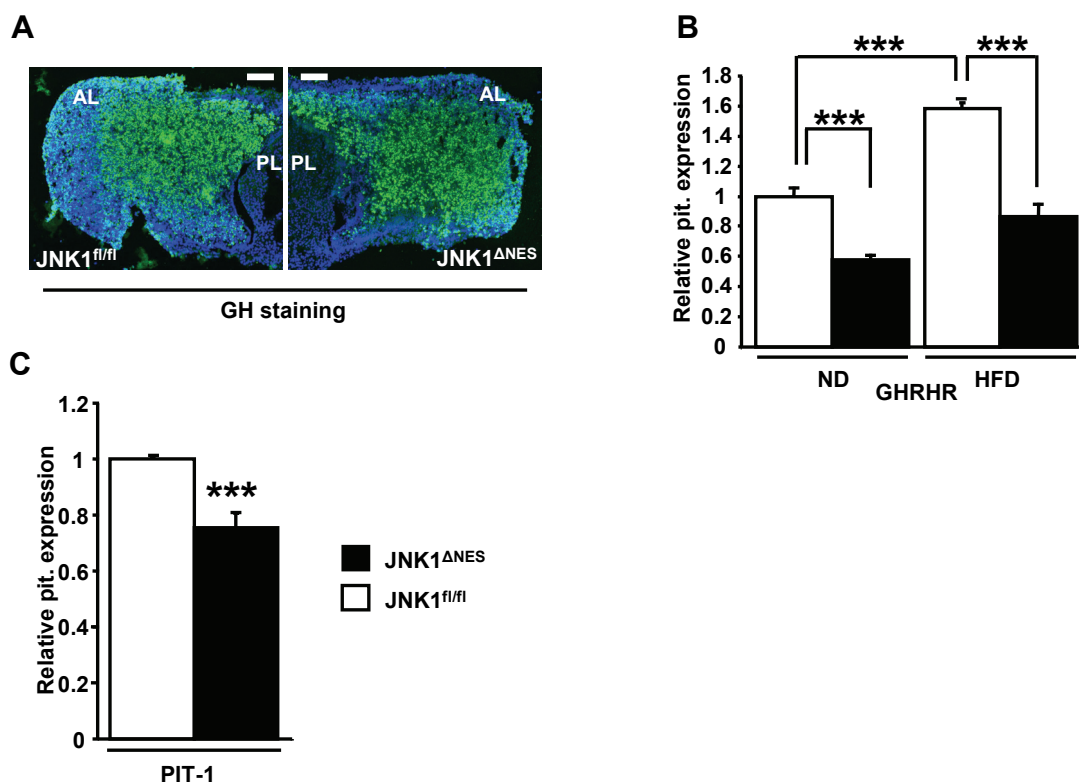


Figure 40: Pituitary expression of PIT-1 and its target GHRHR is regulated in JNK1^{ΔNES} mice

A) Immunohistochemistry for GH from pituitary sections of JNK1^{fl/fl} and JNK1^{ΔNES} mice at the age of 16 weeks (Green, GH; blue, DAPI). At least 3 mice of each genotype were analysed (PL, posterior lobe; AL, anterior lobe; scale bar 80 μ m). B) Pituitary expression of GHRHR of JNK1^{fl/fl} and JNK1^{ΔNES} mice fed ND or HFD at the age of 16 weeks as measured by Real-Time PCR (n= 6 per group). C) Pituitary expression of Pituitary-specific positive transcription factor 1 (PIT-1) of JNK1^{fl/fl} and JNK1^{ΔNES} mice fed ND at the age of 16 weeks as measured by Real-Time PCR (n= 6 per group). ***, p \leq 0.001.

3.22 JNK1^{ΔNES} mice show increased activation of the thyroid axis

To further define the role of JNK1 in the pituitary, it was asked whether JNK1 deficiency also affects other pituitary functions besides the somatotropic axis. As mentioned before, pituitary expression and release of the POMC cleavage product adrenocorticotrophic hormone (ACTH) stimulates release of adrenal corticosterone (in rodents) or cortisol (in humans) (136). Corticosterone and cortisol are known to be antagonists of insulin action, and loss of circulating corticosterone might explain the increased insulin sensitivity of JNK1^{ΔNES} mice. Nonetheless, corticosterone concentrations were unchanged between control and JNK1^{ΔNES} mice (Figure 41A), indicating that general pituitary function was not severely impaired.

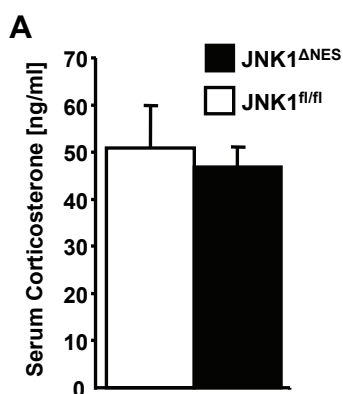


Figure 41: Corticosterone levels are normal in JNK1^{ANES} mice

A) Unchanged circulating corticosterone in JNK1^{ANES} mice. Serum corticosterone in control and JNK1^{ANES} mice at the age of 10 weeks was measured by ELISA (n= 8 per group).

Besides somatotrophs and corticotrophs, thyrotrophs in the pituitary play an important role in energy homeostasis. Thyrotrophs are stimulated by hypothalamic thyroid releasing hormone (TRH) to express and release thyroid stimulating hormone (TSH) β , which acts on the thyroid gland, increasing circulating triiodothyronine (T3) (and thyroxine (T4)) levels, who eventually stimulate energy expenditure. Serum T3 levels were increased in JNK1^{ANES} mice (Figure 42A). In line with increased T3 levels and increased oxygen consumption as monitored by calorimetric analysis, brown adipocytes in interscapular brown adipose tissue (BAT) of JNK1^{ANES} mice appeared smaller, which is a hallmark of increased energy expenditure (Figure 42B). Examination of BAT expression of uncoupling proteins revealed a trend for increased uncoupling protein (UCP)1 mRNA, which is crucial for energy dissipation by proton leakage across the mitochondrial membrane, but not in UCP2 and UCP3 mRNA levels, whose role in energy expenditure is controversial (276-278)(Figure 42C).

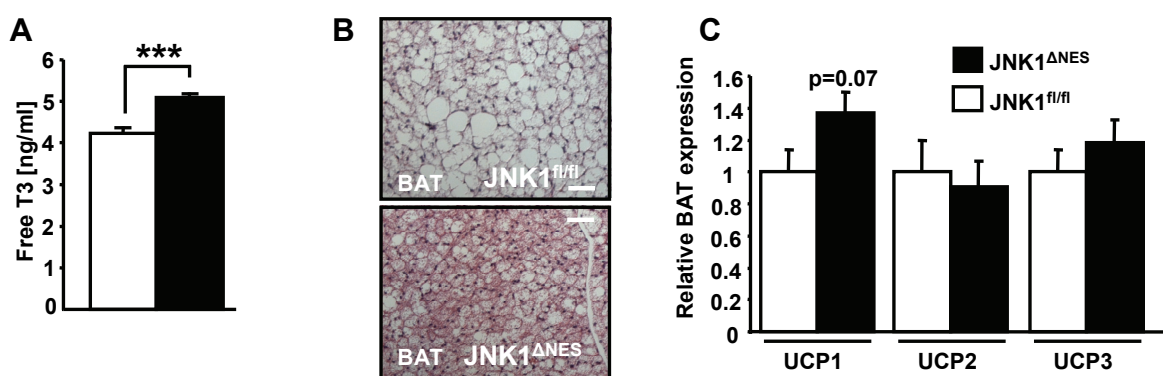


Figure 42: JNK1^{ANES} mice show increased activation of the thyrotropic axis

A) Serum free T3 concentration of JNK1^{fl/fl} and JNK1^{ANES} mice on ND at the age of 10 weeks (n= 8 per group). B) Representative H&E staining of brown adipose tissue of control and JNK1^{ANES} mice on HFD at the age of 16 weeks. BAT sections of 3 mice per genotype were analysed. Scale bars, 40 μ m. C) Brown adipose tissue expression of UCP1, 2 and 3 of JNK1^{fl/fl} and JNK1^{ANES} mice on HFD at the age of 16 weeks as measured by Real-Time PCR (n= 6 per group). ***, p \leq 0.001.

To find out if changes in hypothalamic mRNA expression of TRH were underlying the increased energy expenditure, Real-Time analysis was performed. This revealed no consistent change in TRH mRNA expression, again pointing to a pituitary autonomous phenotype (Figure 43A). In line with the finding of increased circulating T3 concentrations, a more than threefold increase of TSH β mRNA expression was detected in pituitaries of JNK1^{ANES} mice (Figure 43B). Importantly, and inverse to what was found with pituitary GHRHR mRNA levels, TRH receptor (TRHR) expression was increased in pituitaries of JNK1^{ANES} mice (Figure 43C).

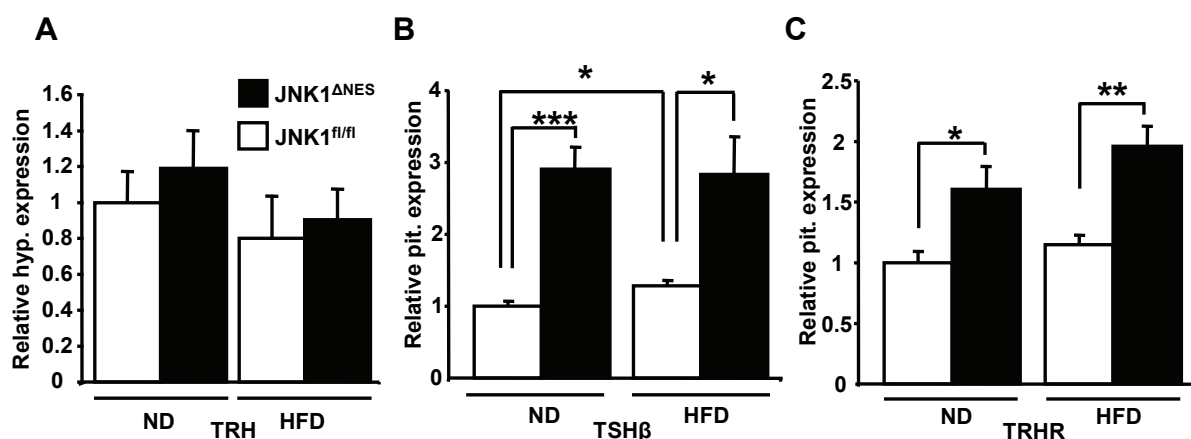


Figure 43: Elevated pituitary activation of the thyrotropic axis in JNK1^{ANES} mice

A) Hypothalamic expression of TRH as measured by Real-Time PCR analysis (n= 5 per group). B) Pituitary expression of TSH β of JNK1^{fl/fl} and JNK1^{ANES} mice on ND or HFD at the age of 16 weeks as measured by Real-Time PCR (n= 6 per group). C) Pituitary expression of TRHR of JNK1^{fl/fl} and JNK1^{ANES} mice on ND or HFD at the age of 16 weeks as measured by Real-Time PCR (n= 6 per group). *, p \leq 0.05; **, p \leq 0.01; ***, p \leq 0.001.

Immunohistological analysis of TSH β positive cells did not show significant structural alterations in pituitaries of JNK1^{ANES} mice, indicating that TRHR expression, but not a change in TSH β cell number underlies the increased expression of TSH β mRNA (Figure 44A). To study the pituitary cell-autonomous regulation of TRHR expression, a rat pituitary cell line (GH4C1) was employed which has been previously used to study TRHR expression (279). GH4C1 cells were incubated with vehicle, JNK inhibitor (SP600125), as well as PI3K (LY294002) and ERK (PD98059) inhibitors to gain further insight into control of TRHR expression. While incubation with either PI3K or ERK inhibitor did not have an effect on TRHR expression, incubation with a JNK inhibitor significantly increased TRHR expression by 70%, which is similar to the increase also seen in JNK1^{ANES} mice *in vivo* (Figure 44B). Thus, in line with the increase in pituitary TRHR expression of JNK1^{ANES} mice, this finding highlights the importance of JNK1-dependent signalling in pituitary-autonomous regulation

of the thyroid axis. Taken together, $JNK1^{\Delta NES}$ mice show increased thyroid action caused by an increase in pituitary $TSH\beta$ and TRHR expression.

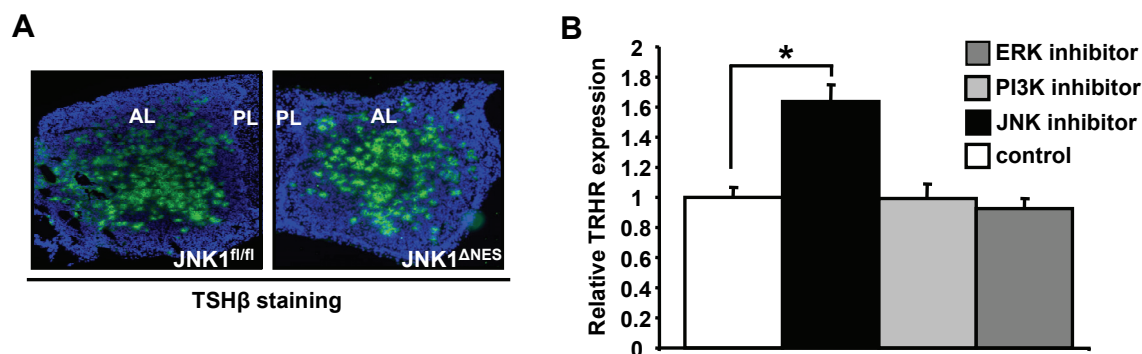


Figure 44: JNK inhibition increases TRHR expression *in vitro*

A) Immunohistochemistry for $TSH\beta$ from pituitary sections of $JNK1^{fl/fl}$ and $JNK1^{\Delta NES}$ mice at the age of 16 weeks (Green, $TSH\beta$; blue, DAPI). At least 2 mice of each genotype were analysed (Original magnification, 100x. PL, posterior lobe; AL, anterior lobe). B) Expression of TRHR in the rat pituitary cell line GH4C1. Expression of TRHR was measured after 16h incubation with control (0.1% DMSO), JNK (SP600125), PI3K (LY294002) or ERK (PD98059) inhibitor. For each sample within an experiment, triplicate values were averaged and then the means of the Real-Time PCR results from three independent experiments were compared. *, $p \leq 0.05$.

3.23 $JNK1^{\Delta NES}$ mice are protected from hepatic dysfunction upon HFD

Central and peripheral insulin sensitization as well as increased thyroid activity have been shown to protect from hepatic steatosis and deregulated gluconeogenesis during obesity, whereas GH action is thought to induce hepatic gluconeogenesis by its negative effect on insulin sensitivity, although very recently a direct role of GH on hepatic lipid and glucose metabolism has also been documented (151, 280-283). Therefore, hepatic tissue morphology in control and $JNK1^{\Delta NES}$ mice fed HFD was investigated. Relative liver weight was decreased in $JNK1^{\Delta NES}$ mice compared to controls, which could point to decreased lipid accumulation (Figure 45A). In line with this notion, Oil-Red O staining showed a reduction in stainable neutral lipids in livers of $JNK1^{\Delta NES}$ mice fed HFD (Figure 45B).

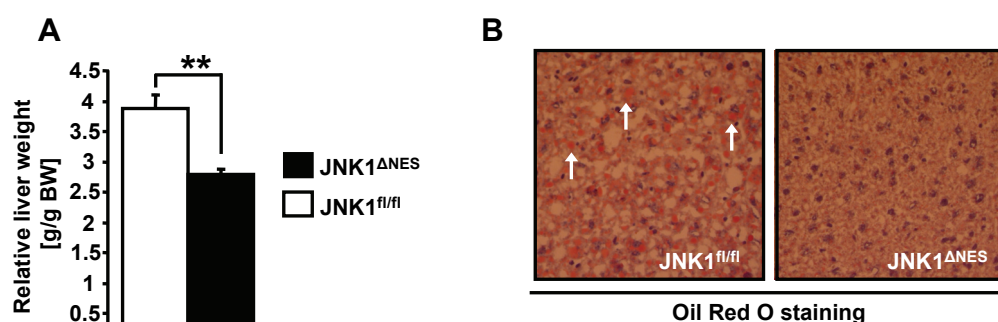


Figure 45: JNK1^{ANES} mice are protected from diet-induced hepatosteatosis

A) Relative liver weight of JNK1^{fl/fl} and JNK1^{ANES} mice on high-fat diet at the age of 16 weeks (n= 12 per group). Relation of liver mass to body weight was calculated individually for each mouse. B) Representative Oil red O staining of hepatic tissue of JNK1^{fl/fl} and JNK1^{ANES} mice on high-fat diet at the age of 16 weeks (Original magnification 100x). Liver sections of 3 animals per genotype were analysed. **, p ≤ 0.01.

Chromatographic analysis of liver extracts revealed a specific reduction in diacylglyceride (DG) and triacylglyceride (TG) content in JNK1^{ANES} mice without changes in free fatty acids or cholesterol (Figure 46A, B).

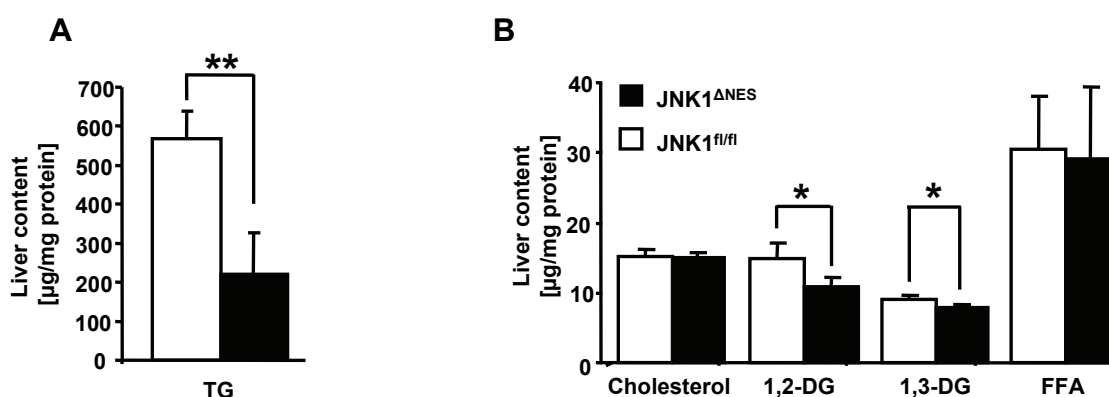


Figure 46: Reduced hepatic triglyceride content in HFD-fed JNK1^{ANES} mice

A) Hepatic triglyceride (TG) content of JNK1^{fl/fl} and JNK1^{ANES} mice on high-fat diet at the age of 16 weeks (n= 4 per group). B) Hepatic cholesterol, 1,2- and 1,3-Diacylglycerides (DG), and free fatty acid (FFA) content of JNK1^{fl/fl} and JNK1^{ANES} mice on high-fat diet at the age of 16 weeks (n= 4 per group). *, p ≤ 0.05; **, p ≤ 0.01.

Since JNK1^{ANES} mice also showed resistance to obesity-induced glucose tolerance, it was analysed if besides protection against hepatic steatosis, JNK1^{ANES} mice also exhibited an amelioration of obesity-associated elevations of hepatic glucose production (HGP). Hence, pyruvate tolerance tests (PTT) were performed in control and JNK1^{ANES} mice to investigate regulation of hepatic gluconeogenesis during fasting, since pyruvate is rapidly taken up and metabolized to glucose in livers of fasting animals. Importantly, JNK1^{ANES} mice showed significantly decreased glucose levels in PTTs, indicating that reduced HGP contributes to the

improved glucose homeostasis of $JNK1^{\Delta NES}$ mice (Figure 47A). Several groups have independently shown that insulin action on (AgRP) neurons decreases HGP via local expression of IL6 in liver (151, 163). In line with increased hypothalamic insulin action found in $JNK1^{\Delta NES}$ mice, significantly increased hepatic IL6 mRNA expression was found concurrent with mildly reduced expression of the key gluconeogenic enzyme glucose-6-phosphatase (G6P) (Figure 47B).

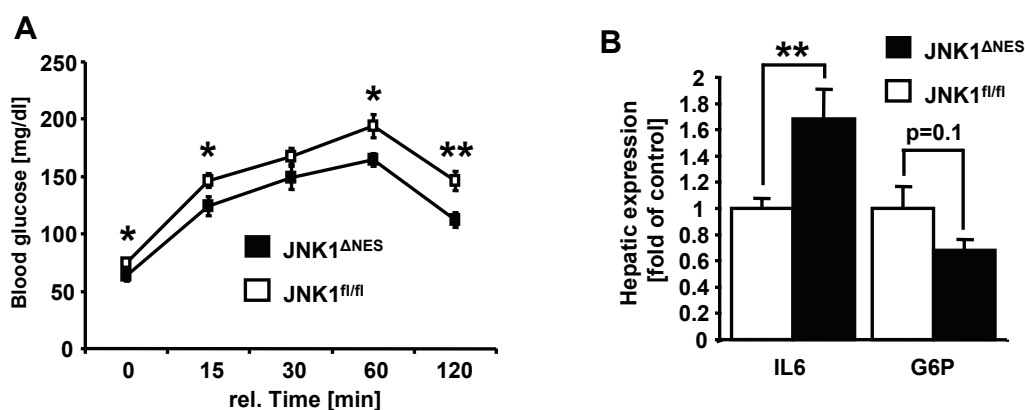


Figure 47: Ameliorated hepatic glucose production in diet-induced obese $JNK1^{\Delta NES}$ mice

A) Pyruvate tolerance test in $JNK1^{fl/fl}$ and $JNK1^{\Delta NES}$ mice on high-fat diet at the age of 10 weeks (n= 8-14 per group). B) Real-Time analysis of hepatic IL6 and G6P mRNA expression in $JNK1^{fl/fl}$ and $JNK1^{\Delta NES}$ mice on HFD at the age of 16 weeks (n= 8 per group). *, $p \leq 0.05$; **, $p \leq 0.01$.

Lastly, hepatic insulin sensitivity was directly assessed. After intraperitoneal insulin injection, liver of $JNK1^{\Delta NES}$ mice showed increased phosphorylation of the key insulin downstream target AKT, indicating that direct insulin action on liver is also retained under HFD conditions (Figure 48A, B). Taken together, hypothalamic and pituitary JNK1 deficiency results in amelioration of obesity-induced hepatic steatosis and dysregulated HGP.

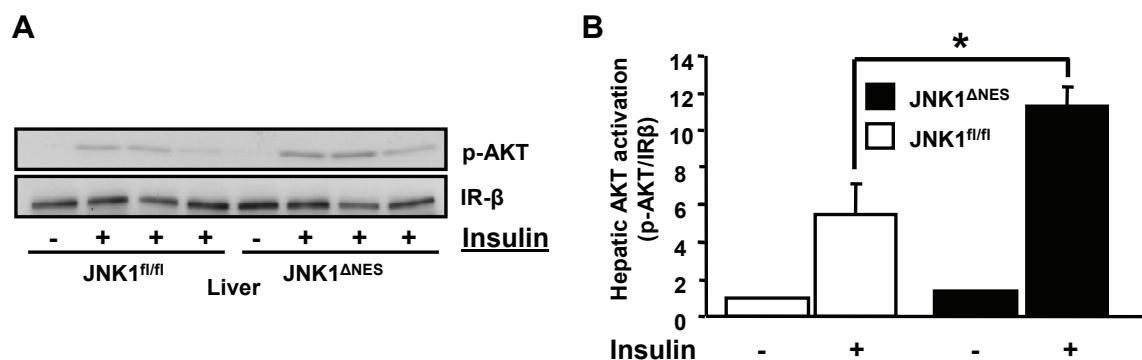


Figure 48: Elevated hepatic insulin sensitivity in diet-induced obese $JNK1^{\Delta NES}$ mice

A) Hepatic AKT activation upon intraperitoneal insulin treatment is improved in diet-induced obese $JNK1^{\Delta NES}$ mice. $JNK1^{fl/fl}$ and $JNK1^{\Delta NES}$ mice on HFD at the age of 10 weeks were fasted for 16h, injected with saline or 1.5U/kg body weight insulin and sacrificed 30min later. Immunoblot was performed for phosphorylated (activated) AKT and IR- β as loading control (n= 3 per injected group). B) Quantification of insulin-induced AKT phosphorylation compared to total IR- β content shown in A). *, $p \leq 0.05$.

3.24 JNK1^{ΔNES} mice are protected from HFD-induced adipose tissue inflammation and dysfunction

Research during the last 15 years has revealed that adipose tissue expresses and releases a plethora of hormones, called adipokines, with leptin being the most prominent one (284, 285). While leptin acts as a “messenger” of WAT to the brain, it has become clear that hormones acting in the brain also regulate adipose tissue metabolism. For example, insulin and leptin acting in the central nervous system regulate gene expression and lipid uptake in WAT, likely through the sympathetic nervous system (161, 286). One of these studies could show that chronic insulin infusion in the CNS, at a low dose that did not affect food intake, led to an increase in WAT expression of lipoprotein lipase (LPL), which catalyses a key step in lipid uptake into WAT (161). In line with this, epigonadal adipose tissue mass was reportedly increased after central insulin infusion (161). Since it was shown here that JNK1^{ΔNES} mice show increased central insulin sensitivity, the structure of white adipose tissue was further examined.

Although NMR studies had revealed unchanged relative fat content of control and JNK1^{ΔNES} mice fed HFD, relative eWAT (but not BAT) mass was increased in JNK1^{ΔNES} mice, indicating differential fat accumulation in these mice compared to control animals (Figure 49A). Notably, under fasting conditions, eWAT lipids appeared to be released at a higher rate compared to eWAT lipids from control animals, since fasting lead to a significant reduction in eWAT mass only in JNK1^{ΔNES} mice fed HFD (Figure 49B).

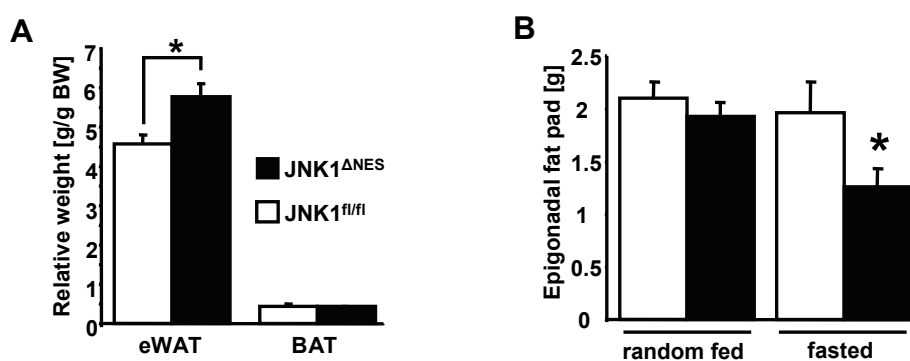


Figure 49: Increased eWAT mass in diet-induced obese JNK1^{ΔNES} mice

A) Relative epigonadal white and brown adipose tissue weight of JNK1^{fl/fl} and JNK1^{ΔNES} mice on high-fat diet at the age of 16 weeks (n= 12 per group). Relation of epigonadal adipose tissue mass and brown adipose tissue mass to body weight was calculated individually for each mouse. B) Absolute epigonadal adipose tissue mass of control and JNK1^{ΔNES} mice on high-fat diet at the age of 16 weeks either random fed or after overnight (16 hour) fasting (n= 8 per group). *, p ≤ 0.05.

Adipocyte size was monitored from control and JNK1^{ΔNES} mice on either diet. JNK1^{ΔNES} mice fed ND showed significantly increased adipocyte size (Figure 50A). This is in line with the notion that improved insulin sensitivity as induced by reduced GH levels can

lead to moderately increased lipid uptake and adipocyte size in human patients (287). In contrast, when adipocyte size was determined from animals fed HFD, adipocyte size from control animals was massively increased indicating lipid-induced hypertrophy, while adipocyte size of $JNK1^{\Delta NES}$ mice was comparable to ND adipocyte size (Figure 50B).

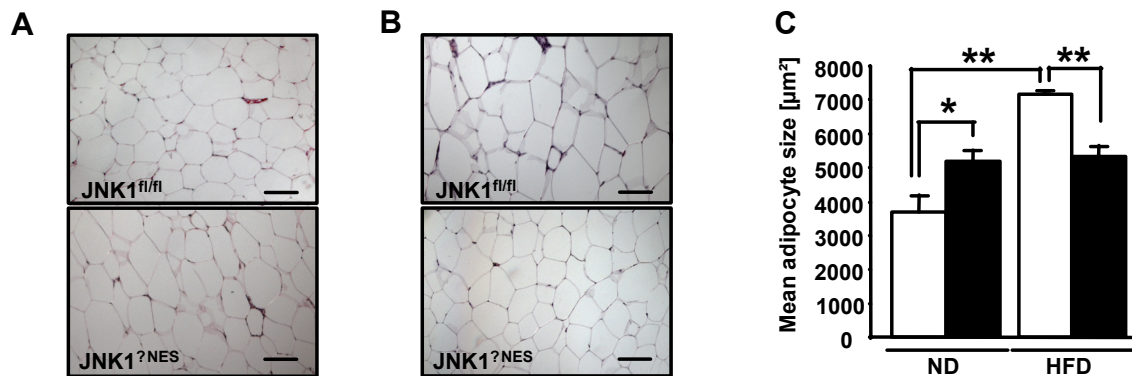


Figure 50: Obese $JNK1^{\Delta NES}$ mice are protected from adipocyte hypertrophy

A) Representative H&E stain of epigonadal adipose tissue of control and $JNK1^{\Delta NES}$ mice on normal diet at the age of 16 weeks. Scale bar: 100 μm . B) Representative H&E stain of epigonadal adipose tissue of control and $JNK1^{\Delta NES}$ mice on high-fat diet at the age of 16 weeks. Scale bar: 100 μm . C) Quantification of adipocyte surface in epigonadal adipose tissue of $JNK1^{fl/fl}$ and $JNK1^{\Delta NES}$ mice on normal chow diet and high-fat diet at the age of 16 weeks (n= 3-6 per group). *, $p \leq 0.05$; **, $p \leq 0.01$.

To gain insight into this apparent discrepancy, expression of key enzymes involved in lipid uptake and lipolysis were measured. LPL regulates triglyceride breakdown, allowing transport of FFAs into adipocytes. LPL mRNA levels tended to be increased under ND conditions and were significantly elevated in eWAT from $JNK1^{\Delta NES}$ mice fed HFD compared to controls, indicating improved uptake of TGs into eWAT (Figure 51A). Although this might partially explain the increase in adipocyte size under ND conditions, adipocytes from $JNK1^{\Delta NES}$ mice fed HFD were smaller compared to controls. One key enzyme controlling lipid efflux from adipocytes is hormone sensitive lipase (HSL). HSL expression is reduced in WAT biopsies of insulin resistant patients, which is thought to render adipocytes unable to reduce TG storage levels, leading to lipid overload and inhibiting weight loss (288). In line with increased peripheral insulin sensitivity of $JNK1^{\Delta NES}$ mice, HSL mRNA levels were increased in eWAT taken from HFD fed $JNK1^{\Delta NES}$ mice (Figure 51A). Since eWAT mass changed more dynamically upon fasting in $JNK1^{\Delta NES}$ mice, these findings indicate that eWAT lipids are more readily accessible during periods of negative energy balance (by elevated HSL action). Taken together, eWAT adipocytes of $JNK1^{\Delta NES}$ mice are resistant to obesity-induced hypertrophy.

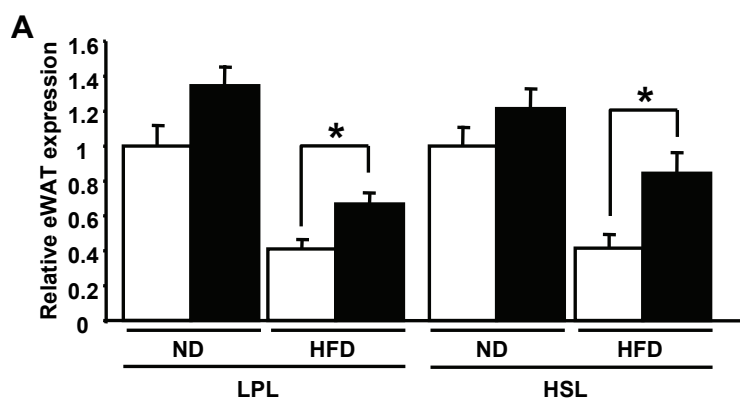


Figure 51: JNK1^{ANES} mice show ameliorated eWAT lipid metabolism enzyme expression

A) Expression of lipoprotein lipase (LPL) and hormone-sensitive lipase (HSL) in epigonadal white adipose tissue of JNK1^{fl/fl} and JNK1^{ANES} mice (n=8 per group) as measured by real-time PCR. *, $p \leq 0.05$.

WAT inflammation is thought to be a crucial event in the pathophysiology of obesity and DM, since macrophage infiltration and local inflammation will eventually lead to systemic, low-grade chronic inflammation (202, 203, 208, 223). There is evidence that lipid overload leads to apoptotic death of adipocytes (209). In line with this finding, activated macrophages are frequently found around dead or dying adipocytes, appearing as crown-like structures (209). Since adipocyte lipid load was reduced in JNK1^{ANES} mice, it was hypothesized that eWAT inflammation may be reduced. While control animals showed increased expression of TNF α , the critical pro-inflammatory cytokine upon HFD, this was completely prevented in WAT of JNK1^{ANES} mice (Figure 51A). Local inflammation accompanied by increased lipid deposition leads to reduced WAT expression of adiponectin, a key adipokine which increases insulin sensitivity in liver and skeletal muscle (284, 285, 289, 290). In line with decreased expression of TNF α and reduced lipid load of WAT adipocytes, adiponectin mRNA expression was significantly increased in JNK1^{ANES} mice fed HFD (Figure 52B). Moreover, this increase was also detected in serum samples from JNK1^{ANES} mice (Figure 52C).

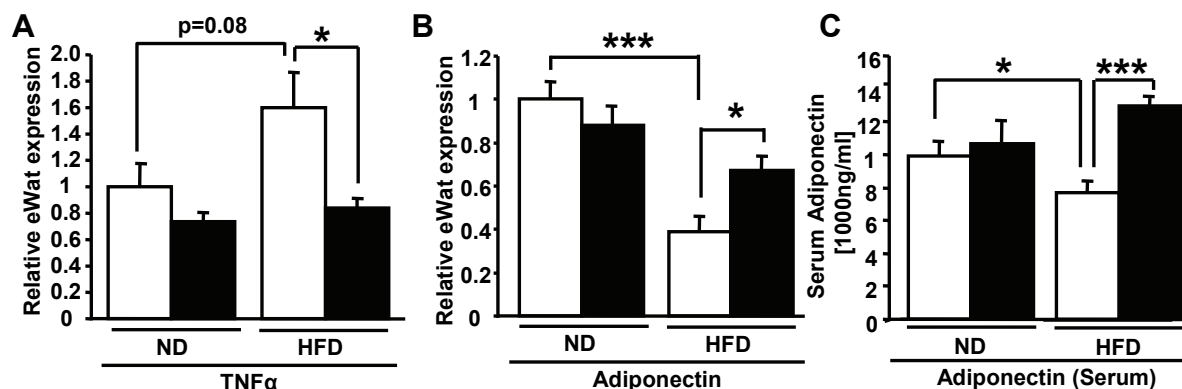


Figure 52: JNK1^{ANES} mice are protected from obesity-induced WAT inflammation

A) Expression of TNF α in epigonadal white adipose tissue of JNK1^{fl/fl} and JNK1^{ANES} mice (n=8 per group) as measured by Real-time PCR. B) Expression of Adiponectin in epigonadal white adipose tissue of JNK1^{fl/fl} and JNK1^{ANES} mice (n=8 per group) as measured by Real-time PCR. C) Serum Adiponectin in control and JNK1^{ANES} mice at the age of 10 weeks was measured by ELISA (n= 8 per group). *, p \leq 0.05; ***, p \leq 0.001.

It has been demonstrated that adipose tissue inflammation can elicit reduced expression of the key adipocyte transcription factor peroxisome proliferator-activated receptor (PPAR) γ , which regulates adipocyte biogenesis (183, 291, 292). In line with this, adipose tissue samples from control animals fed HFD showed significantly reduced expression of PPAR γ , while this was blunted in JNK1^{ANES} mice (Figure 53A). One of the key target genes of PPAR γ is glucose transporter (GLUT) 4, and reduced WAT GLUT4 expression in diet-induced obesity is thought to contribute to persistent hyperglycemia, which is one of the major complications of obesity and diabetes (183, 293). In line with improved glucose tolerance and reduced serum glucose levels, eWAT GLUT4 expression was significantly increased in JNK1^{ANES} mice fed HFD (Figure 53B). PPAR γ deficiency reduces leptin expression (294). In accordance to mildly increased PPAR γ expression, circulating leptin levels tended to be decreased in JNK1^{ANES} mice fed HFD (Figure 53C). Taken together, epigonadal WAT inflammation is reduced in JNK1^{ANES} mice, ameliorating expression of adiponectin, PPAR γ and GLUT4.

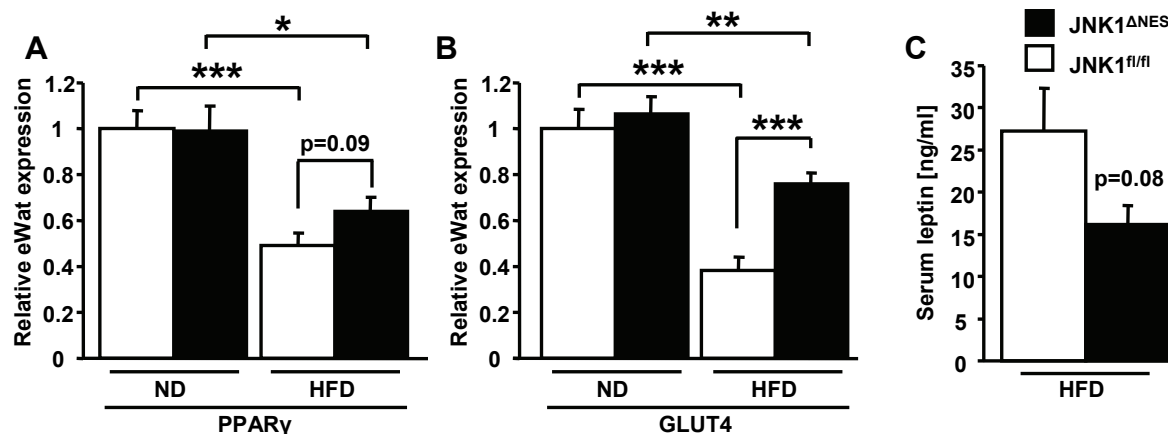


Figure 53: GLUT4 expression in eWAT is increased in obese JNK1^{ANES} mice

A) Expression of PPAR γ in epigonadal white adipose tissue of JNK1^{fl/fl} and JNK1^{ANES} mice (n=8 per group) as measured by real-time PCR. B) Expression of GLUT4 in epigonadal white adipose tissue of JNK1^{fl/fl} and JNK1^{ANES} mice (n=8 per group) as measured by real-time PCR. C) Serum leptin in control and JNK1^{ANES} mice fed HFD at the age of 10 weeks was measured by ELISA (n= 7-8 per group). *, $p \leq 0.05$; **, $p \leq 0.01$; ***, $p \leq 0.001$.

4 Discussion

Obesity is a major risk factor for the most prevalent causes of death in western societies and may pose a potential danger to future generations due to the epigenetic effects of maternal obesity (2, 11, 16, 19, 295-298). Hence, it is of paramount importance to gain insight into regulatory (patho-) physiological mechanisms in energy homeostasis.

It has been demonstrated that both the pancreatic hormone insulin as well as the adipocyte-derived hormone leptin are crucial regulators of body weight, food intake, energy expenditure and physical activity. Evidence exists that leptin mediates most of its effects on energy homeostasis, i.e. reduction of food intake, elevation of energy expenditure, and physical activity by acting on its receptor expressed on CNS neurons (40). While the leptin signalling cascade involves activation of the transcription factor STAT3, a parallel activation of the PI3K cascade previously known to be insulin's main signalling cascade has also been described (46-48, 299).

The ability of insulin to modulate glucose and lipid metabolism by acting on liver, muscle and adipose tissue has been well documented (300-303). Findings in multiple animal models and humans define insulin action in the CNS as a pivotal regulator of energy homeostasis (56, 155, 304-308). Hence, icv application (in rodents) or intranasal application (in men) reduces acute and long-term food intake, and consecutively, body weight (158, 304). On the other hand, in parallel to peripheral resistance in diabetic patients, obesity induces CNS insulin and leptin resistance (184, 305).

Modern mouse genetics as well as studies in cohorts of patients have revealed the critical importance of hypothalamic neuronal populations in regulation of body weight and glucose homeostasis. Ablation of hypothalamic insulin or leptin receptors elevates body weight, whereas intrahypothalamic injection of insulin, insulin mimetics or leptin has the opposite effect (40, 127, 128, 309, 310). Further investigation has revealed a critical role of the POMC neuron population in the hypothalamus in control of energy intake and expenditure both in animal models as well as in humans (131, 152, 153, 172). Hence, leptin's and insulin's ability to modulate energy homeostasis is diminished by antagonizing the receptor for the POMC-derived neuropeptide α -MSH (156, 311, 312).

The key regulator downstream of insulin-mediated PI3K activation is the protein kinase AKT, which has been shown to regulate protein translation, synaptic rewiring and cell survival in neurons (313, 314). To delineate the role of insulin-mediated signalling downstream of PI3K activation, the AKT-activating kinase PDK1, which is itself directly

downstream of the PI3K product PIP3 and only exists in one isoform, was selectively ablated in all POMC expressing cells (PDK1^{ΔPOMC} mice).

4.1 Inactivation of PDK1 in POMC cells

Double-immunostaining of hypothalamic tissue sections confirmed lack of immunoreactive PDK1 protein in more than 90% of POMC neurons of PDK1^{ΔPOMC} mice. Notably, 30% of all POMC neurons from control mice also lacked immunoreactive PDK, which is in line with previous findings that insulin or leptin stimulation activates the respective signalling cascades only in a percentage of all POMC neurons. This indicates that there may be several POMC subpopulations lacking for example PDK1 or STAT3, which cannot be distinguished as of now due to a lack of any marker protein (105). Taken together, PDK1^{ΔPOMC} mice were shown to be a viable tool to study downstream signalling of the PI3K in hypothalamic POMC neurons, and pituitary POMC-expressing cells.

4.2 PDK1 in POMC cell function

PDK1^{ΔPOMC} mice presented with hyperphagia, increased body weight and impaired glucose metabolism during early life, while later on, body weight was normalized, insulin sensitivity was increased, and fat mass was even decreased compared to control animals. Considering that hypothalamic POMC mRNA expression was found to be decreased in young and adult PDK1^{ΔPOMC} mice, which is expected to lead to chronic hyperphagia and obesity, another, anorexigenic input seemed to exist. Real-Time analysis as well as immunohistochemistry analyses demonstrated a severe reduction in pituitary POMC mRNA content, which was reflected in a progressive loss of circulating corticosterone in PDK1^{ΔPOMC} mice over time. Upon further examination, and in contrast to unchanged hypothalamic POMC neuron survival, adult PDK1^{ΔPOMC} mice presented with an 80% loss of corticotrophs (and melanotrophs) in the pituitary, indicating that PDK1 is essential for postnatal survival of these cell types. Thus, PDK1^{ΔPOMC} mice showed a phenotype akin to human Addison's disease.

Addison's disease is invariably connected to low circulating cortisol, and can be caused by pituitary adenomas which block ACTH release, or adrenal insufficiency, among others. Symptoms include loss of appetite and weight, hypoglycemia, and increased insulin sensitivity, all of which were found in adult PDK1^{ΔPOMC} mice. Similarly, mice following adrenalectomy are lean due to reduced hypothalamic AgRP expression and restoration of circulating corticosterone will normalize feeding and body weight (251).

Thus, in line with previous findings that restoration of corticosterone in POMC null mice exacerbates hyperphagia, obesity, and glucose intolerance, corticosterone treatment of PDK1^{ΔPOMC} mice by implantation of osmotic minipumps increased food intake, body weight and fat pad size. These findings indicate that the progressive hypocortisolism due to corticotroph loss negated the orexigenic effect of strongly reduced hypothalamic POMC expression in PDK1^{ΔPOMC} mice.

4.3 The PDK1-FOXO1 axis in hypothalamic POMC expression

Previous findings implicated the insulin-PI3K signalling as a positive modulator of hypothalamic POMC expression. Consistent with this, PDK1 deficiency severely reduced POMC mRNA levels. Although PI3K/PDK1 signalling is known to regulate many pathways including SGK1, mTOR or PKC isoforms, *in vitro* data suggested that the AKT-target transcription factor FOXO1 is able to bind to and compete with leptin-activated STAT3 for access to adjacent binding sites on the POMC promoter (42). To examine the role of FOXO1 in POMC neurons *in vivo*, a mouse with Cre-inducible expression of a FOXO1 mutant (FOXO1^{Δ256}) was generated. This FOXO1 mutant lacks its transactivation domain, and moreover, the nuclear export sequence, sequestering it in the nucleus, where it binds to FOXO1 binding sites and blocks access of endogenous FOXO1 (89). Importantly, PDK1^{ΔPOMC} mice expressing FOXO1^{Δ256} in POMC cells (FOXO1^{Δ256}:PDK1^{ΔPOMC} mice) displayed normal food intake, body weight, and crucially, ameliorated hypothalamic POMC mRNA levels. Furthermore, expression of the anorexigenic neuropeptide cocaine and amphetamine regulated transcript (CART), which is expressed in a subset of POMC neurons, was also normalised, similar to reports published previously (50).

Thus, the results presented in this work suggest that insulin de-inhibits POMC expression by excluding FOXO1 from the nucleus, allowing leptin-activated STAT3 binding, resulting in increased POMC mRNA expression (Figure 54). In addition, leptin's stimulating effect on electrical activity will induce α -MSH release (153). Accordingly, low levels of AKT activation as simulated in PDK1^{ΔPOMC} mice diminishes leptin stimulated POMC transcription, since FOXO1 bound to the POMC promoter blocks STAT3 binding (42, 238). Since obese patients suffer from CNS insulin resistance (305), insulin signalling in POMC neurons will not be able to inhibit FOXO1 from binding to the POMC promoter, consolidating low levels of POMC expression and thus obesity. In line with this model, POMC mRNA expression is low and hypothalamic α -MSH release is impaired in obese mice (181).

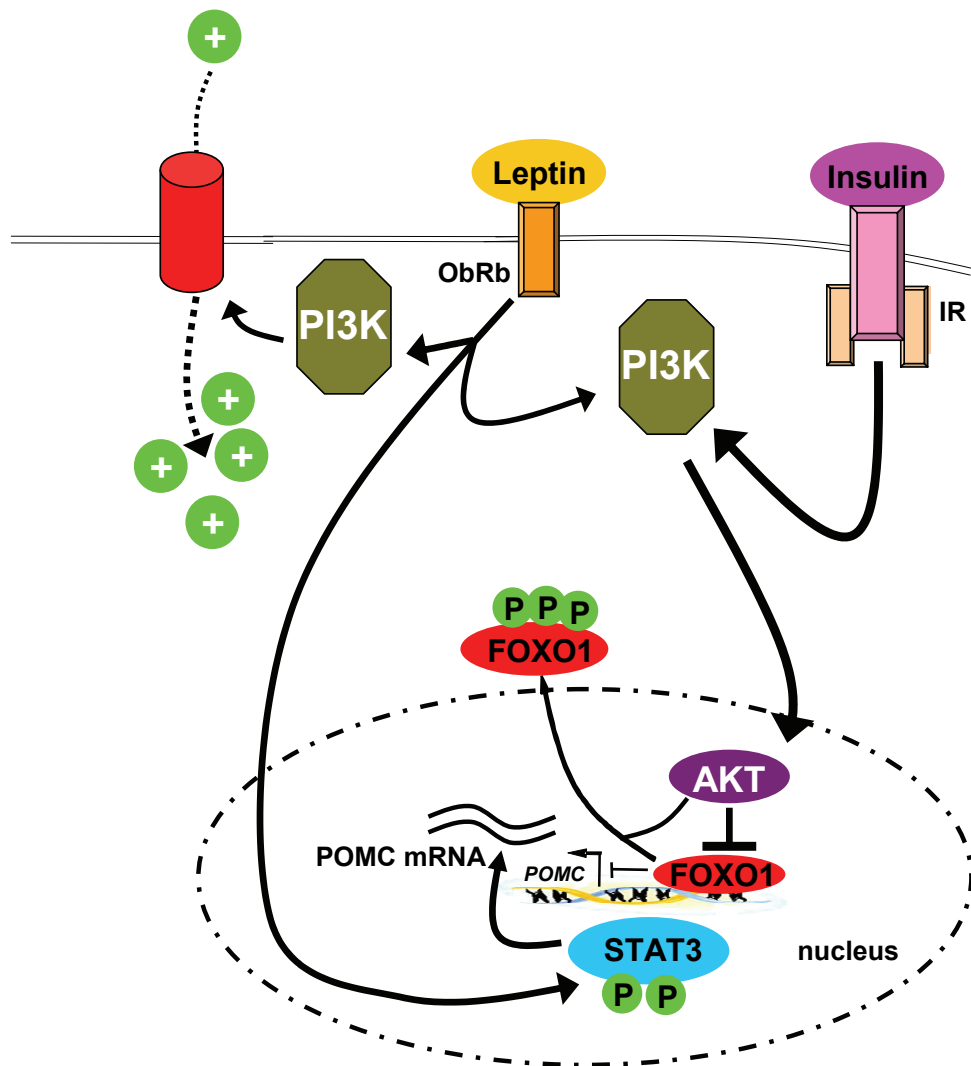


Figure 54: Model of post-developmental POMC neuron activity and POMC mRNA expression

Insulin activates PI3K signalling in POMC neurons. PI3K activation leads to PDK1-mediated phosphorylation and activation of AKT, which is subsequently imported into the nucleus. Here, AKT-mediated phosphorylation induces nuclear export of FOXO1, and thus abrogates FOXO1's inhibition of POMC expression. Leptin-activated STAT3 competes with FOXO1 for adjacent binding sites in the POMC promoter. Leptin may also induce opening of an undefined cation channel to depolarise the neuron by PI3K activation, leading to increased POMC neuron firing and thus α -MSH release. AKT, protein kinase B; FOXO1, forkhead box O1; IR, insulin receptor; ObRb, long (signalling) isoform of the leptin receptor; PI3K, phosphatidylinositol dependent kinase; POMC, proopiomelanocortin; STAT3, signal transducer and activator of transcription 3; +, cations. Figure originally prepared for (105).

Taken together, analyses reported in this work have unravelled the importance of PI3K-FOXO1 signalling in control of hypothalamic POMC neuron function *in vivo* and underlined the role of hypothalamic insulin signalling in control of energy homeostasis.

4.4 The PDK1-FOXO1 axis in corticotroph cell survival

In parallel to the rescue of the hypothalamic phenotype, $\text{FOXO1}^{\Delta 256}; \text{PDK1}^{\Delta \text{POMC}}$ mice might demonstrate survival of corticotrophs in the pituitary. Nonetheless, both $\text{PDK1}^{\Delta \text{POMC}}$

mice and FOXO1^{Δ256};PDK1^{ΔPOMC} mice exhibited loss of corticotrophs and circulating corticosterone levels. Pituitary expression analysis revealed that in young PDK1^{ΔPOMC} mice, the pro-apoptotic genes Bax and Bak were already up-regulated. Additionally, Zac1, which had been demonstrated to be modulated in pituitary cell lines by PI3K signalling *in vitro*, also tended to be increased (254). Although these data demonstrate increased expression of pro-apoptotic genes, further analysis with regards to protein expression of these genes, and careful analysis of corticotroph survival during postnatal development is necessary to understand the phenotype in its entirety.

Bax, Bak and Zac1 mRNA expression was reduced to normal levels in FOXO1^{Δ256};PDK1^{ΔPOMC} mice. Since corticotroph survival was not rescued, PDK1-dependent, FOXO1-independent pathways necessary for corticotroph survival must exist. Mice lacking IR or PTEN in corticotrophs do not show any changes in corticotroph number, survival or function, therefore the ability of PDK1 to ensure corticotroph survival appears to be independent of insulin signalling or PI3K activation (151, 168). Since it has been noted that PDK1 presence is necessary for maturation and function of several PKC isoforms as well as SGK1, it is possible, but so far experimentally untested, that these kinases mediate the pro-survival effect of PDK1 in corticotrophs (247). Taken together, PDK1 inhibition might represent a therapeutic target to treat pituitary (ACTH secreting) adenomas, in line with PDK1 inhibitors undergoing testing for several types of cancer (315).

4.5 Hypothalamic cytokine expression in diet-induced obesity

CNS and hypothalamic insulin and leptin resistance is a major determinant in obesity and impaired glucose metabolism. Inflammatory and stress kinase signalling pathways such as IKK and JNK have been shown to be activated in obesity in peripheral tissues. Experiments in animal models have now provided evidence that JNK and IKK activation also occurs in the hypothalamus in diet-induced obesity (184). Hyperlipidemia and especially peripherally produced cytokines have been indicated in inducing hypothalamic insulin and leptin resistance by inducing JNK and IKK signalling, hence TNF α and IL6 protein content in hypothalamic tissue of diet-induced obese rats have been shown to be increased (214). Nonetheless, these experiments did not clarify if these cytokines originated in peripheral tissues such as WAT or in the hypothalamus itself.

In the present work, using lean and obese wild type mice, it was demonstrated that hypothalamic mRNA expression of inflammatory cytokines TNF α and IL6 is up-regulated.

IL6 has been shown to either induce or inhibit insulin resistance in peripheral tissues such as liver, indicating that duration or intensity plays a role in the outcome of IL6 signalling (151, 219). On the other hand, IL6 null mice show adult-onset obesity, partially due to lower energy expenditure (221, 316). Thus, elevated IL6 levels in the hypothalamus might be beneficial by inducing body weight loss, in line with findings of icv IL6 treatment in rats (221). Notably, the leptin and insulin sensitizing effect of physical activity has been linked to hypothalamic IL6 signalling. Ablation of neuronal IL6 signalling will allow defining the CNS role of IL6 with regards to body weight and energy expenditure.

TNF α signalling activates JNK and IKK signalling, leading to serine phosphorylation of IRS proteins, and possibly also elevating expression of SOCS3, a key regulator both of leptin and insulin signalling in the CNS (184, 317). Nonetheless, CNS TNF α signalling has been linked to anorexia and cachexia during chronic diseases such as AIDS and certain types of cancer (216, 218). These two contradicting findings might be explained by the notion that during obesity, TNF α levels may be elevated by 200-300%, while in cachexic patients suffering from chronic diseases such as AIDS, TNF α levels have been reported to be elevated by up to 1200%, thus depending on the dosage, TNF α may have either orexigenic or anorexigenic effects (318, 319).

In the current work, the duality of TNF α signalling was demonstrated by icv injections. Whereas high dose TNF α application acutely reduced food intake and body weight gain during re-feeding, low dose TNF α application induced hyperphagia and escalated body weight gain compared to vehicle. Thus, in combination with the finding that hypothalamic TNF α expression is up-regulated two to three fold in diet-induced obese mice, these findings implicate hypothalamic TNF expression and signalling in the etiology of hyperphagia and obesity. Moreover, hypothalamic TNF α expression is not readily reversible by body weight loss due to a reduction in fat consumption. It is well known that upon body weight loss, many patients suffer from “rebound” weight gain. Consequently, TNF α may play a role in setting an obesogenic hypothalamic environment, although it is currently unknown how under conditions of weight loss and improved glucose metabolism, TNF α expression is further increased. Interestingly, TNF α has anti-apoptotic properties in the CNS (320). Since obesity may induce loss of hypothalamic neurons, up-regulated TNF α in hypothalami of diet-induced obese mice may be a counterregulatory phenomenon to ameliorate neuronal apoptosis with the fallout of further inhibiting the anorexigenic effects of leptin and insulin ending in a vicious circle of cell loss, TNF α induction and insulin/leptin resistance (321). However, it remains to be delineated by which molecular mechanism TNF α induced hyperphagia/body

weight gain in the paradigm of re-feeding, i.e. by inducing acute insulin/leptin resistance or by other means, and in which cell type TNF α expression is elevated.

4.6 Hypothalamic/pituitary JNK activation in obesity

Diet-induced obesity leads to JNK activation in several tissues, including liver, muscle, and adipose tissue (185, 199, 207). Similar to findings in rats, HFD increased JNK activity also in the hypothalamus of mice (214). Furthermore, JNK activity was also increased in the pituitary of obese wild type mice. To further gain insight into the role of hypothalamic/pituitary JNK1 activation during obesity, mice with Nestin cell-specific JNK1 deletion were generated (JNK1 ^{Δ Nes} mice). The use of Nestin-Cre mice allows ablation of JNK1 in the two tissues where JNK activation was found to be present in diet-induced obesity: the CNS including the hypothalamus, and the pituitary. Therefore, JNK1 immunoreactivity and JNK1 mRNA expression was found to be critically reduced in the hypothalamus. In line with the notion that Nestin expressing stem cells generate the majority of somatotrophs and thyrotrophs but only 20% of all pituitary cells, pituitary JNK1 deletion was detected but not complete in pituitaries of JNK1 ^{Δ Nes} mice (264). Taken together, JNK1 ^{Δ Nes} mice are a viable tool to examine the role of CNS/pituitary JNK1 activation with regards to energy homeostasis.

4.7 JNK1 as a regulator of somatic growth

JNK1 null mice are protected from diet-induced obesity including reduced fat mass and amelioration of hyperphagia and glucose intolerance upon HFD (199). Nonetheless, in that study neither food intake nor energy expenditure was reported to be changed, leaving open the question, how and where exactly JNK1 ablation improves body weight and metabolism in diet-induced obesity.

In the current study, ND fed JNK1 ^{Δ Nes} mice demonstrated significantly reduced body weight, although total fat content was unchanged. Food intake, when corrected for lean mass, was unchanged. Concurrently, JNK1 ^{Δ Nes} mice did not show any alterations in leptin sensitivity independently of diet, therefore it was concluded that CNS JNK1 activation does not impair leptin signalling, whereas lipid-mediated CNS IKK activation has a more pronounced role in the development of leptin resistance (263).

The lower weight seen in JNK1 ^{Δ Nes} mice was thus not due to changes in total body composition. Examination of naso-anal length led to the discovery that body length is reduced

by 8% under ND and 12% under HFD conditions, explaining the differences in body weight. Since a hypothalamus-pituitary-liver axis regulates body length and somatic growth, neuropeptides and hormones involved in this circuit were measured. Notably, neither GHRH nor somatostatin expression was altered in hypothalami of JNK1^{ΔNes} mice, indicating that regulation of somatic growth is not disturbed at the level of the hypothalamus. Instead, expression of GH was shown to be decreased in JNK1^{ΔNes} mice by approximately 40%. In line with these findings, circulating GH and IGF-1 were found to be reduced by up to 50% in adult JNK1^{ΔNes} mice. Upon further examination, it was revealed that pituitary expression of the receptor for GHRH, GHRHR was reduced in JNK1^{ΔNes} mice. Furthermore, the transcription factor PIT-1, which is crucial for GHRHR expression was down-regulated. Notably, immunoreactive somatotroph numbers appeared to be similar between control and JNK1^{ΔNes} mice, thus reduced GH levels are not due to cell loss. Thus, it appears that pituitary expression of PIT-1 and GHRHR desensitised the somatotrophs to the effects of hypothalamic GHRH, leading to decreased release of GH, less expression and release of hepatic IGF-1, finally reducing linear growth. It has been demonstrated that under conditions where at least some GH signalling is present, somatic growth will be preserved at a high level, explaining why JNK1^{ΔNes} mice show IGF-1 level reduced by up to 50%, but only a minor (8-12%) decrease in body length (322).

There is a clear correlation between energy status and somatic growth. Wild type mice show increased linear growth when fed HFD, and overweight children grow faster compared to controls (323). Interestingly, the melanocortin circuit has been shown to be involved in this phenomenon. POMC and MC4R null mice have an increased body length, and patients with MC4R mutations show an increase in average height (134, 138, 324). Nonetheless, insight into the pathways involved in this phenomenon has been limited.

In the current study, a role for JNK1 in regulation of pituitary expression of GH, GHRHR and PIT1 was revealed. Diet-induced obese controls showed elevated pituitary expression of GHRHR and GH, which was abrogated in JNK1^{ΔNes} mice. These findings are in line with a previous report, which demonstrated a specific increase in GH expression in HFD-fed young mice (accompanied by increased somatic growth), although in that study, the authors did not measure GHRHR expression (268). Thus, these findings indicate that JNK1 signalling in somatotroph regulates the GH/IGF1 axis, and that this circuit might sense caloric overabundance through activation of JNK1.

Partially impeded by the lack of pituitary cell lines expressing endogenous GHRHR, signalling cascades involved in GHRHR gene transcription are not well understood. Studies

in patients have revealed a significant role for PIT-1-mediated transcriptional activation (325). Concerning PIT-1 expression, several AP-1 binding sites in its promoter exist, and in addition, cAMP response elements in the PIT-1 promoter may be transactivated by MAPK (including JNK) signalling (326). Therefore, PIT-1 expression may be directly regulated by JNK1-dependent activation of the c-Jun/AP-1 class of transcription factors, although this hypothesis has not been experimentally addressed yet. Here, c-Jun ablation specifically in the somatotroph lineage may be helpful to delineate its function in PIT-1 and/or GHRHR expression, since both GHRHR-Cre transgenic mice as well as mice with loxP-flanked c-Jun alleles have been generated (327, 328). Moreover, it remains undetermined which stimulus activates JNK signalling in somatotrophs to regulate somatic growth. In the current study, elevated levels of ER stress markers were detected in pituitaries of HFD fed mice. Thus, hypothetically, ER stress, for example induced by elevated circulating lipid concentrations, may play a role in regulation of somatic growth by activation of JNK1. Future work will be necessary to understand the upstream activators and downstream targets of pituitary JNK1 signalling.

4.8 JNK1 as a negative regulator of the thyrotrophic axis

JNK1^{ΔNes} mice were found to show mildly increased energy expenditure. Surprisingly, pituitary expression of TSHβ was found to be increased by approximately 300%. In line with this finding, circulating free T3 levels were elevated in JNK1^{ΔNes} mice, and BAT UCP1 levels were mildly increased. Concurrently, BAT morphology was changed in JNK1^{ΔNes} mice in the way of smaller adipocytes, indicating higher levels of lipid expenditure, or differences in lipid deposition in BAT compared to other tissues. Notably, neither respiratory quotient nor body composition was different between control and JNK1^{ΔNes} mice, indicating that although lipolysis appears to be increased in BAT, glucose catabolism must be proportionally increased as well.

Pituitary TSHβ expression is under control of TRH, which itself is released by PVN neurons (329). Since hypothalamic TRH levels were similar in control and JNK1^{ΔNes} mice, increased TSHβ may be due to a pituitary-autonomous phenomenon. Indeed, TRHR expression was found to be elevated in JNK1^{ΔNes} mice. In line with the notion of a pituitary-autonomous effect of JNK1 signalling, JNK inhibitor, but not PI3K or ERK inhibitor treatment increased TRHR expression *in vitro*. Thus, these data suggest that thyrotrophic JNK1 signalling may reduce TRHR expression, resulting in decreased TRH sensitivity and TSHβ expression, and consequently, reduced energy expenditure.

Control of TRHR expression appears to be complex as both PIT-1 and glucocorticoid receptor binding elements have been demonstrated in the TRHR promoter (279). Nonetheless, *in vitro*-based work indicates a PIT-1 independent mechanism involved in JNK1-mediated control of TRHR expression. While JNK inhibition was sufficient to induce TRHR expression *in vitro*, PIT-1 expression was unaltered. Since experimental evidence exists that direct JNK-mediated phosphorylation negatively regulates glucocorticoid receptor signalling, and glucocorticoid receptor signalling increases TRHR expression *in vitro*, future work will be aiming to examine the status of glucocorticoid signalling in the pituitary of JNK1^{ΔNes} mice (330, 331).

4.9 JNK1 action and hypothalamic insulin sensitivity

Hypothalamic insulin signalling has been shown to inhibit peripheral glucose production, and induce glucose uptake, thereby improving glucose tolerance (151, 166). Hypothalamic JNK signalling may induce local insulin resistance, which subsequently would lead to glucose and insulin intolerance in peripheral tissues. In line with this idea, JNK activity in hypothalamic tissue of obese mice was found to be increased.

While leptin's ability to reduce body weight gain and insulin sensitivity was indistinguishable between control and JNK1^{ΔNes} mice, icv administration of insulin exerted potent anorexigenic effects only in JNK1^{ΔNes} mice and independently of diet, while control animals did not show any effect on food intake or body weight at the insulin dose chosen. Thus, JNK1^{ΔNes} mice show elevated CNS insulin efficacy. In addition, hypothalamic activation of insulin's signalling cascade in both groups fed HFD was evaluated using phosphorylation (= activation) of AKT as a marker. In line with the findings on food intake and body weight, icv insulin application induced more than three-fold higher hypothalamic AKT activation in JNK1^{ΔNes} mice compared to controls, further demonstrating that PI3K signalling is negatively affected by hypothalamic JNK1 signalling, possibly due to serine phosphorylation of IRS residues (201). Taken together, JNK1 regulates hypothalamic insulin but not leptin sensitivity.

4.10 Systemic effects of CNS/pituitary JNK1 signalling

JNK1^{ΔNes} mice showed reduced circulating glucose levels both in the fasted and random fed state, indicating improved glycemic control. In line with this, circulating insulin levels were reduced, and JNK1^{ΔNes} mice showed improved systemic insulin sensitivity.

Several lines of experimental evidence indicate that decreased HGP is responsible for the improved glucose levels. Hypothalamic insulin signalling regulates HGP by increasing hepatic IL6 levels (151, 163). In parallel to improved hypothalamic insulin sensitivity, hepatic IL6 expression was elevated in JNK1^{ΔNes} mice. Secondly, glucose levels in JNK1^{ΔNes} mice remained low when injected with a substrate for gluconeogenesis (pyruvate), further pointing to a reduction in hepatic glucose output. Lastly, hepatic insulin action itself was improved in JNK1^{ΔNes} mice under conditions of diet-induced obesity. Since GH signalling negatively affects hepatic insulin sensitivity, hypothalamic insulin signalling and the reduction of circulating GH may additively improve liver insulin action (332, 333).

Besides glucose metabolism, profound changes in lipid metabolism and storage were detected in JNK1^{ΔNes} mice. Hence, hepatic steatosis was prevented in HFD fed JNK1^{ΔNes} mice. Hepatic steatosis may increase the risk of developing hepatocarcinomas, and liver lipid content has also been directly connected to hepatic insulin resistance (334, 335). Thus, in addition to improved hypothalamic insulin signalling and reduced GH levels, reduced hepatic lipogenesis or elevated lipoprotein secretion may be an underlying factor in the decreased hepatic glucose output demonstrated in JNK1^{ΔNes} mice. Nonetheless, since liver insulin resistance may induce hepatic accumulation of lipids, it remains unknown if reduced steatosis is cause or effect of improved hepatic insulin action in JNK1^{ΔNes} mice (336).

Since a decrease in hepatic lipid content may be due to increased lipid deposition in adipose tissue, WAT structure and function was assessed in JNK1^{ΔNes} mice. In line with unchanged total body composition, ND fed JNK1^{ΔNes} mice showed the same relative epigonadal fat mass. Nonetheless, analysis of adipocyte structure revealed an increase in adipocyte size in ND fed JNK1^{ΔNes} mice. Koch and colleagues have demonstrated that chronic low-level CNS insulin application will increase adipocyte size and epigonadal fat mass (161). In that study, the authors demonstrated that WAT LPL expression was up-regulated by CNS insulin action (161). LPL catalyzes fatty acid entry into adipocytes (86). In line with the notion that increased CNS insulin action might be causing the increased adipocyte size, JNK1^{ΔNes} mice showed a tendency for increased LPL expression. Nonetheless, since GH induces adipocyte insulin resistance, increased insulin-mediated inhibition of lipolysis due to low circulating GH may be a second pathway explaining the increased size of adipocytes (337).

In obese patients as well as animal models, adipocyte volume is increased due to lipid influx. Consequently, adipocytes of HFD fed control animals showed a massive increase in adipocyte size. Notably, adipocyte size was unchanged between ND and HFD fed JNK1^{ΔNes}

mice. Further analysis of lipid enzyme expression revealed significantly increased LPL and HSL mRNA expression in $JNK1^{\Delta Nes}$ mice under HFD conditions. HSL-mediated hydrolysis of triglycerides is the rate-limiting step in mobilisation of fat stores. Notably, the disability of adipocytes of obese patients to release lipids into the bloodstream is thought to lead to lipid overload, ending in adipocyte apoptosis, and further recruitment of macrophages (288). Thus, enzymes necessary for lipid uptake (LPL) and lipid release (HSL) are up-regulated, indicating improved and dynamic lipid disposition in eWAT of $JNK1^{\Delta Nes}$ mice. Conversely, fasting induced a 40% reduction in eWAT mass of $JNK1^{\Delta Nes}$ mice, while control animals did not show a significant eWAT weight loss.

In accordance with the eWAT showing signs of improved function (i.e. ameliorated LPL and HSL expression under HFD conditions), adiponectin expression and circulating adiponectin levels were increased in $JNK1^{\Delta Nes}$ mice when challenged with HFD. Adiponectin has been shown to be essential for hepatic insulin sensitivity, and its obesity-induced reduction is one of the key events in development of DM (289). Expression of $PPAR\gamma$, a key transcription factor in adipocyte metabolism and its target gene GLUT4 were also found to be increased (292, 294). Since increased GLUT4 levels will raise glucose uptake, adipocytes may act as a glucose sink, which together with reduced HGP, improves glucose tolerance in $JNK1^{\Delta Nes}$ mice.

Taking into account the reduced hepatic lipid content and decreased circulating glucose levels, it appears that lipids and glucose are redirected to eWAT of $JNK1^{\Delta Nes}$ mice, mediated by up-regulated expression of LPL and GLUT4, as a consequence of increased CNS insulin action and reduced circulating GH levels. At the same time, adipocyte lipid overload is inhibited by HSL-mediated lipid hydrolysis as well as increased adipocyte biogenesis mediated by $PPAR\gamma$, precluding adipocyte lipid overload and thus in combination preventing local inflammation and maintaining adiponectin expression.

In addition to these local effects, the increased thyroid tone likely plays into the complex phenotype of $JNK1^{\Delta Nes}$ mice. Mice with a severe reduction of BAT mass are insulin resistant and suffer from obesity, hyperlipidemia, and WAT inflammation (281). Correspondingly, the increased thyroid tone may partially be responsible for the overall improvement of hepatic and eWAT function.

Taken together, $JNK1^{\Delta Nes}$ mice are protected from obesity-associated glucose intolerance, hepatic steatosis and adipose tissue inflammation. Although they are also hypersensitive to the anorexigenic effects of insulin, they are unexpectedly not protected from obesity per se, and do not eat less compared to control animals when challenged with HFD.

Of note, PPAR γ has been shown to decrease leptin expression, and was moderately increased in eWAT of JNK1 $^{\Delta Nes}$ mice (293, 294). In comparison with control animals, circulating leptin levels tended to be decreased in JNK1 $^{\Delta Nes}$ mice under HFD conditions and thus were no longer correlated with adipose tissue mass, while systemic and central leptin sensitivity of these mice was clearly unaltered.

Another cause of the reduced circulating leptin and/or the unchanged obesity might lie in the increased thyroid tone in JNK1 $^{\Delta Nes}$ mice. Reduced GH and/or IGF-1 levels would be expected to increase leptin levels, in contrast to what is seen in JNK1 $^{\Delta Nes}$ mice (338, 339). While hypothyroidism induces weight gain and obesity due to reduced energy expenditure, T3 has some orexigenic properties, possibly to offset its ability to considerably induce energy expenditure (281, 340). In addition, hyperthyroidism has been shown to decrease WAT leptin expression through the activation of adrenergic signalling (341, 342). Taken together, the results presented in this work suggest that the elevated thyroid tone in combination with higher glucose and lipid uptake into WAT counterbalances the anorexic drive induced by increased CNS insulin sensitivity, resulting in unchanged hypothalamic neuropeptide expression, food intake and body composition. Future studies will aim to further delineate the complex roles of hypothalamic and pituitary JNK1 function.

4.11 Caloric restriction, aging and JNK1

A phenotype of reduced activation of the somatotrophic axis in combination with improved glucose tolerance and insulin sensitivity is very similar to what is seen in animal models undergoing caloric restriction (CR), which is the only intervention repeatedly shown to prolong life. Thus, CR improves glucose metabolism, insulin sensitivity and importantly, prolongs life span and reduces aging-associated disabilities in multiple animal models (343, 344). Molecular analysis has revealed that decreased activation of the somatotrophic axis is necessary for the beneficial effects of CR (345, 346). In a similar vein, aging-induced cellular GH/IGF-1 resistance confers beneficial resistance against oxidative stress (347). In the present study, the crucial role for CNS/pituitary JNK1 in regulation of the somatotrophic and thyrotrophic axis as well as CNS insulin sensitivity was demonstrated. Although these results point at JNK1 as a pharmacological target to mimic CR, careful analysis of life span in JNK1 $^{\Delta Nes}$ mice and possible side effects of specific JNK1 inhibitors *in vivo* will be necessary to substantiate this notion.

4.12 Perspective

The obesity pandemic in combination with a rapidly aging society endangers developed societies by severely increasing health costs, as well as reducing quality of life for people of all age groups. The molecular and endocrine bases for development of obesity and aging are mostly unknown at this time, although control of body weight, insulin sensitivity and aging-related diseases are clearly linked.

In the present study, inactivation of PDK1 and subsequently inhibiting FOXO1 function in POMC cells revealed new insights into development of CNS insulin and leptin resistance as well as regulation of energy homeostasis by both hormones. In addition, this study expanded the knowledge of regulation of pituitary cell survival with implications in the treatment of pituitary cancer.

Moreover, ablation of JNK1 in the CNS and the pituitary uncovered the crucial role of a kinase previously connected to insulin resistance and inflammatory signalling in regulation of somatic growth and thyroid function, and thus linked ambient energy levels to linear growth on a molecular level. Furthermore, since low circulating GH and IGF-1 levels are implied to confer the beneficial effects of CR, further analysis will define the role of CNS and pituitary JNK1 signalling in the context of aging. Insight into the molecular mechanisms linking insulin resistance and inflammation-associated cellular stress are necessary to uncover new treatments to treat the plethora of aging- and obesity-related diseases in the 21st century.

5 Summary

Insulin and leptin action in the central nervous system (CNS) controls food intake, energy expenditure and glucose metabolism, partially by regulating the activity of hypothalamic proopiomelanocortin (POMC) neurons. Moreover, insulin- and leptin-stimulated phosphatidylinositol-3 kinase (PI3K) activation has been demonstrated to play a critical role in the control of energy homeostasis. To delineate the importance of pathways downstream of PI3K specifically in POMC cell regulation, mice with selective inactivation of 3-phosphoinositide-dependent protein kinase-1 (PDK1) in POMC-expressing cells (PDK1^{ΔPOMC} mice) were generated. PDK1^{ΔPOMC} mice initially display hyperphagia, increased body weight and impaired glucose metabolism caused by reduced hypothalamic POMC expression. In contrast, older PDK1^{ΔPOMC} mice exhibit normalized food intake and body weight as well as enhanced insulin and glucose sensitivity, due to a progressive loss of POMC-expressing corticotrophs in the pituitary and subsequent severe hypocortisolism. Expression of a dominant negative mutant of FOXO1 specifically in POMC cells is sufficient to prevent initial hyperphagia, transiently increased body weight and reduced hypothalamic POMC expression in PDK1^{ΔPOMC} mice, but cannot restore regular pituitary function. These results reveal important but differential roles for PDK1 signaling in hypothalamic and pituitary POMC cell function and survival in control of energy homeostasis and stress response.

To understand potential pathomechanisms involved in neuronal insulin and leptin resistance, the effect of obesity on hypothalamic expression of inflammatory mediators was examined. High-fat feeding was found to induce hypothalamic expression of cytokines such as tumor necrosis factor α , which was not readily reversible by switching to low-fat diet. Since cytokines and lipids are known to activate c-Jun N-terminal kinases (JNKs), mice with JNK1 deficiency in Nestin-expressing cells (which include neurons and pituitary stem cells) were generated (JNK1^{ΔNes} mice).

These mice demonstrated increased hypothalamic insulin sensitivity, as well as reduced activation of the somatotrophic axis and elevated activation of the thyrotrophic axis, resulting in improved glucose tolerance, elevated systemic insulin sensitivity, and were protected against obesity-induced hepatosteatosis and adipose tissue dysfunction. Taken together, obesity-induced JNK1 activation in the hypothalamus and pituitary is a crucial event in the induction of CNS insulin resistance and systemic glucose intolerance caused by obesity.

6 Zusammenfassung

Insulin und Leptin-aktivierte Signalkaskaden im zentralen Nervensystem (ZNS) regulieren Nahrungsaufnahme, Energieverbrauch und Blutzuckerkonzentrationen, insbesondere durch ihren Effekt auf hypothalamische Proopiomelanokortin (POMC)-Neurone. Insulin und Leptin stimulieren die Phosphatidylinositol-3 Kinase (PI3K), und diese Aktivierung ist notwendig für die gewichtssenkenden Effekte von beiden Hormonen. Um den Effekt der Signalkaskaden abwärts von PI3K insbesondere in POMC-Neuronen zu untersuchen, wurden Mäuse mit Inaktivierung der 3-Phosphatidylinositol-abhängigen Kinase (PDK1) in POMC-exprimierenden Zellen ($PDK1^{\Delta POMC}$ Mäuse) generiert. Junge $PDK1^{\Delta POMC}$ Mäuse zeigten erhöhte Nahrungsaufnahme, Körpergewicht und Blutzucker verursacht durch erniedrigte hypothalamische POMC Expression. Adulte $PDK1^{\Delta POMC}$ Mäuse hingegen demonstrierten normale Nahrungsaufnahme und Körpergewicht, und erhöhte Insulinsensitivität sowie Glukosetoleranz. Dies war auf einen progressiven Verlust der POMC-exprimierenden corticotrophen Zellen in der Hypophyse zurückzuführen, was zu krankhaft niedrigen Kortisol-Konzentrationen führte. Expression einer dominant-negativen FOXO1-Mutante in POMC-Zellen normalisierte Nahrungsaufnahme, Körpergewicht und hypothalamische POMC Expression, jedoch verhinderte nicht den Verlust der corticotrophen Zellen der Hypophyse. Zusammengenommen haben diese Ergebnisse die differentielle Rolle von PDK1 in der hypothalamischen Regulation des Energiehaushalts sowie der Stressantwort der Hypophyse aufgedeckt. Um die Mechanismen der Adipositas-assoziierten ZNS Leptin- und Insulinresistenz zu verstehen, wurde der Effekt von Adipositas auf die hypothalamische Expression von Zytokinen untersucht. Eine fettreiche Diät erhöhte die Expression von Zytokinen wie Tumor Nekrose Factor α , was nicht kurzfristig durch eine fettarme Ernährung umkehrbar war. Da Zytokine und Fette bekanntermaßen die c-Jun N-terminalen Kinasen (JNKs) aktivieren, wurden Mäuse mit JNK1-Defizienz in Nestin-exprimierenden Zellen (d.h. im ZNS sowie in Stammzellen der Hypophyse) generiert ($JNK1^{\Delta Nes}$ Mäuse). Diese Mäuse zeigten erhöhte hypothalamische Insulinsensitivität, reduzierte Aktivität der somatotrophen Achse und gesteigerte Aktivität der thyrotrophen Achse, was zu einer verbesserten systemischen Insulinsensitivität führte. $JNK1^{\Delta Nes}$ Mäuse waren auch vor Adipositas-induzierter Fettleber sowie Fettgewebestörungen geschützt. Zusammengenommen haben diese Daten gezeigt, dass Adipositas-medierte JNK1 Aktivierung im Hypothalamus sowie der Hypophyse ein entscheidender Punkt in der Entstehung von Insulinresistenz und Glukoseintoleranz ist.

7 References

1. WHO, *World health organisation* (2009).
2. H. R. Wyatt, *Prim Care* **30**, 267 (Jun, 2003).
3. J. C. Seidell, *Br J Nutr* **83 Suppl 1**, S5 (Mar, 2000).
4. A. Berghofer *et al.*, *BMC Public Health* **8**, 200 (2008).
5. K. M. Flegal, M. D. Carroll, C. L. Ogden, C. L. Johnson, *Jama* **288**, 1723 (Oct 9, 2002).
6. E. Jequier, *Clin Endocrinol Metab* **13**, 563 (Nov, 1984).
7. E. Ravussin, *Diabetes Care* **16**, 232 (Jan, 1993).
8. J. E. Blundell, N. A. King, *Ciba Found Symp* **201**, 138 (1996).
9. V. Vaidya, *Adv Psychosom Med* **27**, 73 (2006).
10. M. A. Permutt, J. Wasson, N. Cox, *J Clin Invest* **115**, 1431 (Jun, 2005).
11. E. E. Calle, M. J. Thun, *Oncogene* **23**, 6365 (Aug 23, 2004).
12. C. F. Semenkovich, *J Clin Invest* **116**, 1813 (Jul, 2006).
13. H. A. van Leiden *et al.*, *Diabetes Care* **25**, 1320 (Aug, 2002).
14. A. Gastaldelli *et al.*, *Diabetes* **49**, 1367 (Aug, 2000).
15. P. Hogan, T. Dall, P. Nikolov, *Diabetes Care* **26**, 917 (Mar, 2003).
16. G. A. Bray, T. Bellanger, *Endocrine* **29**, 109 (Feb, 2006).
17. K. Wroblewska-Seniuk, E. Wender-Ozegowska, J. Szczapa, *Pediatr Diabetes* (May 19, 2009).
18. A. M. Stuebe, M. R. Forman, K. B. Michels, *Int J Obes (Lond)* **33**, 743 (Jul, 2009).
19. H. Chen, D. Simar, M. J. Morris, *PLoS ONE* **4**, e6259 (2009).
20. C. Gemma *et al.*, *Obesity (Silver Spring)* **14**, 2193 (Dec, 2006).
21. M. B. Heyman *et al.*, *Am J Physiol* **263**, R250 (Aug, 1992).
22. I. L. Bernstein, E. C. Lotter, P. J. Kulkosky, D. Porte, Jr., S. C. Woods, *Proc Soc Exp Biol Med* **150**, 546 (Nov, 1975).
23. R. J. Seeley *et al.*, *Am J Physiol* **271**, R819 (Sep, 1996).
24. S. B. Roberts *et al.*, *Jama* **272**, 1601 (Nov 23-30, 1994).
25. J. P. Newnham, C. E. Pennell, S. J. Lye, J. Rampono, J. R. Challis, *Obstet Gynecol Clin North Am* **36**, 227 (Jun, 2009).
26. J. R. Krebs, *Am J Clin Nutr* **90**, 707S (Sep, 2009).
27. A. Bellisari, *Obes Rev* **9**, 165 (Mar, 2008).
28. A. M. Sharma, *J Mol Med* **76**, 568 (Jul, 1998).
29. D. E. Cummings, M. W. Schwartz, *Nat Genet* **26**, 8 (Sep, 2000).
30. M. W. Schwartz, S. C. Woods, D. Porte, Jr., R. J. Seeley, D. G. Baskin, *Nature* **404**, 661 (Apr 6, 2000).
31. M. W. Schwartz, *Ann Endocrinol (Paris)* **63**, 117 (Apr, 2002).
32. L. Plum, B. F. Belgardt, J. C. Bruning, *Journal of Clinical Investigation* **116** (July 2006, 2006).
33. J. L. Halaas *et al.*, *Science* **269**, 543 (Jul 28, 1995).
34. R. C. Frederich *et al.*, *J Clin Invest* **96**, 1658 (Sep, 1995).
35. M. Ozata, I. C. Ozdemir, J. Licinio, *J Clin Endocrinol Metab* **84**, 3686 (Oct, 1999).
36. L. A. Tartaglia *et al.*, *Cell* **83**, 1263 (Dec 29, 1995).
37. C. Vaisse *et al.*, *Nat Genet* **14**, 95 (Sep, 1996).
38. M. Maffei *et al.*, *Nat Med* **1**, 1155 (Nov, 1995).
39. J. T. Smith, P. J. Mark, B. J. Waddell, *J Endocrinol* **184**, 535 (Mar, 2005).
40. P. Cohen *et al.*, *J Clin Invest* **108**, 1113 (Oct, 2001).
41. A. S. Banks, S. M. Davis, S. H. Bates, M. G. Myers, Jr., *J Biol Chem* **275**, 14563 (May 12, 2000).

42. T. Kitamura *et al.*, *Nat Med* **12**, 534 (May, 2006).
43. G. Fruhbeck, *Biochem J* **393**, 7 (Jan 1, 2006).
44. C. Bjorbaek, J. K. Elmquist, J. D. Frantz, S. E. Shoelson, J. S. Flier, *Mol Cell* **1**, 619 (Mar, 1998).
45. C. Duan, M. Li, L. Rui, *J Biol Chem* **279**, 43684 (Oct 15, 2004).
46. A. Z. Zhao, J. N. Huan, S. Gupta, R. Pal, A. Sahu, *Nat Neurosci* **5**, 727 (Aug, 2002).
47. S. Mirshamsi *et al.*, *BMC Neurosci* **5**, 54 (Dec 6, 2004).
48. C. D. Morrison, G. J. Morton, K. D. Niswender, R. W. Gelling, M. W. Schwartz, *Am J Physiol Endocrinol Metab* **289**, E1051 (Dec, 2005).
49. K. Ning *et al.*, *Embo J* (May 4, 2006).
50. M. S. Kim *et al.*, *Nat Neurosci* **9**, 901 (Jul, 2006).
51. L. Rosenfeld, *Clin Chem* **48**, 2270 (Dec, 2002).
52. D. F. Steiner, D. E. James, *Diabetologia* **35 Suppl 2**, S41 (Dec, 1992).
53. A. Massaglia, F. Pennisi, U. Rosa, S. Ronca-Testoni, C. A. Rossi, *Biochem J* **108**, 247 (Jun, 1968).
54. F. M. Ashcroft, *Biochem Soc Trans* **34**, 243 (Apr, 2006).
55. J. C. Bruning *et al.*, *Mol Cell* **2**, 559 (Nov, 1998).
56. J. C. Bruning *et al.*, *Science* **289**, 2122 (Sep 22, 2000).
57. M. D. Michael *et al.*, *Mol Cell* **6**, 87 (Jul, 2000).
58. M. Bluher *et al.*, *Dev Cell* **3**, 25 (Jul, 2002).
59. R. N. Kulkarni *et al.*, *Cell* **96**, 329 (Feb 5, 1999).
60. J. Baumgartl *et al.*, *Cell Metab* **3**, 247 (Apr, 2006).
61. C. Ward *et al.*, *Acta Physiol (Oxf)* **192**, 3 (Jan, 2008).
62. M. G. Myers, Jr., M. F. White, *Annu Rev Pharmacol Toxicol* **36**, 615 (1996).
63. M. G. Myers, Jr., X. J. Sun, M. F. White, *Trends Biochem Sci* **19**, 289 (Jul, 1994).
64. M. G. Myers, Jr., M. F. White, *Diabetes* **42**, 643 (May, 1993).
65. S. Boura-Halfon, Y. Zick, *Am J Physiol Endocrinol Metab* **296**, E581 (Apr, 2009).
66. E. Van Obberghen *et al.*, *Eur J Clin Invest* **31**, 966 (Nov, 2001).
67. M. H. Lima *et al.*, *Endocrine* **18**, 1 (Jun, 2002).
68. Y. R. Hadari *et al.*, *J Biol Chem* **267**, 17483 (Sep 5, 1992).
69. T. Ito, Y. Sasaki, J. R. Wands, *Mol Cell Biol* **16**, 943 (Mar, 1996).
70. Y. Terauchi *et al.*, *Nat Genet* **21**, 230 (Feb, 1999).
71. D. A. Fruman *et al.*, *Nat Genet* **26**, 379 (Nov, 2000).
72. D. R. Alessi *et al.*, *Curr Biol* **7**, 261 (Apr 1, 1997).
73. D. A. Cross, D. R. Alessi, P. Cohen, M. Andjelkovich, B. A. Hemmings, *Nature* **378**, 785 (Dec 21-28, 1995).
74. K. Inoki, Y. Li, T. Zhu, J. Wu, K. L. Guan, *Nat Cell Biol* **4**, 648 (Sep, 2002).
75. O. Meyuhas, *Int Rev Cell Mol Biol* **268**, 1 (2008).
76. M. Ashcroft *et al.*, *Oncogene* **21**, 1955 (Mar 27, 2002).
77. J. A. Le Good *et al.*, *Science* **281**, 2042 (Sep 25, 1998).
78. C. Belham, S. Wu, J. Avruch, *Curr Biol* **9**, R93 (Feb 11, 1999).
79. M. R. Williams *et al.*, *Curr Biol* **10**, 439 (Apr 20, 2000).
80. M. A. Lawlor *et al.*, *Embo J* **21**, 3728 (Jul 15, 2002).
81. H. Cho, J. L. Thorvaldsen, Q. Chu, F. Feng, M. J. Birnbaum, *J Biol Chem* **276**, 38349 (Oct 19, 2001).
82. P. R. Shepherd, B. B. Kahn, *N Engl J Med* **341**, 248 (Jul 22, 1999).
83. E. E. Kershaw *et al.*, *Diabetes* **55**, 148 (Jan, 2006).
84. K. Jaworski, E. Sarkadi-Nagy, R. E. Duncan, M. Ahmadian, H. S. Sul, *Am J Physiol Gastrointest Liver Physiol* **293**, G1 (Jul, 2007).
85. K. J. Claycombe *et al.*, *Am J Physiol* **274**, R1253 (May, 1998).

86. C. F. Semenkovich, M. Wims, L. Noe, J. Etienne, L. Chan, *J Biol Chem* **264**, 9030 (May 25, 1989).
87. T. N. Stitt *et al.*, *Mol Cell* **14**, 395 (May 7, 2004).
88. H. Huang, D. J. Tindall, *J Cell Sci* **120**, 2479 (Aug 1, 2007).
89. J. Nakae, T. Kitamura, D. L. Silver, D. Accili, *J Clin Invest* **108**, 1359 (Nov, 2001).
90. X. Zhang *et al.*, *J Biol Chem* **277**, 45276 (Nov 22, 2002).
91. P. Puigserver *et al.*, *Nature* **423**, 550 (May 29, 2003).
92. H. Cassuto *et al.*, *J Biol Chem* **280**, 33873 (Oct 7, 2005).
93. K. Lin, J. B. Dorman, A. Rodan, C. Kenyon, *Science* **278**, 1319 (Nov 14, 1997).
94. S. Ogg *et al.*, *Nature* **389**, 994 (Oct 30, 1997).
95. D. Weigel, G. Jurgens, F. Kuttner, E. Seifert, H. Jackle, *Cell* **57**, 645 (May 19, 1989).
96. M. E. Giannakou *et al.*, *Science* **305**, 361 (Jul 16, 2004).
97. M. C. Wang, D. Bohmann, H. Jasper, *Cell* **121**, 115 (Apr 8, 2005).
98. K. S. Lee *et al.*, *J Biol Chem* (Aug 31, 2009).
99. R. M. Buijs, S. J. Chun, A. Nijijima, H. J. Romijn, K. Nagai, *J Comp Neurol* **431**, 405 (Mar 19, 2001).
100. N. Quinson, H. L. Robbins, M. J. Clark, J. B. Furness, *Arch Histol Cytol* **64**, 281 (Aug, 2001).
101. M. Bamshad, V. T. Aoki, M. G. Adkison, W. S. Warren, T. J. Bartness, *Am J Physiol* **275**, R291 (Jul, 1998).
102. A. Pocai *et al.*, *Nature* **434**, 1026 (Apr 21, 2005).
103. L. Plum *et al.*, *Cell Metab* **6**, 431 (Dec, 2007).
104. D. Daniels, R. R. Miselis, L. M. Flanagan-Cato, *J Neurobiol* **48**, 278 (Sep 15, 2001).
105. B. F. Belgardt, T. Okamura, J. C. Bruning, *J Physiol* (Sep 21, 2009).
106. A. C. Konner, T. Klockener, J. C. Bruning, *Physiol Behav* **97**, 632 (Jul 14, 2009).
107. C. Sanchez-Lasheras, A. Christine Konner, J. C. Bruning, *Front Neuroendocrinol* (Sep 1, 2009).
108. S. Fulton *et al.*, *Neuron* **51**, 811 (Sep 21, 2006).
109. J. D. Hommel *et al.*, *Neuron* **51**, 801 (Sep 21, 2006).
110. V. K. Yadav *et al.*, *Cell* **138**, 976 (Sep 4, 2009).
111. G. M. Leininger *et al.*, *Cell Metab* **10**, 89 (Aug, 2009).
112. J. G. Quinn, E. O'Hare, A. S. Levine, E. M. Kim, *Brain Res* **991**, 206 (Nov 21, 2003).
113. L. K. Heisler *et al.*, *Ann NY Acad Sci* **994**, 169 (Jun, 2003).
114. Y. Xu *et al.*, *Neuron* **60**, 582 (Nov 26, 2008).
115. N. E. Miller, C. J. Bailey, J. A. Stevenson, *Science* **112**, 256 (Sep 1, 1950).
116. J. M. Delgado, B. K. Anand, *Am J Physiol* **172**, 162 (Jan, 1953).
117. W. Wyrwicka, C. Dobrzecka, *Science* **132**, 805 (Sep 23, 1960).
118. M. K. Lewinska, A. Romaniuk, *Acta Biol Exp (Warsz)* **26**, 285 (1966).
119. L. D. Devenport, S. Balagura, *Science* **172**, 744 (May 14, 1971).
120. P. J. Morgane, *Science* **133**, 887 (Mar 24, 1961).
121. C. Bernard, *Baillère et Fils* **296-313** (1855).
122. F. B. Krasne, *Science* **138**, 822 (Nov 16, 1962).
123. J. G. Mercer *et al.*, *J Neuroendocrinol* **8**, 733 (Oct, 1996).
124. J. G. Mercer *et al.*, *FEBS Lett* **387**, 113 (Jun 3, 1996).
125. D. G. Baskin, A. J. Sipols, M. W. Schwartz, M. F. White, *Regul Pept* **48**, 257 (Oct 20, 1993).
126. S. Obici, Z. Feng, G. Karkanias, D. G. Baskin, L. Rossetti, *Nat Neurosci* **5**, 566 (Jun, 2002).
127. E. L. Air, S. C. Benoit, D. J. Clegg, R. J. Seeley, S. C. Woods, *Endocrinology* **143**, 2449 (Jun, 2002).
128. E. L. Air *et al.*, *Nat Med* **8**, 179 (Feb, 2002).

129. K. D. Niswender *et al.*, *Nature* **413**, 794 (Oct 25, 2001).
130. J. Z. Kiss *et al.*, *Brain Res* **329**, 169 (Mar 11, 1985).
131. H. Krude *et al.*, *Nat Genet* **19**, 155 (Jun, 1998).
132. Y. S. Lee *et al.*, *Cell Metab* **3**, 135 (Feb, 2006).
133. B. G. Challis *et al.*, *Hum Mol Genet* **11**, 1997 (Aug 15, 2002).
134. L. Yaswen, N. Diehl, M. B. Brennan, U. Hochgeschwender, *Nat Med* **5**, 1066 (Sep, 1999).
135. J. L. Smart, V. Tolle, M. J. Low, *J Clin Invest* **116**, 495 (Feb, 2006).
136. A. P. Coll, I. S. Farooqi, B. G. Challis, G. S. Yeo, S. O'Rahilly, *J Clin Endocrinol Metab* **89**, 2557 (Jun, 2004).
137. G. W. Millington, *Clin Exp Dermatol* **31**, 407 (May, 2006).
138. I. S. Farooqi *et al.*, *J Clin Invest* **106**, 271 (Jul, 2000).
139. G. S. Yeo *et al.*, *Nat Genet* **20**, 111 (Oct, 1998).
140. M. Benzinou *et al.*, *Nat Genet* **40**, 943 (Aug, 2008).
141. M. F. Dallman, *Endocr Res* **10**, 213 (1984).
142. E. R. Simpson, M. R. Waterman, *Annu Rev Physiol* **50**, 427 (1988).
143. S. R. Bornstein, G. P. Chrousos, *J Clin Endocrinol Metab* **84**, 1729 (May, 1999).
144. C. Jung, W. J. Inder, *Med J Aust* **188**, 409 (Apr 7, 2008).
145. J. L. Rees, *Annu Rev Genet* **37**, 67 (2003).
146. T. M. Hahn, J. F. Breininger, D. G. Baskin, M. W. Schwartz, *Nat Neurosci* **1**, 271 (Aug, 1998).
147. M. M. Ollmann *et al.*, *Science* **278**, 135 (Oct 3, 1997).
148. A. Ishihara *et al.*, *Proc Natl Acad Sci U S A* **103**, 7154 (May 2, 2006).
149. E. Groppe *et al.*, *Nat Neurosci* **8**, 1289 (Oct, 2005).
150. S. Luquet, F. A. Perez, T. S. Hnasko, R. D. Palmiter, *Science* **310**, 683 (Oct 28, 2005).
151. A. C. Konner *et al.*, *Cell Metab* **5**, 438 (Jun 6, 2007).
152. N. Balthasar *et al.*, *Neuron* **42**, 983 (Jun 24, 2004).
153. M. A. Cowley *et al.*, *Nature* **411**, 480 (May 24, 2001).
154. A. W. Xu *et al.*, *J Clin Invest* **115**, 951 (Apr, 2005).
155. S. C. Woods, E. C. Lotter, L. D. McKay, D. Porte, Jr., *Nature* **282**, 503 (Nov 29, 1979).
156. S. C. Benoit *et al.*, *J Neurosci* **22**, 9048 (Oct 15, 2002).
157. T. Masaki *et al.*, *Obes Res* **12**, 878 (May, 2004).
158. L. M. Brown, D. J. Clegg, S. C. Benoit, S. C. Woods, *Physiol Behav* **89**, 687 (Dec 30, 2006).
159. M. W. Schwartz *et al.*, *Endocrinology* **130**, 3608 (Jun, 1992).
160. L. Plum *et al.*, *Nat Med* **15**, 1195 (Oct, 2009).
161. L. Koch *et al.*, *J Clin Invest* **118**, 2132 (Jun, 2008).
162. A. M. van den Hoek *et al.*, *Diabetes* **53**, 2529 (Oct, 2004).
163. H. Inoue *et al.*, *Cell Metab* **3**, 267 (Apr, 2006).
164. D. S. Edgerton *et al.*, *J Clin Invest* **116**, 521 (Feb, 2006).
165. R. W. Gelling *et al.*, *Cell Metab* **3**, 67 (Jan, 2006).
166. S. Obici, B. B. Zhang, G. Karkanas, L. Rossetti, *Nat Med* **8**, 1376 (Dec, 2002).
167. T. Maehama, J. E. Dixon, *J Biol Chem* **273**, 13375 (May 29, 1998).
168. L. Plum *et al.*, *J Clin Invest* **116**, 1886 (Jul, 2006).
169. G. G. MacGregor *et al.*, *Proc Natl Acad Sci U S A* **99**, 2726 (Mar 5, 2002).
170. T. Baukrowitz *et al.*, *Science* **282**, 1141 (Nov 6, 1998).
171. L. Plum, B. F. Belgardt, J. C. Bruning, *J Clin Invest* **116**, 1761 (Jul, 2006).
172. A. W. Xu, L. Ste-Marie, C. B. Kaelin, G. S. Barsh, *Endocrinology* **148**, 72 (Jan, 2007).
173. J. W. Hill *et al.*, *J Clin Invest* **118**, 1796 (May, 2008).

174. D. Spanswick, M. A. Smith, V. E. Groppi, S. D. Logan, M. L. Ashford, *Nature* **390**, 521 (Dec 4, 1997).
175. X. Ma, L. Zubcevic, F. M. Ashcroft, *Proc Natl Acad Sci U S A* **105**, 9811 (Jul 15, 2008).
176. H. Munzberg, J. S. Flier, C. Bjorbaek, *Endocrinology* **145**, 4880 (Nov, 2004).
177. M. B. Ernst *et al.*, *J Neurosci* **29**, 11582 (Sep 16, 2009).
178. A. Sahu, *Neurosci Lett* **440**, 125 (Aug 1, 2008).
179. K. K. Bence *et al.*, *Nat Med* **12**, 917 (Aug, 2006).
180. J. M. Zabolotny *et al.*, *J Biol Chem* **283**, 14230 (May 23, 2008).
181. P. J. Enriori *et al.*, *Cell Metab* **5**, 181 (Mar, 2007).
182. S. C. Benoit *et al.*, *J Clin Invest* **119**, 2577 (Sep, 2009).
183. S. H. Chiang *et al.*, *Cell* **138**, 961 (Sep 4, 2009).
184. X. Zhang *et al.*, *Cell* **135**, 61 (Oct 3, 2008).
185. G. K. Bandyopadhyay, J. G. Yu, J. Ofrecio, J. M. Olefsky, *Diabetes* **54**, 2351 (Aug, 2005).
186. J. E. Davis, N. K. Gabler, J. Walker-Daniels, M. E. Spurlock, *Horm Metab Res* **41**, 523 (Jul, 2009).
187. M. S. Radin, S. Sinha, B. A. Bhatt, N. Dedousis, R. M. O'Doherty, *Diabetologia* **51**, 336 (Feb, 2008).
188. M. S. Jin, J. O. Lee, *Immunity* **29**, 182 (Aug 15, 2008).
189. M. S. Jin, J. O. Lee, *Curr Opin Immunol* **20**, 414 (Aug, 2008).
190. J. E. Davis, N. K. Gabler, J. Walker-Daniels, M. E. Spurlock, *Obesity (Silver Spring)* **16**, 1248 (Jun, 2008).
191. H. Shi *et al.*, *J Clin Invest* **116**, 3015 (Nov, 2006).
192. F. Kim *et al.*, *Circ Res* **100**, 1589 (Jun 8, 2007).
193. M. Poggi *et al.*, *Diabetologia* **50**, 1267 (Jun, 2007).
194. M. J. Song, K. H. Kim, J. M. Yoon, J. B. Kim, *Biochem Biophys Res Commun* **346**, 739 (Aug 4, 2006).
195. D. M. Tsukumo *et al.*, *Diabetes* **56**, 1986 (Aug, 2007).
196. Q. Li, I. M. Verma, *Nat Rev Immunol* **2**, 725 (Oct, 2002).
197. D. Cai *et al.*, *Nat Med* **11**, 183 (Feb, 2005).
198. K. A. Posey *et al.*, *Am J Physiol Endocrinol Metab* **296**, E1003 (May, 2009).
199. J. Hirosumi *et al.*, *Nature* **420**, 333 (Nov 21, 2002).
200. M. A. Bogoyevitch, *Bioessays* **28**, 923 (Sep, 2006).
201. G. S. Hotamisligil *et al.*, *Science* **271**, 665 (Feb 2, 1996).
202. K. E. Wellen, G. S. Hotamisligil, *J Clin Invest* **115**, 1111 (May, 2005).
203. G. S. Hotamisligil, *Nature* **444**, 860 (Dec 14, 2006).
204. M. A. Bogoyevitch, B. Kobe, *Microbiol Mol Biol Rev* **70**, 1061 (Dec, 2006).
205. G. Solinas *et al.*, *Cell Metab* **6**, 386 (Nov, 2007).
206. S. N. Vallerie, M. Furuhashi, R. Fucho, G. S. Hotamisligil, *PLoS ONE* **3**, e3151 (2008).
207. G. Sabio *et al.*, *Science* **322**, 1539 (Dec 5, 2008).
208. G. S. Hotamisligil, N. S. Shargill, B. M. Spiegelman, *Science* **259**, 87 (Jan 1, 1993).
209. S. Cinti *et al.*, *J Lipid Res* **46**, 2347 (Nov, 2005).
210. C. N. Lumeng, J. L. Bodzin, A. R. Saltiel, *J Clin Invest* **117**, 175 (Jan, 2007).
211. D. Gordin *et al.*, *Ann Med* **40**, 627 (2008).
212. M. T. Nguyen *et al.*, *J Biol Chem* **280**, 35361 (Oct 21, 2005).
213. W. A. Banks, A. J. Kastin, R. D. Broadwell, *Neuroimmunomodulation* **2**, 241 (Jul-Aug, 1995).
214. C. T. De Souza *et al.*, *Endocrinology* **146**, 4192 (Oct, 2005).
215. R. M. Ransohoff, V. H. Perry, *Annu Rev Immunol* **27**, 119 (2009).

216. M. Fantino, L. Wieteska, *Physiol Behav* **53**, 477 (Mar, 1993).
217. T. Romanatto *et al.*, *Peptides* **28**, 1050 (May, 2007).
218. C. R. Plata-Salaman, G. Sonti, J. P. Borkoski, C. D. Wilson, J. M. b. French-Mullen, *Physiol Behav* **60**, 867 (Sep, 1996).
219. S. Franckhauser *et al.*, *Diabetologia* **51**, 1306 (Jul, 2008).
220. F. T. Wunderlich, Brüning, J.C., *in preparation* (2009).
221. V. Wallenius *et al.*, *Nat Med* **8**, 75 (Jan, 2002).
222. U. Ozcan *et al.*, *Science* **306**, 457 (Oct 15, 2004).
223. G. S. Hotamisligil, *Int J Obes (Lond)* **32 Suppl 7**, S52 (Dec, 2008).
224. M. Schroder, *Mol Biotechnol* **34**, 279 (Oct, 2006).
225. M. Schroder, *Cell Mol Life Sci* **65**, 862 (Mar, 2008).
226. I. Kim, W. Xu, J. C. Reed, *Nat Rev Drug Discov* **7**, 1013 (Dec, 2008).
227. C. Xu, B. Bailly-Maitre, J. C. Reed, *J Clin Invest* **115**, 2656 (Oct, 2005).
228. B. Vodenik, J. Rovira, J. M. Campistol, *Transplant Proc* **41**, S31 (Jul-Aug, 2009).
229. Y. Koketsu *et al.*, *Am J Physiol Endocrinol Metab* **294**, E719 (Apr, 2008).
230. S. Mordier, P. B. Iynedjian, *Biochem Biophys Res Commun* **362**, 206 (Oct 12, 2007).
231. P. Hu, Z. Han, A. D. Couvillon, R. J. Kaufman, J. H. Exton, *Mol Cell Biol* **26**, 3071 (Apr, 2006).
232. C. Zhang *et al.*, *Biochem Biophys Res Commun* **289**, 718 (Dec 7, 2001).
233. L. Ozcan *et al.*, *Cell Metab* **9**, 35 (Jan 7, 2009).
234. J. Sambrook, Russel, D.W., *Molecular cloning: a laboratory manual* (CSHL Press, 2001), pp.
235. R. Janoschek *et al.*, *Proc Natl Acad Sci U S A* **103**, 10707 (Jul 11, 2006).
236. P. Signorelli, Y. A. Hannun, *Methods Enzymol* **345**, 275 (2002).
237. D. L. Silver, *Mouse genetics: concepts and applications* (Oxford University press, 1995), pp.
238. B. F. Belgardt *et al.*, *Cell Metab* **7**, 291 (Apr, 2008).
239. F. Tronche *et al.*, *Nat Genet* **23**, 99 (Sep, 1999).
240. C. Canibano *et al.*, *Embo J* **26**, 2015 (Apr 18, 2007).
241. P. Kievit *et al.*, *Cell Metab* **4**, 123 (Aug, 2006).
242. A. Mora *et al.*, *Embo J* **22**, 4666 (Sep 15, 2003).
243. J. Seibler *et al.*, *Nucleic Acids Res* **31**, e12 (Feb 15, 2003).
244. L. J. Muglia *et al.*, *J Clin Invest* **105**, 1269 (May, 2000).
245. J. L. Smart, V. Tolle, V. Otero-Corchon, M. J. Low, *Endocrinology* **148**, 647 (Feb, 2007).
246. N. Hashimoto *et al.*, *Nat Genet* **38**, 589 (May, 2006).
247. A. Mora, D. Komander, D. M. van Aalten, D. R. Alessi, *Semin Cell Dev Biol* **15**, 161 (Apr, 2004).
248. A. Mora, C. Lipina, F. Tronche, C. Sutherland, D. R. Alessi, *Biochem J* **385**, 639 (Feb 1, 2005).
249. A. Novak, C. Guo, W. Yang, A. Nagy, C. G. Lobe, *Genesis* **28**, 147 (Nov-Dec, 2000).
250. S. Ten, M. New, N. Maclaren, *J Clin Endocrinol Metab* **86**, 2909 (Jul, 2001).
251. L. Jacobson, *Endocrinology* **140**, 310 (Jan, 1999).
252. R. H. Medema, G. J. Kops, J. L. Bos, B. M. Burgering, *Nature* **404**, 782 (Apr 13, 2000).
253. S. J. Kim *et al.*, *J Biol Chem* **280**, 22297 (Jun 10, 2005).
254. M. Theodoropoulou *et al.*, *Cancer Res* **66**, 1576 (Feb 1, 2006).
255. S. W. Oh *et al.*, *Proc Natl Acad Sci U S A* **102**, 4494 (Mar 22, 2005).
256. V. Aguirre, T. Uchida, L. Yenush, R. Davis, M. F. White, *J Biol Chem* **275**, 9047 (Mar 24, 2000).
257. Z. B. Andrews *et al.*, *Nature* **454**, 846 (Aug 14, 2008).

258. L. A. Velloso, E. P. Araujo, C. T. de Souza, *Neuroimmunomodulation* **15**, 189 (2008).
259. A. Hezi-Yamit *et al.*, *Proc Natl Acad Sci U S A* **102**, 12077 (Aug 23, 2005).
260. L. Haversen, K. N. Danielsson, L. Fogelstrand, O. Wiklund, *Atherosclerosis* **202**, 382 (Feb, 2009).
261. S. Lindmark, J. Buren, J. W. Eriksson, *Clin Endocrinol (Oxf)* **65**, 301 (Sep, 2006).
262. B. Tian, D. E. Nowak, A. R. Brasier, *BMC Genomics* **6**, 137 (2005).
263. A. Kleinridders *et al.*, *Cell Metab* **in press** (2009).
264. A. S. Gleiberman *et al.*, *Proc Natl Acad Sci U S A* **105**, 6332 (Apr 29, 2008).
265. C. Y. Kuan *et al.*, *Neuron* **22**, 667 (Apr, 1999).
266. E. A. Roman *et al.*, *Mol Cell Endocrinol* (Aug 19, 2009).
267. A. S. Metlakunta, M. Sahu, A. Sahu, *Endocrinology* **149**, 1121 (Mar, 2008).
268. L. Kappeler *et al.*, *Endocrinology* **150**, 314 (Jan, 2009).
269. N. M. Martin *et al.*, *Int J Obes (Lond)* **30**, 430 (Mar, 2006).
270. A. Giustina, G. Mazziotti, E. Canalis, *Endocr Rev* **29**, 535 (Aug, 2008).
271. Y. Kato, Y. Murakami, M. Sohmiya, M. Nishiki, *Intern Med* **41**, 7 (Jan, 2002).
272. J. M. Gertner, M. P. Wajnrach, R. L. Leibel, *Horm Res* **49 Suppl 1**, 9 (1998).
273. C. J. Phelps, G. E. Hoffman, *Peptides* **8**, 1127 (Nov-Dec, 1987).
274. B. D. Gaylinn, *Receptors Channels* **8**, 155 (2002).
275. C. Lin, S. C. Lin, C. P. Chang, M. G. Rosenfeld, *Nature* **360**, 765 (Dec 24-31, 1992).
276. F. E. Sluse *et al.*, *Biochim Biophys Acta* **1757**, 480 (May-Jun, 2006).
277. D. Ricquier, *Proc Nutr Soc* **64**, 47 (Feb, 2005).
278. K. S. Echtay, *Free Radic Biol Med* **43**, 1351 (Nov 15, 2007).
279. P. I. Hovring, V. Matre, A. K. Fjeldheim, O. P. Loseth, K. M. Gautvik, *Biochem Biophys Res Commun* **257**, 829 (Apr 21, 1999).
280. H. Z. Lin *et al.*, *Nat Med* **6**, 998 (Sep, 2000).
281. A. Hamann, J. S. Flier, B. B. Lowell, *Endocrinology* **137**, 21 (Jan, 1996).
282. Y. Fan *et al.*, *J Biol Chem* **284**, 19937 (Jul 24, 2009).
283. R. A. Rizza, L. J. Mandarino, J. E. Gerich, *Diabetes* **31**, 663 (Aug, 1982).
284. N. Rasouli, P. A. Kern, *J Clin Endocrinol Metab* **93**, S64 (Nov, 2008).
285. K. Rabe, M. Lehrke, K. G. Parhofer, U. C. Broedl, *Mol Med* **14**, 741 (Nov-Dec, 2008).
286. C. Buettner *et al.*, *Nat Med* **14**, 667 (Jun, 2008).
287. M. Rosenbaum, J. M. Gertner, R. L. Leibel, *J Clin Endocrinol Metab* **69**, 1274 (Dec, 1989).
288. J. W. Jocken *et al.*, *J Clin Endocrinol Metab* **92**, 2292 (Jun, 2007).
289. E. Hu, P. Liang, B. M. Spiegelman, *J Biol Chem* **271**, 10697 (May 3, 1996).
290. U. B. Pajvani, P. E. Scherer, *Curr Diab Rep* **3**, 207 (Jun, 2003).
291. M. I. Lefterova, M. A. Lazar, *Trends Endocrinol Metab* **20**, 107 (Apr, 2009).
292. G. Medina-Gomez, S. Gray, A. Vidal-Puig, *Public Health Nutr* **10**, 1132 (Oct, 2007).
293. J. Rieusset, J. Auwerx, H. Vidal, *Biochem Biophys Res Commun* **265**, 265 (Nov, 1999).
294. N. Kubota *et al.*, *Mol Cell* **4**, 597 (Oct, 1999).
295. D. W. Haslam, W. P. James, *Lancet* **366**, 1197 (Oct 1, 2005).
296. J. A. Luchsinger, D. R. Gustafson, *J Alzheimers Dis* **16**, 693 (Apr, 2009).
297. H. M. Salihu, S. M. Bonnema, A. P. Alio, *Maturitas* **63**, 7 (May 20, 2009).
298. A. Plagemann, *J Matern Fetal Neonatal Med* **21**, 143 (Mar, 2008).
299. K. D. Niswender *et al.*, *Diabetes* **52**, 227 (Feb, 2003).
300. K. N. Frayn, *Proc Nutr Soc* **60**, 375 (Aug, 2001).
301. W. Nolte, H. Hartmann, G. Ramadori, *Exp Clin Endocrinol Diabetes* **103**, 63 (1995).
302. K. F. Petersen, G. I. Shulman, *Am J Cardiol* **90**, 11G (Sep 5, 2002).
303. U. Smith *et al.*, *Ann N Y Acad Sci* **892**, 119 (Nov 18, 1999).
304. M. Hallschmid *et al.*, *Diabetes* **53**, 3024 (Nov, 2004).

305. M. Hallschmid, C. Benedict, B. Schultes, J. Born, W. Kern, *Int J Obes (Lond)* **32**, 275 (Feb, 2008).
306. K. D. Kimura, H. A. Tissenbaum, Y. Liu, G. Ruvkun, *Science* **277**, 942 (Aug 15, 1997).
307. C. A. Wolkow, K. D. Kimura, M. S. Lee, G. Ruvkun, *Science* **290**, 147 (Oct 6, 2000).
308. E. J. Rulifson, S. K. Kim, R. Nusse, *Science* **296**, 1118 (May 10, 2002).
309. R. J. Jacob *et al.*, *Diabetes* **46**, 150 (Jan, 1997).
310. N. Satoh *et al.*, *Neurosci Lett* **224**, 149 (Mar 21, 1997).
311. N. Satoh *et al.*, *Neurosci Lett* **249**, 107 (Jun 19, 1998).
312. R. J. Seeley *et al.*, *Nature* **390**, 349 (Nov 27, 1997).
313. D. E. Read, A. M. Gorman, *Cell Mol Life Sci* **66**, 2975 (Sep, 2009).
314. H. Zhao, R. M. Sapolsky, G. K. Steinberg, *Mol Neurobiol* **34**, 249 (Dec, 2006).
315. R. I. Feldman *et al.*, *J Biol Chem* **280**, 19867 (May 20, 2005).
316. A. Benrick *et al.*, *J Neuroendocrinol* **21**, 620 (Jul, 2009).
317. H. Mori *et al.*, *Nat Med* **10**, 739 (Jul, 2004).
318. A. Katsuki *et al.*, *J Clin Endocrinol Metab* **83**, 859 (Mar, 1998).
319. N. Wig *et al.*, *AIDS Patient Care STDS* **19**, 212 (Apr, 2005).
320. I. Figiel, *Acta Neurobiol Exp (Wars)* **68**, 526 (2008).
321. J. C. Moraes *et al.*, *PLoS ONE* **4**, e5045 (2009).
322. K. T. Coschigano *et al.*, *Endocrinology* **144**, 3799 (Sep, 2003).
323. M. Vignolo, A. Naselli, E. Di Battista, M. Mostert, G. Aicardi, *Eur J Pediatr* **147**, 242 (Apr, 1988).
324. D. Huszar *et al.*, *Cell* **88**, 131 (Jan 10, 1997).
325. R. Salvatori, X. Fan, P. E. Mullis, A. Haile, M. A. Levine, *Mol Endocrinol* **16**, 450 (Mar, 2002).
326. A. Garcia, C. V. Alvarez, R. G. Smith, C. Dieguez, *Mol Endocrinol* **15**, 1484 (Sep, 2001).
327. K. Yamamoto *et al.*, *Biochem Biophys Res Commun* **363**, 908 (Nov 30, 2007).
328. Z. Yin, L. Williams-Simons, L. Rawahneh, S. Asa, L. S. Kirschner, *Genesis* **46**, 37 (Jan, 2008).
329. M. Perello *et al.*, *Endocrinology* **147**, 2705 (Jun, 2006).
330. L. Davies *et al.*, *Mol Endocrinol* **22**, 1331 (Jun, 2008).
331. J. Yang, A. H. Tashjian, Jr., *Endocrinology* **133**, 487 (Aug, 1993).
332. I. Hansen *et al.*, *Am J Physiol* **250**, E269 (Mar, 1986).
333. L. R. MacGorman, R. A. Rizza, J. E. Gerich, *J Clin Endocrinol Metab* **53**, 556 (Sep, 1981).
334. T. C. Schreuder, B. J. Verwer, C. M. van Nieuwkerk, C. J. Mulder, *World J Gastroenterol* **14**, 2474 (Apr 28, 2008).
335. P. Bjorntorp, *Arteriosclerosis* **10**, 493 (Jul-Aug, 1990).
336. M. S. Brown, J. L. Goldstein, *Cell Metab* **7**, 95 (Feb, 2008).
337. J. P. del Rincon *et al.*, *Diabetes* **56**, 1638 (Jun, 2007).
338. H. Wei, J. Fang, M. Wang, *J Tongji Med Univ* **21**, 332 (2001).
339. H. Yamaza *et al.*, *J Gerontol A Biol Sci Med Sci* **62**, 27 (Jan, 2007).
340. W. M. Kong *et al.*, *Endocrinology* **145**, 5252 (Nov, 2004).
341. J. N. Fain, E. C. Coronel, M. J. Beauchamp, S. W. Bahouth, *Biochem J* **322 (Pt 1)**, 145 (Feb 15, 1997).
342. L. Zabrocka, J. Klimek, J. Swierczynski, *Life Sci* **79**, 1114 (Aug 8, 2006).
343. C. K. Lee, D. B. Allison, J. Brand, R. Weindruch, T. A. Prolla, *Proc Natl Acad Sci U S A* **99**, 14988 (Nov 12, 2002).
344. K. Flurkey, J. Papaconstantinou, R. A. Miller, D. E. Harrison, *Proc Natl Acad Sci U S A* **98**, 6736 (Jun 5, 2001).

345. M. S. Bonkowski *et al.*, *PLoS ONE* **4**, e4567 (2009).
346. M. S. Bonkowski, J. S. Rocha, M. M. Masternak, K. A. Al Regaiey, A. Bartke, *Proc Natl Acad Sci U S A* **103**, 7901 (May 16, 2006).
347. G. A. Garinis *et al.*, *Nat Cell Biol* **11**, 604 (May, 2009).

8 Acknowledgements

I would like to thank Professor Jens C. Brüning for allowing me to work in his lab, and for investing time, resources and energy in mentoring me during my graduation.

Furthermore, I would like to thank Professor Peter Kloppenburg, Professor Matthias Hammerschmidt and Dr. Ursula Lichtenberg for agreeing to form my thesis committee.

I would like to thank all my past and current colleagues in the Bruning lab for providing assistance and insightful discussions. I especially thank Dr. Jan Mauer, who discussed, helped and taught me a lot as a colleague and as a friend. I would also like to thank Dr. Eva Rother, Dr. Christine Könner and Dr. Sabine Jordan, who always offered me support, friendship and a good time. I would like to thank Dr. F. Thomas Wunderlich and Marianne Ernst for providing help and material during the studies. I cordially thank Dr. Sabine Jordan, Dr. Christine Könner, Dr. Jan Mauer, Dr. Hella Brönneke and Marianne Ernst for proofreading my thesis. I am deeply indebted to Brigitte Hampel for her help with immunohistochemistry and beyond. I would also like to thank Dr. Hella Brönneke and Sonja Becker for kind support in all (mouse) matters.

I am forever indebted to my parents Friedrich-Wilhelm & Anneliese Belgardt for their never-ending love, encouragement and support. I also would like to thank my sister Pia and my friends Marco, Steve, OJ, Frank, Peter and Darko for being there (even when I once again “disappeared” in work). Last but not least, I thank Anne Heppekausen for her support, friendship and love throughout the last 5 years.

9 Erklärung

Ich versichere, daß ich die von mir vorgelegte Dissertation selbständig angefertigt, die benutzten Quellen und Hilfsmittel vollständig angegeben und die Stellen der Arbeit einschließlich Tabellen, Karten und Abbildungen, die anderen Werken im Wortlaut oder dem Sinn nach entnommen sind, in jedem Einzelfall als Entlehnung kenntlich gemacht habe; dass diese Dissertation noch keiner anderen Fakultät oder Universität zur Prüfung vorgelegen hat; dass sie – abgesehen von unten angegebenen Teilpublikationen – noch nicht veröffentlicht worden ist sowie, dass ich eine solche Veröffentlichung vor Abschluß des Promotionsverfahren nicht vornehmen werde. Die Bestimmungen dieser Promotionsordnung sind mir bekannt. Die von mir vorgelegte Dissertation ist von Prof. Dr. Jens C. Brüning betreut worden.

Köln, 29. Oktober 2009, Bengt F. Belgardt

Teilpublikationen:

Belgardt BF, Husch A, Rother E, Ernst MB, Wunderlich FT, Hampel B, Klöckener T, Alessi D, Kloppenburg P, Brüning JC: “PDK1-deficiency in POMC-expressing cells reveals FOXO1-dependent and -independent pathways in control of energy homeostasis and stress response”. *Cell Metab.* 2008 Apr;7(4):291-301.

Kleinridders A*, Schenten D*, Könner AC*, **Belgardt BF***, Mauer J, Okamura T, Wunderlich FT, Medzhitov R, Brüning JC: “Myd88 signalling in the CNS is required for development of fatty acid induced leptin resistance and diet-induced obesity”. *Cell Metab.* 2009 Oct;10(4):249-59. *equally contributing first author

10 Curriculum vitae

Persönliche Daten

Name	Bengt-Frederik Belgardt
Geburtsdatum	16.01.1981
Geburtsort	Köln, Deutschland
Nationalität	Deutsch
Derzeitige Adresse	Pfälzer Str. 21, 50677 Köln
Email-Adresse	Bengt.Belgardt@uni-koeln.de

Bildungsweg

2000	Stadtgymnasium Köln-Porz, Abschluss: Allgemeine Hochschulreife
2000 - 2001	Wehrdienst, Deutsche Luftwaffe in den Niederlanden und in Deutschland
2001-2006	Biologie-Studium an der Universität zu Köln, Deutschland mit Abschluss des Biologie-Studiums mit Diplomprüfungen im Hauptfach Genetik und Nebenfächern Biochemie und Organische Chemie
Juni 2006	Abschluss Diplomarbeit in der Abteilung Mausgenetik und Metabolismus mit Titel „Die Rolle von PDK1 in der Energie-Homöostase“
Seit Juli 2006	Promotion in der Abteilung Mausgenetik und Metabolismus

Publikationen

Rother E, **Belgardt BF**, Brüning JC: Neuroendokrine Kontrolle des Energiestoffwechsels. Neuroforum 3/06. Review.

Plum L, Ma X, Hampel B, Balthasar N, Coppari R, Munzberg H, Shanabrough M, Burdakov D, Rother E, Janoschek R, Alber J, **Belgardt BF** et al.: Enhanced PIP3 signalling in POMC neurons causes KATP channel activation and leads to diet-sensitive obesity. J. Clin Invest. 2006 Jul;116(7):1886-901

Plum L, **Belgardt BF**, Brüning JC.: Central insulin action in energy and glucose homeostasis. J Clin Invest. 2006 Jul;116(7):1761-6. Review.

Belgardt BF, Husch A, Rother E, Ernst M, Wunderlich FT, Hampel B, Klöckener T, Alessi D, Kloppenburg P, Brüning JC: Inactivation of PDK1 in POMC-expressing cells reveals FOXO1-dependent and independent pathways in control of energy homeostasis and stress response.

Cell Metab. 2008 April;7(4):291-301.

Kleinridders A, Schenten D, Koenner AC, **Belgardt BF***, Mauer J, Okamura T, Wunderlich FT, Medzhitov R, Brüning JC: MyD88 signalling in the CNS is required for development of fatty acid induced leptin resistance and diet-induced obesity

Cell Metab. 2009 Oct;10(4):249-59. *equally contributing first author

Belgardt BF, Okamura T, Brüning JC: Hormone and glucose signalling in POMC and AgRP neurons
J Physiol. 2009 Sep 21. Review. [Epub ahead of print].

Belgardt BF, Mauer J, Wunderlich FT, Ernst MB, Pal M, Spohn G, Brönneke H, Brodesser S, Schauss AC, Brüning JC: Hypothalamic-pituitary JNK1 action controls Somatic growth and Glucose Metabolism

-in preparation-

Bailly-Maitre B, **Belgardt BF***, Jordan S, Coornaert B, Svorcova M, Kleinridders A, Mauer J, Cuddy M, Kress CL, Willmes D, Essig M, Hampel B, Protzer U, Reed JC, Brüning JC: Hepatic Bax-inhibitor (BI)-1 protects from obesity-associated insulin resistance and glucose intolerance via IRE1 α inhibition

-in preparation for resubmission- *equally contributing first author

Vorträge

TOBI – targeting obesity-associated inflammation, Vienna, Austria, Oct. 2009

Title: “Central JNK1 signalling regulates inflammation in adipose tissue”

Leopoldina Symposium on Developmental origins of health and disease, Greifswald, Germany, Sept. 2009

Title: “Perinatal re-programming of the melanocortin system”

PENS Summer School 2009, Günzburg, Germany, July 2009

Title: “Novel insights into control of energy homeostasis”

Days of Endocrinology Meeting, Eckernförde, Germany, May 2009

Title: “Über die Regulation des Energiehaushalts“

TOBI – targeting obesity-associated inflammation, Brussels, Belgium, March 2009

Title: “The role of JNK1 signalling in inflammation”

10th annual meeting Young active research, Cologne, Germany, Sept. 2008

Title: "BI-1 as a therapeutical target for treatment of diabetes"